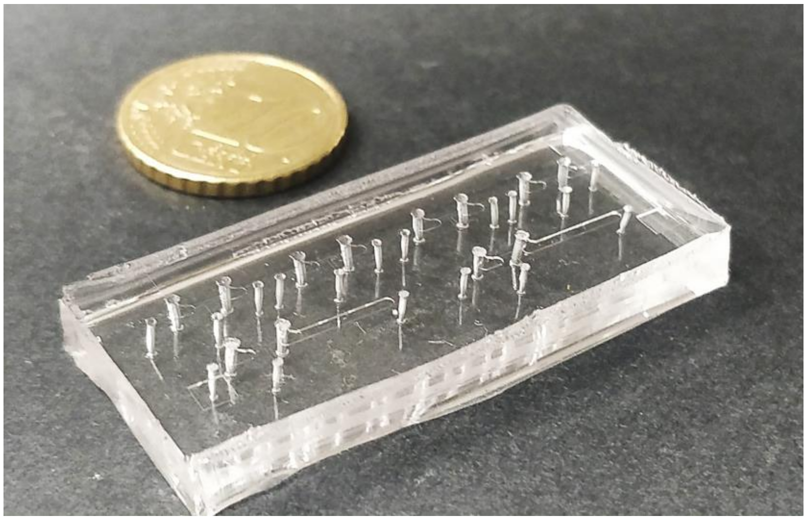

Enzyme Immobilization in porous micro beads in microfluidics for continuous production of L- DOPA and dopamine

Cristiana Maria Filipe Domingues

Thesis to obtain the Master of Science Degree in

Biotechnology

Supervisor (s): Prof. João Pedro Estrela Rodrigues Conde and Dr. Pedro Carlos de Barros Fernandes

Examination Committee

Chairperson: Prof. Arsénio do Carmo Sales Mendes Fialho

Supervisor: Prof. João Pedro Estrela Rodrigues Conde

Member of the Committee: Dr. Filipe Daniel Ramos de Carvalho

November 2019

Preface

The work presented in this thesis was performed at INESC MN and Institute for Bioengineering and Biosciences of Instituto Superior Técnico (Lisbon, Portugal), during the period August-November 2018-2019, under the supervision of Professor João Pedro Estrela Rodrigues Conde and Professor Pedro Carlos de Barros Fernandes.

Declaration

I declare that this document is an original work of my own authorship and that it fulfills all the requirements of the Code of Conduct and Good Practices of the Universidade de Lisboa.

Acknowledgments

In first place, I would like to thank for the support, cooperation, motivation and mentorship given by my supervisors Prof. Dr. João Pedro Conde and Prof. Dr. Pedro Fernandes. I really would like to emphasis my gratitude in allowing me to work on this project. It was a pleasure to work under yours involved supervision and in such a motivating and supporting environment throughout this last semester. I wish to thank Dr. Virginia Chu for all the support and advice during the entire project.

I would like to thank all my colleagues from INESC-MN for all the support, advices and the awesome environment provided during work. A special thanks to Eduardo Brás for the dedication, friendship and mentorship in every phase of this project, Pedro Monteiro, Catarina Caneira and Catarina Bombaça for all the good advices, help during troubleshooting times and the encouragement. Not only them, but everyone else who contributed in some way to help me grow during this project, and for all the fun times and cheerful spirit in the lab!

I would like to thank Andreia Jardim, Ricardo Serrão, Inês Domingos and Martim Costa for the amazing week in Germany- Summer School “Meeting Point – Functional Layers” in University of Applied Sciences Kaiserslautern, Campus Zweibrücken.

I would like to thank Andreia Jardim, who started out as a lab colleague and now a great friend, for friendship, advice, laughter, help and encouragement. Without her it would not have been the same. Thanks for everything.

I would like to thank my childhood friends, Cátia Gomes, Liliana Caetano, Raquel Freire and Catarina Gomes, for proving that despite the absence, our friendship prevails and even becomes stronger.

I would, also, like to thank my friends from the Biochemistry bachelor, Catarina Pedro, Diana Julião and Filipa Falcato for all the support and shared moments that made my academic journey awesome. You are the proof that good friendships remain strong even though we followed different paths.

Furthermore, I would like to thank Andreia Pereira and Rita Valente for all the support and friendship, Maria Joana Pinheiro and Mariana Tavares for sharing this amazing and challenging experience with me. The writing of my thesis would not be the same without these amazing people.

Finally, I would like to thank my family for all the support, especially to my parents who have not only supported all the expenses related to my academic training, but above all for all the love and support throughout these academic years, for believing in me, for being my stronghold during difficult times, for being the most important pillar of my life and for always being happy with my achievements. To my brother Telmo Domingues for being the best and for giving the best gift ever, my godson Tiago Domingues. To my grandparents for always being happy for my achievements, even when they did not quite understand what it meant.

Resumo

A síntese de biomoléculas, com potencial terapêutico, por via enzimática é de extrema importância, pois representa um processo de produção mais limpo, com etapas de processamento a jusante mais simples, em comparação com processos baseados em fermentação. Um modo de operação eficiente para prolongar a vida útil da enzima é a imobilização do catalisador num suporte que pode ser usado num reator de leito compactado. É essencial otimizar as condições da reação por meio de estudos de rastreio, a fim de obter as melhores condições para a produção contínua dessas biomoléculas de alto valor. Os biorreatores microfluídicos apresentam uma solução muito atraente para realizar a otimização do processo de maneira económica e rápida, uma vez que permite o uso de pequenas quantidades de reagentes de forma muito controlada. Desta forma, o meu trabalho visa desenvolver um reator microfluídico capaz de ser usado na indústria biotecnológica para rastrear as condições do processo para síntese enzimática de L-DOPA e dopamina, ambos usados como fármacos em casos de doenças neurológicas, em sequências de reação de etapa única e de etapa múltipla, bem como o aumento da produção de L-DOPA para um nível de produção de um reator de bancada.

Em todas essas reações, as conversões obtidas foram semelhantes às obtidas por outros trabalhos relatados na literatura com uma conversão global de aproximadamente 30%. Este trabalho também demonstrou o aumento de escala bem-sucedido do sistema, obtendo resultados semelhantes tanto na microescala quanto na macroescala para a produção de L-DOPA.

Palavras-chave

Biocatálise, Microfluídica, L-DOPA, Dopamina, Imobilização enzimática, Reator de leito compactado

Abstract

The synthesis of biomolecules with therapeutic potential by enzymatic route is of utmost importance as it represents a cleaner production process with simpler downstream processing steps compared to fermentation based processes. An efficient mode of operation for extending enzyme life is the immobilization of the catalyst in a carrier that can be used in a packed-bed reactor. It is essential to optimize the reaction conditions through screening studies in order to obtain the best conditions for the continuous production of these high value biomolecules. Microfluidic bioreactors provide a very attractive solution for cost-effective and rapid process optimization as they allow the use of small quantities of reagents in a very controlled manner. Thus, my work aims to develop a microfluidic reactor that can be used in the biotechnology industry to track the process conditions for L-DOPA and dopamine, both used as drugs in cases of neurological diseases, enzymatic synthesis in single-step and multi-step reaction sequences, as well as the upscale of L-DOPA production to a bench-scale production level.

In all these reactions, the conversions obtained were similar to those obtained by other studies reported in the literature with an overall conversion of approximately 30%. This work also demonstrated the successful upscale of the system, obtaining similar results on both the microscale and bench scale for L-DOPA production.

Keywords

Biocatalysis, Microfluidics, L-DOPA, Dopamine, Enzyme immobilization, Packed-bed reactor

Table of Contents

Preface iii
Declaration v
Acknowledgments vii
Resumo x
Abstract xii
List of Tables xviii
List of Figures xx
Nomenclature xxvii
List of Acronyms xxviii

1. Introduction 1
  1.1. Biomolecule Production 1
  1.2. What are Enzymes? 3
  1.3. Enzyme kinetics 5
  1.4. Enzyme Inhibition 7
  1.5. Enzyme Immobilization 8
  1.6. (Bio) Reactor modes operation 10
  1.7. Enzyme applications 13
    1.7.1. The pharmaceutical industry 13
    1.7.2. The food industry 13
    1.7.3. The chemical industry 14
  1.8. Microtechnology 15
    1.8.1. General concepts 15
      1.8.1.1. Surface to Volume Ratio 15
      1.8.1.2. The Reynolds Numbers 16
      1.8.1.3. The Péclet Number 16
      1.8.1.4. The Schmidt Number 17
      1.8.1.5. The Damkhöler Number 17
    1.8.2. Microfabrication 18

1.8.2.1. **Photolithography** 18
1.8.2.2. **Soft- Lithography** 20
1.8.3. **Instrumentation** 21
1.8.3.1. **Microsensors** 21
1.8.3.2. **Microvalves** 21
1.8.3.3. **Micropumps** 22
1.8.3.4. **Heaters and Coolers** 23
1.9. **Applications for Microfluidics** 24
1.9.1. **Screening Chip** 24
1.9.2. **Microfluidic reactors** 24
1.9.3. **Immobilized Enzyme Microreactors** 25
1.10. **Objectives** 25
2. **Materials and Methods** 26
2.1. **Microfluidic device fabrication** 26
2.1.1. **Hard mask fabrication** 27
2.1.2. **Mold fabrication** 28
2.1.3. **Fabrication of PDMS structures** 30
2.2. **Enzymatic Experiments** 32
2.2.1. **Beads preparation protocol** 32
2.2.1.1. **Detection (autofluorescence and detection)** 32
2.2.1.2. **Production (Enzyme Immobilization)** 33
2.2.2. **Packing beads method** 33
2.2.2.1. **Detection (autofluorescence)** 33
2.2.2.2. **Detection (L-DOPA/Dopamine)** 33
2.2.2.3. **Production (L-DOPA/Dopamine)** 34
2.2.3. **Bradford Method** 34
2.2.4. **Product Detection** 35
2.2.5. **Image Analysis** 36
2.2.6. **Production Experiments – Microscale** 36
2.2.7. **Production Experiments - Macroscale** 38
2.2.8. **Reverse phase High Performance Liquid Chromatography (rp-HPLC)** 38
3. **Results and Discussion** 39
3.1. **L-DOPA detection method** 39

3.1.1. Fluorescence Nanoparticles 39
3.1.2. Autofluorescence 40
3.1.3. With PEG vs without PEG 43
3.1.4. Reducing agent optimization 45
3.2. Calibration Curve of pure L-DOPA solutions. Monitor the amount at reactor output 48
3.3. Microscale Production of L-DOPA. Screening Conditions 52
3.4. Dopamine Detection Method 56
3.5. Microscale Production of Dopamine. Screening Conditions 59
3.6. Cascade Production 63
3.7. Macroscale Production of L-DOPA 65
3.8. HPLC 69
3.8.1. L-DOPA and dopamine standards 69
3.8.2. Artificial mixtures 72
3.8.3. Determination of compounds in samples 73
4. Conclusions and Future Works 75
5. References 78

List of Tables

Table 1. Classification of Enzymes. 4
Table 2. Materials and equipment required for microfluidic device fabrication. 26
Table 3. Summary of the equipment, material and reagents needed for these experiments. 32
Table 4. Different types of beads and their interactions used in this project for to determine which beads can be used to capture L-DOPA. 41
Table 5. Summarizes all absorbance's obtained throughout production. 56
Table 6. Results obtained for DOPA-decarboxylase wash-out studies at microscale experiments. 62
Table 7. Flow properties and resulting working flow rates for both micro and macroscale. 65
Table 8. Results obtained for tyrosinase wash-out studies at macroscale experiments. 67
Table 9. Substrate conversion comparison to literature reports. Conversions marked with "*" refer to the initial 8h working period. CSTR – Continuous Stirred Tank Reactor 68
Table 10. Summarize the retention time (min) and the peak area (A.U) collected based on the chromatograms for the L-DOPA. 71
Table 11. Summarize the retention time (min) and the peak area (A.U) collected based on the chromatograms for the Dopamine. 71

List of Figures

Figure 1. Comparing between enzyme-catalyzed and uncatalyzed reactions, where the terms $\Delta G^{\ddagger}_{uncat}$ and $\Delta G^{\ddagger}_{cat}$, are respectively, the activation energy for the uncatalyzed reaction and the activation energy for the catalyzed reaction. 3

Figure 2. Representation of the 3D structure of Tyrosinase of the RSCB Protein Data – Bank (5M6B) as of January 2019. 5

Figure 3. Effect of substrate concentration on the initial velocity of an enzyme-catalyzed reaction under Michaelis-Menten kinetics. 6

Figure 4. Distinction between competitive inhibition and noncompetitive inhibition. (**A**) Enzyme-substrate complex; **(B)** Competitive inhibition, where the inhibitor binds to the active center, preventing the specific substrate from binding; **(C)** Uncompetitive inhibition, where the inhibitor does not prevent substrate binding, because the inhibitor binds to the enzyme elsewhere. 8

Figure 5: Enzyme immobilization techniques 9

Figure 6. Various modes of reactor operation: **(A)** Batch-mode, **(B)** Continuous- mode and **(C)** Fed-batch mode. Schematic diagrams of different configurations for developing reactions in continuous processes using immobilized enzymes: **(D)** stirred tank reactors, **(E)** packed bed reactor and **(F)** fluidized bed reactor. 12

Figure 7. Steps of fabrication of: 1) aluminum hard masks; 2) SU-8 negative photoresist mold; and 3) PDMS structures used for trapping beads. The photoresists 1 and 2 should be selected to allow the spin-coating of a thinner and thicker SU-8 layer, respectively. 19

Figure 8. Example of a piezoelectric actuated microvalve. (a) Microvalve closed; (b) Microvalve opened 22

Figure 9. A 3D scale diagram of pneumatic actuated valves in a peristaltic pump configuration. The channels are 100 μm wide and 10 μm high 22

Figure 10. Sequence of steps involved in the fabrication of the aluminum hard masks. 28

Figure 11. Sequence of steps involved in the mold fabrication: 20 μm layer exposure, 20 μm layer development and 100 μm layer exposure, 100 μm layer development. 29

Figure 12. Sequence of steps involved in the fabrication of the PDMS structures. 30

Figure 13. (**A**) Microfluidic structure designed using AutoCAD software with two layers: 20 μm (purple) and 100 μm (green); (**L1**) Hard Mask (aluminum) used to fabricate layer with 100 μm of height; (**L2**) Hard Mask used to fabricate layer with 20 μm of height; **(B)** Mold showing layers with different heights, 20 μm and 100 μm; **(C)** PDMS structure. 31

Figure 14. Schematics of the nanoporous microbead used in this work for detection - Q Sepharose bead with strong ion exchange for ionic interactions. The matrix is agarose and these beads have a size of approximately 90 µm. 34

Figure 15. Microfluidic structure used for product detection: **(A)** The Q-Sepharose beads are packed through the side inlet (Red arrow), which is then closed with a closed metallic adapter. The mixture between L-DOPA and NaOH (pipette tip) is then pulling (Blue arrow). The mixture solution was pulling through the column using the polyethylene tubing coupled to an open metallic adapter with an PBS syringe controlled by a syringe pump (Green Arrow), applying a negative pressure at the outlet and **(B)** Bead trapping feature used to trap the beads. 35

Figure 16. Image Analysis: **(A)** Source image and **(B)** Conversion to a green channel, then the value obtained from the outer area is subtracted from the value obtained from the inner area. 36

Figure 17. Step-up of microscale production experiments: **(1)** Inverted fluorescence microscope coupled to a CCD color camera; **(2)** Syringe Pump (Multi-channel) on a pulling mode; **(3)** Hotplate in temperature of 32.5ºC; **(4)** Microreactors (**A**, **B** and **C** – Different microreactors with different geometries used for production of L-DOPA and Dopamine). 37

Figure 18. Step-up of macroscale production experiments: **(A)** An AKTA system for pumping, a hot bath, substrate reservoir which is also in the bath and a collection flask and **(B)** The beads are packed into a stainless steel pre-column holder typically used for HPLC. 38

Figure 19. Fluorescence spectrum. Resulting polymers exhibiting fluorescent properties. [79] 39

Figure 20. Pre-existing column design available at INESC-MN: **(A)** Schematics of the columns used for the screen experiments and dimensions; **(B)** Bead trapping feature used to trap the beads; **(C)** Packed column (brightfield); **(D)** Packed column (UV filter); **(E)** Detail of an only column showing the inlet (pipette tip with containing the bead suspension - blue arrow) and outlet (metal adapter - green arrow) through which the liquid was flowed by applying a negative pressure at the outlet. The accumulated negative pressure would then force the packing solution to enter the column through the column inlet. 40

Figure 21. Autofluorescence: **(A)** Capto Adhere; **(B)** DEAE- Sepharose; **(C)** PPA; **(D)** Q – Sepharose; **(E)** CM – Sepharose; **(F)** HEA HyperCel; **(G)** MEP HyperCel and **(H)** Silica. The conditions of acquisition using Leica DMLM Microscope were exposure time of 2s and gain of 2x. Objective lens: 10x. 42

Figure 22. Detection of L-DOPA. 5 beads were used for this studies: Silica, CM Sepharose, DEAE-Sepharose, HEA HyperCel and Q-Sepharose. First was study the autofluorescence of beads and then was flowed one solution of pure L-DOPA at 100 µM to know if any beads capture the fluorescence nanoparticles of L-DOPA. Using [NaOH] $_{\text{reaction medium}}$ = 0,2M. The conditions of acquisition using Leica DMLM Microscope were exposure time of 2s and gain of 2x. Objective lens: 10x. 43

Figure 23. Detection of L-DOPA at 100 µM using two methods: **Method A** - Without washing the columns with PBS and **Method B** – With washing the columns with PBS. Images captured for 0, 3, 6 and 9 minutes for a pure solution of L-DOPA at 100 µM flow of 1 µL/min using Q-Sepharose beads. Using [NaOH] $_{\text{reaction medium}}$ = 0,2M. The time 0 min corresponds to the beginning of the entry of the mixture solution (L-DOPA + NaOH). The conditions of acquisition using Leica DMLM Microscope were exposure time of 2s and gain of 2x. Objective lens: 10x. 44

Figure 24. Screen studies: **(A)** The fluorescence increase over time for different types of beads: HEA beads Hypercel, Q and DEAE Sepharose when the mixture solution (pure L-DOPA at 100 µM and NaOH) is passed in the column; and **(B)** The fluorescence increase over time for increasing concentrations of pure L- DOPA, using Q-Sepharose beads. [NaOH] reaction medium = 0.2 M. The measurements were performed at a flow rate of 1 µL/min. The conditions of acquisition using Leica DMLM Microscope were exposure time of 2s and gain of 2x. n=2 45

Figure 25. L-DOPA reaction pathway using L- tyrosine as a substrate. Tyrosinase plays a part in several of the reactions that take place, which eventually culminate with the production of melanin. Ascorbic acid is added to the reaction as the reducing agent of choice, to prevent the further oxidation of L-DOPA. Adapted from E.J.S. Brás and co-workers, in peer review. 46

Figure 26. Representation of the fluorescence emission as a function of time, for different concentrations of ascorbic acid in reaction medium. The [L-DOPA] is fixed, 100 µM. Using [NaOH] reaction medium = 0.2 M. The measurements were performed at a flow rate of 1 µL.min^{-1}. The conditions of acquisition using Leica DMLM Microscope were exposure time of 2s and gain of 2x. n=1 47

Figure 27. Representation of the fluorescence emission as a function of time, for different concentrations of NaOH in reaction medium. The [L-DOPA] and the [Ascorbic acid] are fixed, 100 µM and 2 mM, respectively. The measurements were performed at a flow rate of 1 µL.min^{-1}. The conditions of acquisition using Leica DMLM Microscope were exposure time of 2s and gain of 2x. Objective lens: 10x. 48

Figure 28. **(A)** Schematics of the microfluidic structure used for the calibration curves experiments and dimensions. The Q-Sepharose beads are packed through the side inlet (Red arrow), which is then closed with a closed metallic adapter, as described in section **2.2.2.2**. The mixture between L-DOPA, ascorbic acid and NaOH (pipette tip) is then pulling (Blue arrow). The mixture solution was pulling through the column using the polyethylene tubing coupled to an open metallic adapter with a PBS syringe controlled by a syringe pump (Green Arrow), applying a negative pressure at the outlet. **(B)** Brightfield (column packed). **(C) - (E)** Image captured at a long time (UV filter). The conditions of acquisition using Olympus (UV filter) were exposure time of 1s and a gain of 0x. Objective lens: 10x. 49

Figure 29. Experimental Image analysis method. By splitting the full image (RAW Image) in RGB color channels a better signal to ratio is obtained, especially for low concentrations of L-DOPA. Adapted from E.J.S. Brás and co-workers, in peer review. 50

Figure 30. Q-Sepharose beads darkening over the detection time, using brightfield. 51

Figure 31. Calibration Curve for each concentration of ascorbic acid, 0 µM (black), 100 µM (red), 200 µM (blue). Was made with an exposure time of 1s and a gain of 0, microscope CKX41 Olympus. n=4 51

Figure 32. Production and Detection of L-DOPA. Two reactor geometries was used for optimization experiments of production: **(A)** “Short Reactor” and **(B)** “Long Reactor”. The columns were packed with tyrosinase-functionalized beads through the side inlet (Red arrow), which is then closed with a closed metallic adapter (as described in section **2.2.2.3**). The substrate solution (tyrosine and ascorbic acid) is then pushing through the column inlet using the polyethylene tubing coupled to an open metallic adapter with a substrate solution controlled by a syringe pump (Blue arrow). Then the sample for analysis (S.U.A) was recovered at the reactor outlet (Green arrow). **(C)** The microfluidic structure used for the detection protocol, section **2.2.4.** This microfluidic column used for the detection protocol has the same dimensions the column used for production (Short Reactor). 53

Figure 33. Optimization experiments for the production of L-DOPA using tyrosinase as a substrate: **(A)** Flowrate (n=3), **(B)** Reducing agent concentration (n=3) and **(C)** Reactor geometry (n=3) was studied. **(D)** Using the optimal conditions, both reactor geometries were checked for long term viability (n=4). In **(B)**, **(C)** and **(D)** was considered flowrate of 1 µL/min. Adapted from E.J.S. Brás and co-workers, in peer review. 54

Figure 34. Microfluidic structure of Long Reactor after production of L-DOPA. Column darkening throughout production. Byproducts tend to deposit themselves on the microbeads, which leads to mass transport limitations in longer assays. Impossible that new substrates reach the enzyme. 55

Figure 35. Calibration curve obtained using tyrosinase solutions as a standard – Bradford method. 56

Figure 36. Dopamine reaction pathway using L-DOPA as a substrate and DOPA-decarboxylase as am enzyme. 57

Figure 37. Calibration Curves monitoring the fluorescence increase over time: **(A)** Pure dopamine concentrations varied 6 times, using green filter and **(B)** Pure solution of L-DOPA at 100 µM concentration remained constant and the dopamine concentration varied 6 times. 58

Figure 38. Detection of Dopamine. 4 typed of beads were used for these studies: Capto Adhere, CM Sepharose, PPA and MEP HyperCel. The autofluorescence of beads was initially assessed, then a solution of pure Dopamine at 100 µM was flowed to establish if any beads capture the fluorescence nanoparticles of Dopamine. 59

Figure 39. Consumption and Detection of L-DOPA. A reactor used for optimization experiments of production: **(A)** “Short Reactor”. The columns were packed with Dopa-Decarboxylase-functionalized beads through the side inlet (Red arrow), which is then closed with a closed metallic adapter (as described in section **2.2.2.3.**). The substrate solution (pure L-DOPA) is then pushing through the column inlet using the polyethylene tubing coupled to an open metallic adapter with a substrate solution controlled by a syringe pump (Blue arrow). Then the sample for analysis (S.U.A) was recovered at the reactor outlet (Green arrow). **(B)** The microfluidic structure used for the detection protocol, section **2.2.4.** This microfluidic column used for the detection protocol has the same dimensions the column used for production (Short Reactor). 60

Figure 40. Flow rate optimization of the dopamine production. A pure L-DOPA solution was used as a substrate and its consumption was monitored using the aforementioned described method. Adapted from E.J.S. Brás and co-workers, in peer review. 61

Figure 41. Calibration curve using DOPA-decarboxylase solutions as a standard – Bradford method. Adapted from E.J.S. Brás and co-workers, in peer review. 62

Figure 42. Sequential production of both L-DOPA and dopamine in a single microfluidic system and detection of L-DOPA. The chambers were packed, with respectively enzymes, through the side inlet (Red arrow), which is then closed with a closed metallic adapter (as described in section 2.2.2.3.). The substrate solution (tyrosine and ascorbic acid) is then pushing through the column inlet using the polyethylene tubing coupled to an open metallic adapter with a substrate solution controlled by a syringe pump (Blue arrow). Then the sample for analysis (S.U.A) was recovered at the reactor outlet (Green arrow): (A) For the monitoring of L-DOPA production, the outlet is sealed off and the middle outlet is used for sample retrieval and (B) For the detection of dopamine through of the consumption of L-DOPA, the middle outlet is sealed off and the sample is collected at the outlet. (C) Microfluidic structure packed with beads Q-Sepharose, as described in section 2.2.2.2., used for detection of L-DOPA, as described in section 2.2.4…………………………………………………………………...…63

Figure 43. Productivity for the sequential production of both L-DOPA and dopamine in a single microfluidic system, from of tyrosine as substrate. The flowrate used was 1 µL/min. Adapted from E.J.S. Brás and co-workers, in peer review. 64

Figure 44. Comparison between macroscale and microscale production: **(A)** The experiment lasted for 8h for both the Short reactor and **(B)** The experiment lasted for 8h for both the Short reactor. For the macroscale experiments, n=2. Adapted from E.J.S. Brás and co-workers, in peer review. 66

Figure 45. Comparison between the original bead stock (left) and the beads used for 8 h at the macroscale (right). The white substance above the beads in right picture is the cotton used to prevent bead washout from the column. 66

Figure 46. Calibration curve obtained using tyrosinase solutions as a standard – Bradford method. Adapted from E.J.S. Brás and co-workers, in peer review. 67

Figure 47. Chromatogram of different standard solutions with different concentrations: **(A)** L-DOPA and **(B)** Dopamine. In chromatogram of L-DOPA: **a)** [L-DOPA] = 200 µM; **b)** [L-DOPA] = 100 µM and **c)** [L-DOPA] = 50 µM. In chromatogram of L-Dopamine: **a)** [L-DOPA] = 200 µM; **b)** [L-DOPA] = 100 µM, **c)** [L-DOPA] = 50 µM and **d)** [L-DOPA] = 0 µM. For each standard has its retention time, which will be shown in **Table 10** and **Table 11**, respectively for compound L-DOPA and dopamine. 70

Figure 48. Calibration Curves: **(A)** L-DOPA and **(B)** Dopamine for different concentrations of standard solutions: 12.5, 25, 50, 100 and 200 µM. These curves can be used to determine the concentration of L-DOPA and Dopamine compounds in samples... 72

Figure 49. HPLC: **(A)** Step-up and **(B)** Chromatogram obtained for artificial mixtures of different proportions between L-DOPA and dopamine: **Grey** – 75 µM of L-DOPA + 25 µM of dopamine, **Pink** - 50 µM of L-DOPA + 50 µM of dopamine and **Blue** – 25 µM of L-DOPA + 75 µM of dopamine. The retention time for L-DOPA and Dopamine, is approximately, 3.13 and 3.45 minutes, respectively. 73
Figure 50. Chromatogram obtained for real sample. Peaks of L-DOPA and Dopamine compounds are highlighted, depending on retention times, 3.1 minutes for L-DOPA, and 3.45 minutes for Dopamine. 74
Figure 51. Calibration Curve not considered. n=1 79
Figure 52. Different slopes obtained for each concentration of L-DOPA and for each concentration of ascorbic acid in function of time: **(A)** 0 µM of ascorbic acid; **(B)** 100 µM of ascorbic acid and **(C)** 200 µM of ascorbic acid. n=1 86

Nomenclature

Symbols

$\Delta G^{\neq}$	Activation Energy
$\Delta G^{\neq}_{cat}$	Activation Energy of catalyzed reaction
$\Delta G^{\neq}_{uncat}$	Activation Energy of uncatalyzed reaction
r	radius
h	height
ρ	density
U	velocity of the fluid
L	characteristic dimension
μ	viscosity
D	diffusion coefficient
k	thermal diffusity

List of Acronyms

APTES	(3-Aminopropyl)triethoxysilane
ATP	Adenosine triphosphate
CAD	Computer Assisted Design
CSTR	Continuous Stirred Tank Reactor
Da	Damkhöler Number
DI Water	Deionized Water
DWL	Direct Laser Writer
E	Enzyme
EC	Enzyme Commission
ES	Enzyme-Substrate complex
EP	Enzyme-Product complex
FADH	Flavin adenine Dinucleotide
FBR	Fluidized Bed Reactor
HPLC	High Performance Liquid Chromatography
IPA	Isopropanol
K_M	Michaelis-Menten constant
L-DOPA	3,4-dihydroxy-L-phenylalanine
MEMS	Microelectromechanical systems
MS	Mass Spectrometry
NADH	Nicotinamide adenine dinucleotide
NaOH	Sodium Hydroxide
P	Product
PBR	Packed-Bed Reactor
PBS	Phosphate Buffer Saline
PDMS	Polydimethylsiloxane
Pe	Péclet Number
PEG	Polyethylene Glycol
PGMEA	Propylene Glycol Monomethyl Ether Acetate
PVC	Polyvinyl Chloride
Re	Reynolds Number

RP	Reversed Phase
RNA	Ribonucleic Acid
S	Substrate
STR	Stirred Tank Reactor
v_0	Initial reaction rate
V_{max}	Maximum reaction rate
UV	Ultraviolet

Chapter 1

1. Introduction

This project focuses on the development of a microfluidic device capable of producing biomolecules individually, as well as for their continuous production through a cascade of reactions. It also focuses on upscale the optimized production system.

The first chapter presents the concepts of enzymes, enzymatic reactions and their possible applications. The notion of microfluidics will also be explored, with the explanation of general concepts and elaboration of possible instrumentation on chip. Implementation will be highlighted by presenting a few examples of microfluidics systems used for biotechnological applications.

1.1. Biomolecule Production

The ability to continuously produce biomolecules in an efficient and low-cost fashion is of increasing interest for the biotechnology industry, since many of these biomolecules have a high commercial value and are relevant, not only for the pharmaceutical sector, but also for the food and cosmetics industry. [1][2][3] For instance, some biomolecules can be used as drugs to treat neurodegenerative diseases, such as 3,4-dihydroxy-L-phenylalanine (L-DOPA) which is the gold standard treatment used to increase dopamine production in Parkinson's disease.[4] Dopamine and its precursor L-DOPA are important signaling molecules in the human organism, by playing roles as neurotransmitters and in the case of dopamine as a major signaling molecule in the brain reward system.[5][6][7] An imbalance of these molecules can cause several types of neurological disorders such as Parkinson's disease. [8] However, dopamine is not used in the treatment of these types of diseases due to its inability to cross the brain-blood barrier, still it is used in the treatment of low blood pressure and cardiac arrest. [9] The increase in prevalence of neurodegenerative diseases in recent years has helped to boost the interest and the research around the production of these biomolecules.

The production of biomolecules can occur through enzymatic reactions or through fermentation technology, and it should be noticed that purity is a key aspect in the production of biomolecules for pharmaceutical applications, regardless of the process used. While the fermentation process involves a multiplicity of catalytic steps, performed by the cells used, where the substrate and the final product differ substantially, enzymatic reactions involve fewer catalytic steps (usually one or two) and the substrate and the product have structural similarities. Furthermore, the enzymatic process typically decreases the risk of by-products or undesired reactions by other enzymes that could consume substrate for purposes other than intended or degrade the product, which is another advantage over fermentation. However, there are cases where the enzyme chosen will serve as a catalyst for multiple, sequential reactions, as is the case of melanin production via tyrosine oxidation using tyrosinase as the catalyst. [10] The option for a fermentative pathway typically occurs when either the complexity of the metabolic pathway is too large to enable the use of (partially) purified enzymes or when the set of reactions can be performed by an enzymatic cascade, yet the enzymes are very unstable when not in the cellular environment. Thus, when there are enzymatic cascade, fermentation or use of whole cells containing the desired metabolic pathway can be chosen, due to the high costs associated to purification and separation (the higher the number of enzymes, the more expensive the process) and due to enzymes involved in the cascade do not have similar turnovers, accumulation or lack of reagents occurs. [11][12] Furthermore, fermentation is based on microbial biotechnology, where the biomolecules are produced by the cell metabolism and can be characterized as extracellular or intracellular products. Typically, the fermentation broth is a very complex mixture that includes live cells, cell debris, proteins and nucleic acids. Due to this, the downstream processing becomes very challenging due to the different nature of these compounds, in addition to the presence of unconsumed substrate and unwanted metabolic by-products. In contrast, enzymatic reactions present an overall cleaner production process with simpler downstream processing steps, which can influence the choice of production path when working with pharmaceutical applications, as aforementioned. [11]

Optimization of both upstream and downstream processing steps is often very burdensome, both in terms of time as well as in financial terms, which creates a demand to expedite the process in the cheapest way possible. Thus, it is essential to optimize the reaction conditions through screening studies in order to obtain the best conditions for the continuous productions of these high value biomolecules.[13]

Microfluidics technology presents itself as a very attractive solution to perform process optimization in a cost effective and rapid manner since it enables the use of small amounts of reagents in a very controlled form, in terms of both mass and heat transfer, in addition to the reduced reaction times, imposed by small diffusion lengths within the microfluidic device. [13][14]

With this being said, my project aims at developing a microfluidic reactor capable of being used in the biotechnological industry to screen process conditions for enzymatic synthesis in a fast and cost effective way for process optimization (i) and/or for continuous production of biomolecules (ii) as well as to upscale the resulting, optimized, process to a lab bench scale (iii).

1.2. What are Enzymes?

Enzymes are biological catalysts that accelerate chemical reactions. They have molecular weights ranging from about tens of thousands to more than one million Daltons (Da). All enzymes are proteins with the exception of a group of catalytic RNA molecules, ribozymes. [15]

Many reactions in biochemistry are unfavorable or unlikely in the cellular environment. [15] In order to overcome this, enzymes are used, giving a specific environment within which a given reaction can occur more quickly and favorably. The enzyme contains an active site where substrate binding occurs. A simple enzymatic reaction can be depicted as:

$$\mathrm{E + S \rightleftharpoons ES \rightleftharpoons EP \rightleftharpoons E + P}$$

Where E is the enzyme, S the substrate, ES the transient complex of the enzyme with the substrate, P the product, and EP the transient complex of the enzyme with the product. [15]

The role of enzymes is to accelerate the interconversion of S and P without affecting the reaction equilibrium.

The enzymes cause the decrease of the activation energy needed for the reaction to occur, this way increasing the speed of the reaction. The activation energy, $\Delta G^{\ddagger}$ is given by the difference between the ground state energy levels. In **Figure 1** it is possible to see the difference between a catalyzed reaction and an uncatalyzed reaction. Where the activation energy is higher when an uncatalyzed reaction is present, concluding that this reaction is slower. [15]

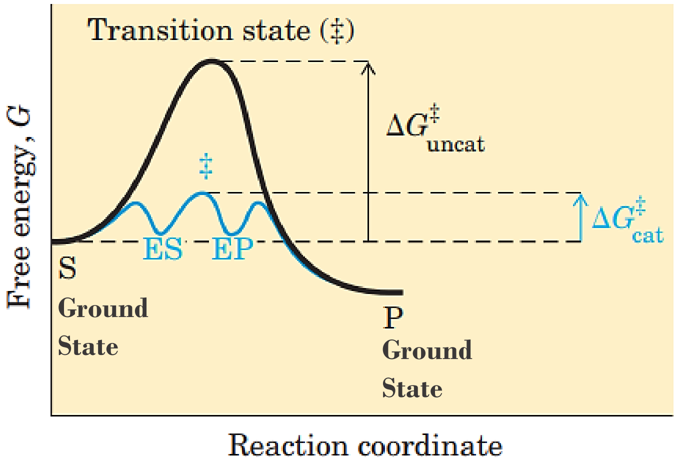

Figure 1. *Comparing between enzyme-catalyzed and uncatalyzed reactions, where the terms* $\Delta G^{\ddagger}_{uncat}$ *and* $\Delta G^{\ddagger}_{cat}$*, are respectively, the activation energy for the uncatalyzed reaction and the activation energy for the catalyzed reaction.* [15]

The enzymes are classified according to the reaction that they catalyze and therefore are divided into seven classes: oxidoreductases, transferases, hydrolases, lyases, isomerases, ligases and translocases. [15] Further details are given in **Table 1**.

***Table 1**. Classification of Enzymes.*

Enzyme Commission number	Class	Reaction Catalyzed
EC 1	Oxidoreductases	Oxidation- reduction reaction (transfer of electrons)
EC 2	Transferases	Group transfer reactions
EC 3	Hydrolases	Hydrolytic cleavage of bonds by the addition of a water molecule
EC 4	Lyases	Elimination reactions of groups in which a double bond is formed
EC 5	Isomerases	Isomerization reactions (transfer of groups within molecules)
EC 6	Ligases	Reactions in which two molecules join together with energy (usually ATP)
EC 7	Translocase	Movement of ions or molecules across membranes or their separation within membranes

Some enzymes require, for activity, an additional chemical component – cofactor (non-protein molecule), that can be organic or inorganic. The organics also called by coenzyme are for example Flavin adenine dinucleotide (FADH), Nicotinamide adenine dinucleotide (NADH) and Biocytin. And the inorganics are for example magnesium (Mg^{2+}), iron (Fe^{2+}), manganese (Mn^{2+}), or zinc (Zn^{2+}). The enzymes that require the cofactor are designed by holoenzymes. [15]

An example of an enzyme which requires an additional chemical component to have activity is tyrosinase (EC 1.14.18.1), which as its molecular structure presented in **Figure 2**. Tyrosinase is a type III copper-containing (two copper ions in the active site) oxidoreductases that are widely distributed in nature. [16][17][18] It is mostly involved in the development of pigments, such as melanins, and other polyphenolic compounds. [19] More exactly this enzyme catalyzes the hydroxylation of L-tyrosine to L-DOPA via cresolase activity and oxidoreduction of L-DOPA to dopaquinone via catecholase activity, which are both coupled to the reduction of molecular oxygen to water. [16][20]

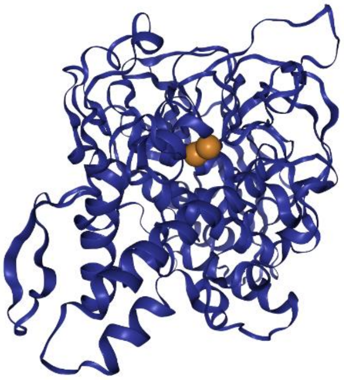

Figure 2. *Representation of the 3D structure of Tyrosinase of the RSCB Protein Data – Bank (5M6B) as of January 2019.*

An important property is the three-dimensional structure of the enzymes. This structure is achieved through weak interactions, such as, hydrogen bonds, electrostatic forces, Van der Waals forces and hydrophobic bonds. When pH or temperature changes occur, some of these forces are compromised, so that the enzymes lose their structure, and consequently alterations occur in the conformation of the active site, limiting the capability of the enzyme to bind its substrate, thus occurring loss of activity. Therefore, the enzymes have optimal temperature and pH values for which their activity is maximal, which will play an important role in the overall productivity of the system. In order to study the mechanism of an enzyme-catalyzed reaction and determine the optimal working conditions for an enzyme, kinetic studies have to be performed. [15]

1.3. Enzyme kinetics

In order to model an enzymatic process, it is essential to understand the kinetics of the enzyme that we are using. For reactions catalyzed for by enzymes that possess a single substrate, the reaction kinetics fall under the Michaelis-Menten model. The Michaelis-Menten model depends on the relatively simple two-step reaction mechanism, a binding step between enzyme and substrate (ES complex – **Figure 4.A**), followed by breakdown of ES complex to form P. In **Figure 3** is depicted the typical kinetic curve for the Michaelis-Menten model. Based on the figure it is possible to see that the reaction rate catalyzed by an enzyme is affected by the concentration of the substrate. As the concentration of the substrate increases, the rate of reaction increases in the same proportion, until it reaches a point where the increase in reaction rate is small as the concentration of the substrate increases. This region is close to the maximum velocity. As far as the enzyme is concerned, the maximum velocity indicates that all active site in the enzyme are filled with substrate. [21] It is possible to see, in **Figure 3**, the Michaelis-Menten equation, where v_0 represents the initial velocity, V_{max} the maximum rate achieved when the system is saturated (more substrate molecules than actual binding sites), [S] the concentration of substrate and K_M the concentration at which half of the maximum reaction rate is achieved, that is K_M is the concentration of substrate at which half the active sites are filled. [15][21] Thus, K_M indicates the affinity between the enzyme and the substrate and gives an idea of the substrate concentration required for significant catalysis to occur. [21]

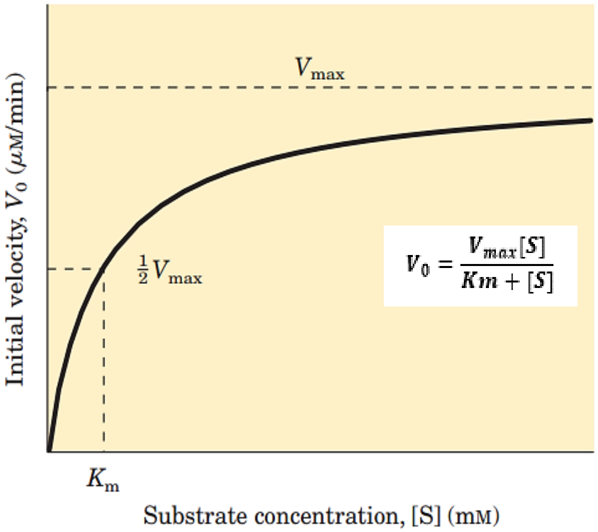

Figure 3. *Effect of substrate concentration on the initial velocity of an enzyme-catalyzed reaction under Michaelis-Menten kinetics.* [15]

In order to calculate relatively simple kinetic parameters such as K_M and V_{max}, there are different linear equations that are rearrangements of the Michaelis-Menten equation (rectangular hyperbole). Within which we have the Lineweaver-Burke, Hanes, and Eadie — Hofstee equations. The Lineweaver-Burke equation allows the determination of kinetic parameters from a plot of $1 / v_0$ versus $1 / [S]_0$ **(Equation 1)**, the Hanes equation from a plot of $[S]_0 / v_0$ versus $[S]_0$ **(Equation 2)** and the Eadie — Hofstee equation from a plot of v_0 versus $v_0 / [S]_0$ **(Equation 3)**. Of the three linear arrangements presented, although Lineweaver-Burke is the most widely used, it is also the least reliable. The most reliable rearrangement is the Hanes equation. [15][22]

$$\frac{1}{v_0} = \frac{K_M}{V_{max}} \times \frac{1}{[S]_0} + \frac{1}{V_{max}} \qquad \text{(Equation 1)}$$

$$\frac{[S]_0}{v_0} = \frac{1}{V_{max}} [S]_0 + \frac{K_M}{V_{max}} \qquad \text{(Equation 2)}$$

$$v_0 = -K_M \left(\frac{v_0}{[S]_0}\right) + V_{max} \qquad \text{(Equation 3)}$$

Many enzymes catalyze reactions with two or more substrates, which involve more complex mechanisms than the mechanism originally suggested for the development of the Michaelis-Menten model that considered a single substrate. These reactions can follow either a ping-pong mechanism or ternary-complex/ double-displacement mechanism. [15] In the first case, conformational changes occur in the enzyme due to the binding of the first substrate. After the product of the previous reaction dissociates, the second substrate attaches to the enzyme with the altered conformational structure obtaining the second product. The formation of a tertiary complex does not occur. In the case of ternary-complex mechanism both substrates are bound to the enzyme simultaneously, in order to form a noncovalent ternary complex, at which the substrates bind to the enzyme sequentially or randomly. After the reaction, two products are released. [15]

Besides the above-mentioned kinetic models there is other, like pre-steady-state kinetics, also relevant for enzymatic analysis and modelling, but that will not be discussed here**.**

1.4. Enzyme Inhibition

Enzyme inhibitors are substances that interfere with catalysis enzymatic reactions. There are two classes of enzyme inhibitors: reversible (competitive, uncompetitive and mixed) and irreversible. A competitive inhibitor (**Figure 4. B**) is a compound similar to the substrate, that competes with the substrate for the active site of an enzyme preventing the substrate from binding and thereby decreasing the activity of the enzyme solution. An uncompetitive inhibitor (**Figure 4. C**) does not bind to the enzyme active center, binding to another region of the enzyme. Therefore in these cases the inhibitor will bind to the ES complex. A mixed inhibitor is similar to the previous inhibitor that is bound at a site distinct from the substrate active site, but in this case the inhibitor may bind to both the enzyme and the ES complex. And finally, the irreversible inhibitors which binds covalently, destroying a functional group of the enzyme, this way altering the activity of this enzyme. [15][21]

Irreversible inhibitors can be divided into three groups: group-specific reagents, substrate analogs and suicide inhibitors. Group-specific reagents react with amino acid-specific R groups of the active site of the enzyme. Substrate analogs, as the name implies, are molecules structurally similar to the enzyme substrate (mimics the normal substrate) that covalently modify residues of the enzyme active site. These inhibitors are more specific for the active site of the enzyme than group specific reagents. [21] And finally, suicide inhibitors are relatively unreactive compounds until they bind to the active site of a specific enzyme. The inhibitor binds to the enzyme as a substrate and the normal enzymatic reaction occurs. However, instead of producing a normal product, the catalysis mechanism generates a chemically reactive intermediate that will inactivate the enzyme. That is, the enzyme catalyzes its own suicide. [15][21]

Environmental factors, such as temperature and pH, can also affect enzyme activity because they disrupt the structure of the enzyme. At very high temperatures protein denaturation can occur, so enzymatic activity decreases dramatically. Regarding pH, each enzyme has an optimal pH, where the enzymatic activity is maximum. Below or above this pH the enzymatic activity decreases. [15]

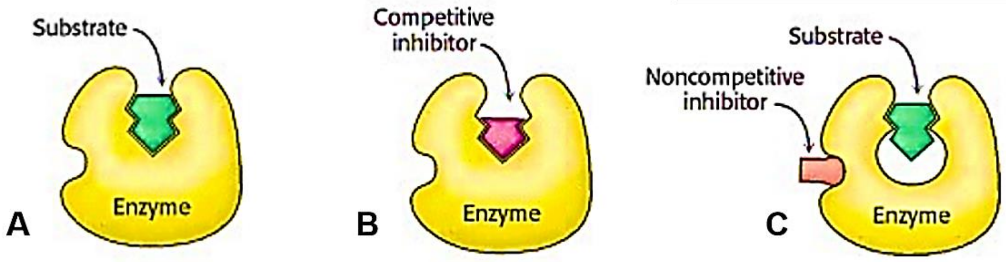

Figure 4. *Distinction between competitive inhibition and noncompetitive inhibition. (**A**) Enzyme-substrate complex; **(B)** Competitive inhibition, where the inhibitor binds to the active center, preventing the specific substrate from binding; **(C)** Uncompetitive inhibition, where the inhibitor does not prevent substrate binding, because the inhibitor binds to the enzyme elsewhere.* [21]

1.5. Enzyme Immobilization

In multiple practical processes the use of the enzymes has presented some obstacles, such as, narrow pH range, low thermal stability, loss of catalytic activity, the high cost of isolation and purification and instability of their structures. The immobilization of enzymes could be a possible solution to overcome some of these obstacles. By binding the enzyme to a surface we promote the protection of the enzyme to the external environment preventing denaturation from occurring. Thus, the immobilized enzymes are more resistant to the external environment and are more stable. Furthermore, the immobilization allows the reuse of the enzymes and prevents the wash-out of the system in the case of a continuous process. [23][24][25]

There are several methods to immobilize enzymes, which can be classified as physical and chemical methods. The physical methods refer to the weak interactions between the enzyme and the carrier. The chemical methods refer to covalent bonds. [24] The general immobilization techniques are adsorption, entrapment and covalence (**Figure 5**). [26] [27]

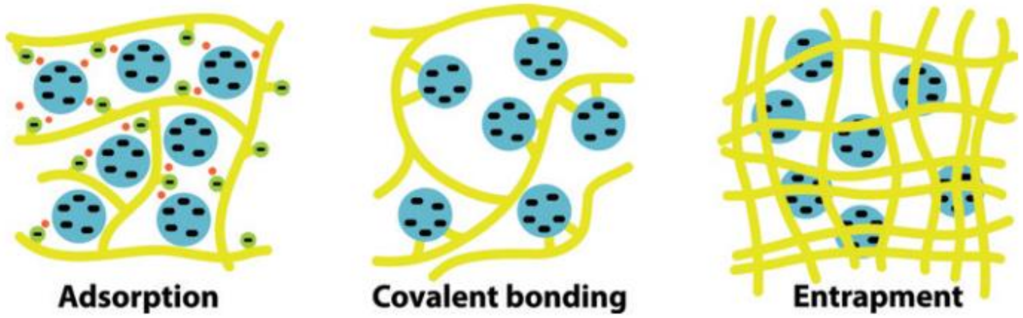

Figure 5: *Enzyme immobilization techniques.* [27]

Immobilization by adsorption is a method of reversible binding between the carrier and the catalyst. Some of the forces involved in the binding are electrostatic forces and Van der Waals forces. Since these forces are weak, no changes occur in the three-dimensional structure of the catalyst, and therefore no active site changes occur and as such, the catalyst maintains its activity. There are two types of carrier, organic and inorganic. Examples of organic are chitosan, cellulose and alginate, and example of inorganic is silica. [23]

The entrapment is a method of irreversible immobilization, where the enzyme is trapped in a polymeric mesh or carrier. This mesh, in spite of preventing the enzyme from escaping, allows the movement of the substrate and the products of the reaction. This type of immobilization promotes decreased leaching and improved enzyme stability, however, typically suffers from higher mass transfer limitations then other methods. [28]

The covalent bonding is another example of irreversible immobilization, which is achieved through the binding of functional groups on the carrier and the side chains of the enzymes. In this case the activity of the enzyme will be minimized if the binding involves amino acids that are present in the active site. [28]

An example, where production using immobilized enzyme has been the alternative to microbial fermentation is in the production of L-DOPA (precursor of dopamine and an essential neural message transmitter, used for the treatment of Parkinson's disease). Although microbial fermentation to L-DOPA exhibits better enantio-selectivity than chemical synthesis of L-DOPA, is a more time-consuming process and the downstream processes are complex. Therefore, the immobilization of the enzymes is the solution adopted to overcome obstacles such as, enzyme denaturation, low productivity. Immobilization also facilitates the separation of the enzyme from the reaction medium. [10]

As previously mentioned, immobilization of the enzymes allows the continuous operation of an enzymatic process, however, there are several reactor designs and modes of operation that can be used and these will be discussed in the following section.

1.6. (Bio) Reactor modes operation

A reactor is a system consisting of a vessel or a series of vessels to perform the desired conversion by enzymatic means to obtain the desired product under strictly controlled conditions. In order to provide higher yields and purity and low pollution and costs, the choice of reactors for a specific process is used. Reactors can operate in batch mode (**Figure 6. A**), continuous mode (**Figure 6. B**) or fed-batch mode (**Figure 6. C**), using enzymes in their free state or in immobilized form. [29][30][31]

In Batch- mode operations, reactors typically consist of a tank containing an agitator (stirred tank reactor, STR) where the culture environment changes continuously. This stirrer allows the content to have relatively uniform properties such as temperature, density and pH. It is a discontinuous reactor that has no feed flow or product. The enzyme and substrate are placed at the beginning of the reaction in the reactor and the reaction is performed until a chosen degree of conversion is achieved. Then the product is discharged and the reactor is cleaned before the next batch is loaded. Generally, the enzyme and substrate have identical residence times within the reactor. Batch- mode reactors are usually preferred when free enzymes are used as biocatalysts. But in these cases, there is no enzyme recovery at the end of production. Already when immobilized enzymes are used, they must be separated from the product stream by a subsequent purification step, such as centrifugation or filtration. Sometimes, these enzyme recovery steps can lead to immobilized enzyme loss, and can lead to inactivation of enzymes, leading to low productivity. [29][30][31]

In Continuous- mode operations, nutrients are continuously supplied to the reactor system and the product stream is continuously recovered. Growth and product formation can be sustained for extended periods. Continuous reactions allow for higher productivity than batch production mainly due to the lower frequency of unproductive time and are especially used for large scale production processes. In continuous operation, the product is uniform in time. The operating costs of batch reactors are higher than in continuous processes due to the need to empty and replenish the reactors. In this type of reactor, immobilized enzymes are used as catalysts, since highly stable enzymes are required to perform continuous processes. [29][32]

In Fed-batch mode operations, also called semi-batch reactors, the feed is introduced continuously or intermittently into the reactor, however there is no continuous removal of the product as in continuous- mode operation. As a result, the reactor volume increases over time. Products obtained from the reaction are only removed at the end of the cycle, as in batch- mode. [29]

As noted above, the choice of reactor varies depending on a specific process and therefore the first decision to make will be the type of reactor to use. However, there is no ideal reactor configuration. Selecting the best option depends on the type of support and reaction kinetics. There are several reactor configurations for developing reactions in continuous processes using immobilized enzymes. Examples of such configurations are the continuous stirred tank reactor (CSTR) (**Figure 6.D**), the packed bed reactor (PBR) (**Figure 6.E**), and the fluidized bed reactor (FBR) (**Figure 6.F**). [31]

Continuous stirred tank reactor (CSTR) is a reactor often used in industrial processes. It usually works at steady state, where the concentration of nutrients and product is constant. Thanks to continuous stirring it is assumed to be perfectly mixed. Consequently, the whole variable (temperature, concentration and reaction rate) is the same within the reactor vessel, with no dependence on these variables. And so, these variables in the output current are modeled as being the same as those inside the reactor. This type of reactor offers a long residence time due to the large volume and has easy temperature control. However, the conversion of reactant to product by reactor volume is small. [33]

Packed bed reactor (PBR) is a cylinder shaped reactor, packed with solid catalyst particles, forming a submerged bed. Most reactors are vertical and allow reagents to flow by gravity. Normally this reactor operates at steady state and reagents are consumed as they flow along the reactor column, which is filled with a certain immobilized biocatalyst. The liquid passing through the reactor must flow evenly so as to be in contact with the entire immobilized biocatalyst. In these reactors, liquid flow and air pressure drop are generally high due to low flow. The pressure drop depends on the fluid velocity, the bed porosity, the shape and surface of the particles, as well as the relationship between the compacted bed height and the particle diameter. Already the porosity of the bed may be affected by the packing mode, the ratio of column to particle diameter, particle shape, particle size distribution, particle surface roughness and lastly by bed height. [29][30][31][34] This type of reactor has a high conversion rate by catalyst weight, and therefore higher production (thanks to greater contact between the reactant and the catalyst). However, temperature control is difficult.

Fluidized bed reactor (FBR) is a vertical cylindrical reactor with a certain packing material through which the fluid flows. Although the content is heterogeneous, the fluidized bed is analogous to CSTR, with uniform temperature distribution throughout the bed. In this reactor the fluid flow is high allowing to keep the particles suspended in the fluid stream and thus often the fluidized bed behaves like a liquid. The pressure drop here is low compared to a compacted bed reactor. [29][30][31] These reactors have the advantages of excellent temperature stability and uniformity, uniform production in batch processes due to the strong solid mixture and the large solid-liquid / gas exchange area due to the small size of solid grains. [35]

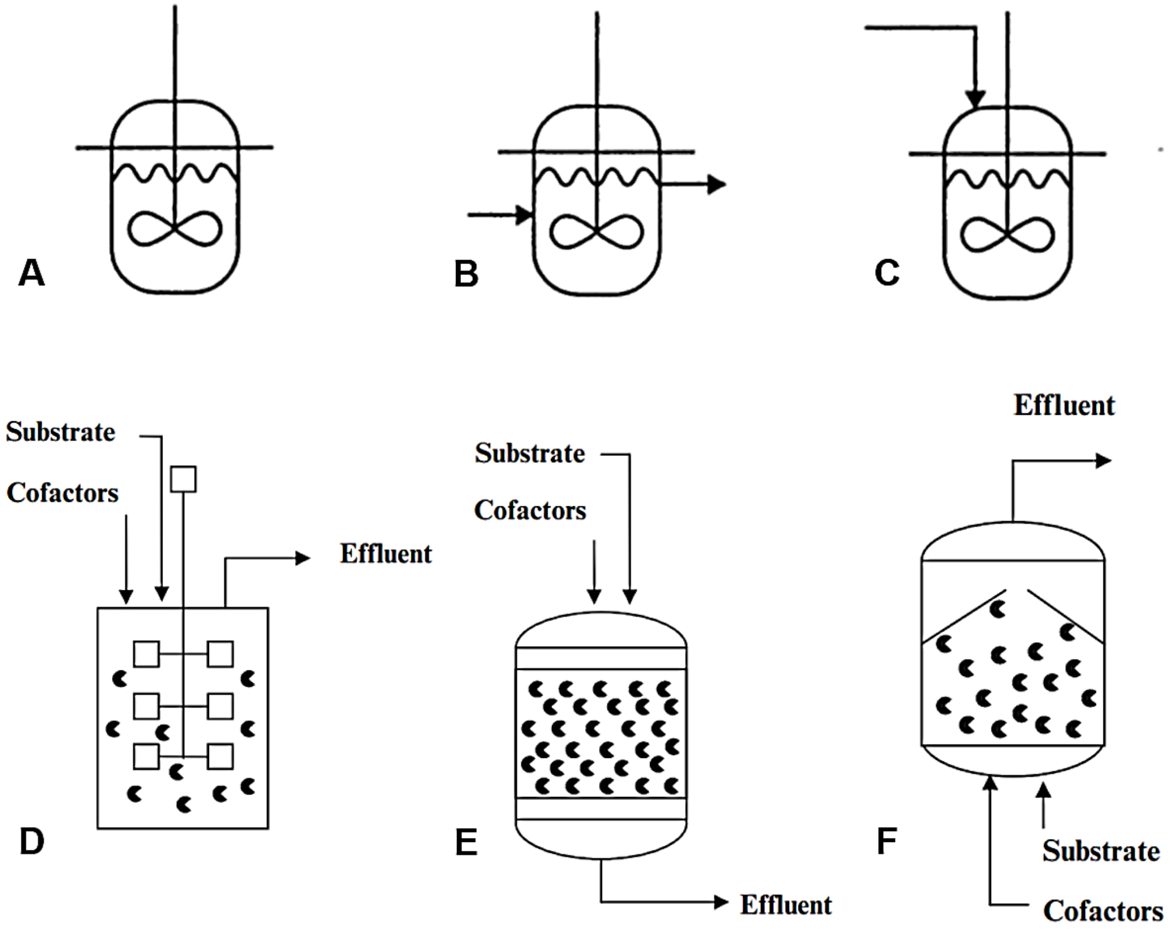

Figure 6. *Various modes of reactor operation:* ***(A)*** *Batch-mode,* ***(B)*** *Continuous- mode and* ***(C)*** *Fed-batch mode. Schematic diagrams of different configurations for developing reactions in continuous processes using immobilized enzymes:* ***(D)*** *stirred tank reactors,* ***(E)*** *packed bed reactor and* ***(F)*** *fluidized bed reactor.* [29][31]

1.7. Enzyme applications

In this section some of the enzyme applications will be discussed, focusing on the food, pharmaceutical and chemical industries as they are those where the use of enzymes is relatively well established. Alternatives will also be addressed, currently used to reduce costs and to make a greener industry.

1.7.1. The pharmaceutical industry

The pharmaceutical industry is one of the biggest industries nowadays, and a lot of financial resources are allocated to this industry due to the active research, development and industrial production of new drugs. About three hundred million euros are spent each year on the pharmaceutical industry into the development of new drugs in Portugal.[36] The pharmaceutical industry also produces large quantities of waste, which has led to the search for innovative solutions to decrease waste production and develop greener production strategies. [37] One possible solution would be to use enzymes. [38] Atorvastatin, which is used to lower blood cholesterol levels, is an example of the use of enzymes for production - halohydin dehalogenase. [39] Another example is Sitagliptin that is used for the treatment of diabetes - transaminase. [40] Boceprevir that is used to treat hepatitis C is another good example of enzyme use - transaminase. [41] The manufacture of small-molecule pharmaceuticals, also uses via biocatalysis, as with the 7-aminocephalosporanic acid molecule, which is the main chemical structure for antibiotic synthesis. [42]

1.7.2. The food industry

The food industry allows the processing of food of animal and plant origin before being consumed. One of the examples is the use of the enzyme carbohydrases (cellulases, amylases, invertases) which catalyzes the breakdown of carbohydrates into sugars (fructose, glucose and galactose). Many carbohydrates are used in order to sweeten the final product, however these have to first be broken down. [43][44] Another example is the use of proteases whose function is to hydrolyze peptide bonds of proteins for brewing or bread making purposes.[45] Other enzymes used in this industry are lipases, which are responsible for the breakdown of fatty acids and also for the production of sugar esters. [46][47][48] Oxidoredutases are also other enzymes used in industry, these are comprised for a vast group of oxidizing enzymes (peroxidases and catalase), which are used as preservatives in food. [49]

1.7.3. The chemical industry

Chemical synthesis of certain compounds can sometimes be hazardous due to high temperatures or the use of hazardous reagents, for example. With this in mind, the development of new enzyme-based techniques has led to safer and faster production of certain substances used in the chemical industry. Some examples where enzymes are currently used for their production are: glycolic acid, which was formerly produced by the reaction between formaldehyde and carbon monoxide, and the polyacrylamide that was once produced by combining copper with sulfuric acid at high temperatures and is now produced through the use of nitrile hydratase under mild conditions.[50][51][52]

1.8. Microtechnology

The need for miniaturization of all types of systems led to the development of microelectromechanical systems (MEMS). This field allowed the creation of devices in the range of 1-300 µm in size. It was established in 1980, but it was only in the 1990s, that the MEMS domain began to include biological, chemical and other scientific applications. The manipulation of the fluid flow in these applications, originated a new discipline, that we today know as microfluidic that can be defined as "(…) the study of flows that are simple or complex, mono- or multiphasic, which are circulating in artificial microsystems (…)", according to the literature. [53]

The main advantages of working in a microfluidic environment are: low sample / reagent consumption, fast analysis time, throughput screening of catalysts and process chemistries. In addition to these, it also enables the incorporation of sample preparation and purification elements. However, working in a microfluidic environment has some drawbacks, such as mixing, number of species present in very small volumes and surface effects.[14]

1.8.1. General concepts

1.8.1.1. Surface to Volume Ratio

In microfluidics it is essential to realize how some geometrical aspects change with the reduction of scale. Taking the geometry of a cylinder, the surface to volume ratio is (**Equation 4**):

$$\frac{Surface}{\mathrm{V\,olume}} = \frac{2\pi(\mathrm{r} \times \mathrm{h} + \mathrm{r}^2)}{\pi \mathrm{r}^2 \times \mathrm{h}} = 2\left(\frac{1}{r} + \frac{1}{h}\right) \qquad \text{(Equation 4)}$$

Where *r* is the radius and *h* the height of the cylinder. It can be seen that the surface to volume ratio will increase rapidly, allowing molecular absorption and surface phenomena such as capillary flow to be more efficient. In this way, the increase of this ratio in microfabricated structures can be exploited to increase the sensitivity of the detector, greatly increasing the interaction of a sensor element with a large sample.[54]

1.8.1.2. The Reynolds Numbers

Fluid flow is characterized by Reynolds Numbers (Re). The Reynolds Number is a dimensionless number used to quantify the relative importance of inertial and viscous forces within a fluid (**Equation 5**):

$$Re = \frac{inertial\, forces}{viscous\, forces} = \frac{\rho UL}{\mu} \quad \text{(Equation 5)}$$

Where *ρ* is the density, *U* the velocity of the fluid, *L* the characteristic dimension and *μ* the viscosity of the fluid. The Reynolds Number allows to evaluate whether the fluid flows in turbulent or laminar form. If the Reynolds number assumes values greater than 2000, this indicates that the flow is turbulent and if to assume values less than 1000, this indicates that the flow is laminar. The region between these boundaries is called the transition region. In the microfluidic laminar flow, indicating that the interactions between the wall of the microchannel and the fluid are strong, and that the fluids are increasingly influenced by viscosity and not by inertia. [14]

1.8.1.3. The Péclet Number

The microfluidic regime is characterized by a dimensionless number, Péclet Number (Pe_H). It describes the ratio between advective and diffusive transport in fluid flows (**Equation 6** and **Equation 7**):

$$Pe_H\,(mass) = \frac{advective}{diffusive} = \frac{UL}{D} \quad \text{(Equation 6)}$$

$$Pe_H\,(heat) = \frac{advective}{diffusive} = \frac{UL}{K} \quad \text{(Equation 7)}$$

Where *U* is the velocity of the fluid, *L* the characteristic dimension, *D* the diffusion coefficient and k the thermal diffusivity of the fluid. If the Péclet Number is greater than one it indicates that advective transport predominates, but if it is less than one it indicates that diffusion transport predominates. The Péclet Number occur in context of mass and heat. For example, in the context of heat transport, the Péclet Number corresponds to the rate with which heat is transported through a moving fluid relative to the heat transfer rate of the channel wall to the fluid flow. [14]

1.8.1.4. The Schmidt Number

Such as the Péclet Number is a dimensionless number that allows to perceive the transportation problems associated with the flow of fluids. But in this case, the Schmidt Number (Sc) qualitatively compares molecular diffusivity with momentum diffusivity (**Equation 8**):

$$Sc = \frac{viscous\ diffusion\ rate}{molecular\ (mass) diffusion\ rate} = \frac{v}{D} = \frac{\mu}{\rho D} \qquad \text{(Equation 8)}$$

Where *v* is the kinematic viscosity, *ρ* is the density, *μ* the viscosity of the fluid and *D* the diffusion coefficient of the species of interest through a particular solvent. If the Schmidt Number is greater than one it indicates that the viscous effects diffuse more rapidly than concentration effects exposing the concentration boundary layer to a linear velocity profile. [55]

1.8.1.5. The Damkhöler Number

Other dimensionless numbers can be defined, such as the Damkhöler Number (Da), which represents the ratio between the reaction flux and the mass transport flux (**Equation 9**):

$$Da = \frac{Reactiveflow}{Diffusive\ flow} \qquad \text{(Equation 9)}$$

If the Da Number is greater than one it indicates that the reaction rate is greater that the diffusion rate distribution (diffusion limited). On the other hand, if the Da Number is less than one it indicates that diffusion occurs much faster than the reaction (reaction limited). [56]

1.8.2. Microfabrication

In this section will be approached some techniques of microfabrication, namely technologies of photolithography and soft-lithography used on this work.

1.8.2.1. Photolithography

Photolithography is a procedure used for patterning substrate carried out in an extremely clean environment, because considering the standard size of airborne particles and the scales used in microfabrication it is possible to conclude that it is difficult to carry out the fabrication of a microfluidic system in a dusty environment. So the fabrication of a microfluidic system is typically carried out in a clean room.

Photolithography is based on the use of a photosensitive organic film, known as photoresist. The photoresist is dissolved in a solvent and puddled onto the substrate to be patterned. This pattern can be defined by direct laser writer (DWL) system or by a previously patterned mask. The coated substrate is then selectively exposed, typically by passing ultraviolet light - the spectral band between 300 and 450 nm (is the most used technology) through a photomask. A photomask can be made of glass (or quartz) substrate on which aluminum (or other UV-opaque film with similar propose) is usually deposited along with a photoresist to be further patterned using a DWL system. The final step is a removal the exposed (or unexposed) resist by a wet etching solvent (typically weak basic solutions and vary from resist to resist), in order to obtain the final features. These photolithographic masks may be reused many times to create reusable molds that contain the same features and are further used in soft-lithography fabrication. [53]

After finishing the mask, the next step is the fabrication the mold on a silicon substrate. The first step is to spin-coat photoresist on a silicon substrate, followed by a short baking step, to remove the solvent that did not evaporate totally during the spin-coat photoresist. For the exposure, the mask is placed on top of the coated substrate and this one is aligned with the mask. When the photoresist coated substrate is exposed at uniform UV light beam, occur chemical reactions in the photoresist, which will alter the solubility in certain solvents, transferring the mask pattern to the photoresist. The photoresist can be classed as positive or negative resists, depending on the solubility. A negative resist is one whose solubility in the developer decrease when it is exposed to UV light and therefore staying in the substrate (insoluble in solvent). Already in the positive resist, the solubility increases and so the zones exposed to the light become soluble and disappear. It is relevant that the photoresists used have a great disparity between the solubility constants of the exposed and unexposed portions, high resistance and high photosensitivity to some chemicals used in afterward steps of microfabrication. [53] The full fabrication of mold (including mask fabrication) is highlighted in **Figure 7. 1) and 2)**: [57]

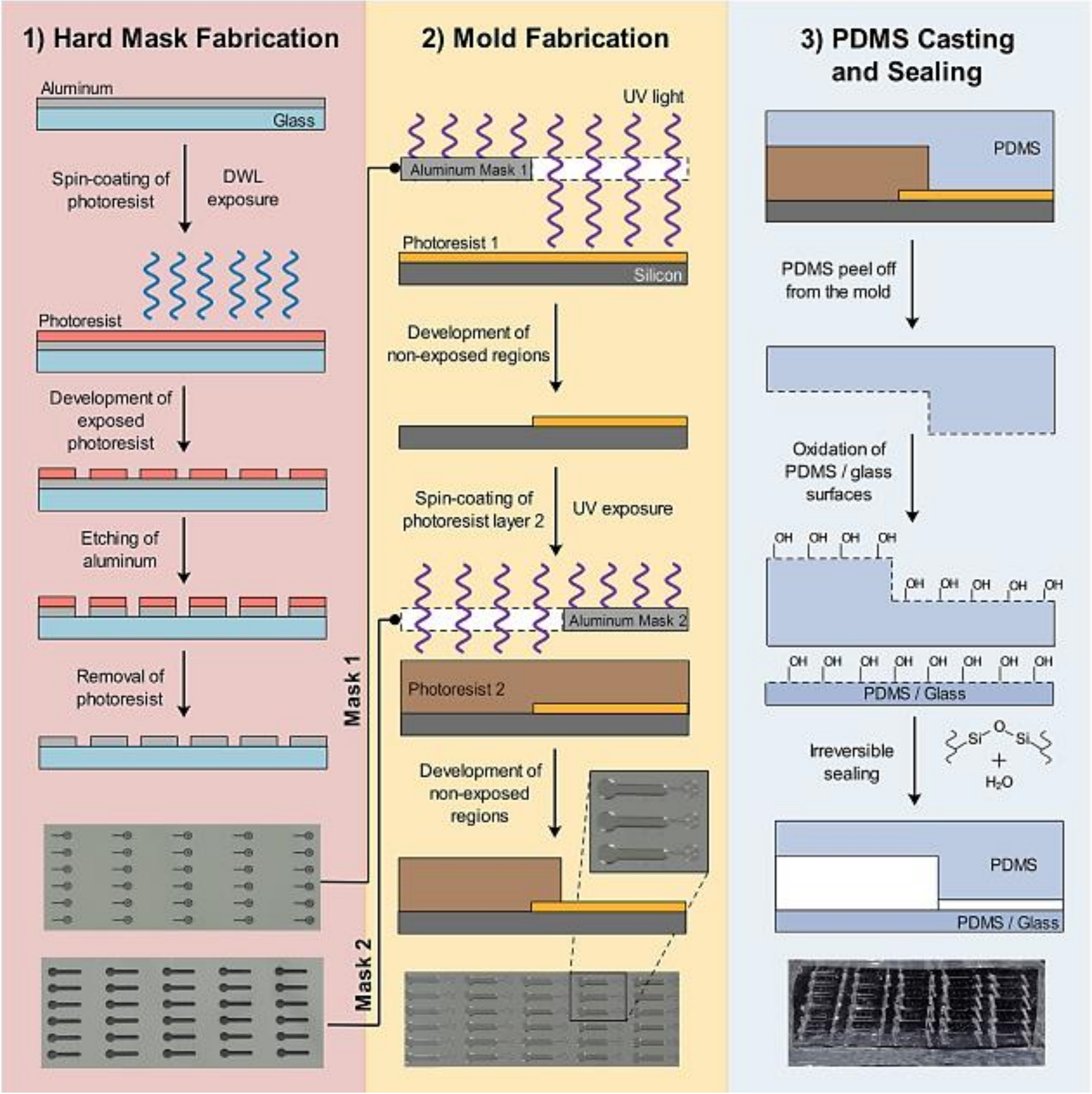
1) Hard Mask Fabrication
Aluminum
Glass
Spin-coating of photoresist
DWL exposure
Photoresist
Development of exposed photoresist
Etching of aluminum
Removal of photoresist
Mask 1
Mask 2
2) Mold Fabrication
UV light
Aluminum Mask 1
Photoresist 1
Silicon
Development of non-exposed regions
Spin-coating of photoresist layer 2
UV exposure
Aluminum Mask 2
Photoresist 2
Development of non-exposed regions
3) PDMS Casting and Sealing
PDMS
PDMS peel off from the mold
Oxidation of PDMS / glass surfaces
OH
PDMS / Glass
Irreversible sealing
Si O Si
+
H₂O
PDMS
PDMS / Glass

Figure 7. *Steps of fabrication of: 1) aluminum hard masks; 2) SU-8 negative photoresist mold; and 3) PDMS structures used for trapping beads. The photoresists 1 and 2 should be selected to allow the spin-coating of a thinner and thicker SU-8 layer, respectively.* [57]

1.8.2.2. Soft- Lithography

A soft-lithography is a non-photolithographic microfabrication technology, in that elastomeric stamp or mold is the key element that transfers the pattern to the substrate, using flexible organic molecules and materials. The PDMS (polydimethylsiloxane) have been the choice to create the structure features, due to great capacity for rapid prototyping and easy fabrication without expensive equipment. There is another types of polymers, like polystyrene, PVC (polyvinyl chloride), polycarbonate, however PDMS is one of the most used techniques. [58] [59]

PDMS belongs to a family of polymers that especially contain silicon oils and it is composed of polymeric chains constructed with repeating units of $-(CH_3)_2SiO_2-$. [60] When PDMS reaches a temperature higher than the polymerization temperature (around 70 ºC) and in the presence of a reticulating agent, it forms an elastomer. [53][61][62] PDMS has very advantageous properties, such as, biocompatibility, elasticity, optical transparency, gas permeability, low impermeable to water, chemical inertia, nontoxic, good thermal stability, low surface tension and ease of molding into (sub) micrometer features. [63][62] Also, untreated PDMS is hydrophobic, and becomes temporarily hydrophilic through treating the surface with plasma (oxidation of the surface by oxygen) and consequently forming self-assembled siloxane monolayers due at oxidation of methyl groups. [64] Oxidized PDMS adheres to silicon, glass or even PDMS itself, if the surfaces receive the same treatment. This treatment is called sealing and resulting in an irreversible sealing at room temperature. [62]

Since the PDMS forms an elastomer, it is possible patterning of channels into the PDMS surface by pouring it into a mold (hard material). Then the mold and PDMS are placed into the oven to be baked, and the PDMS polymerizes, becoming solid. In the end the PDMS structure is peeling off from the mold, obtaining a PDMS structure with microchannels like mold. But, to allow liquid flow in the channels it is necessary the sealing this structure against glass or a PDMS. The soft-lithography is highlighted in **Figure 7. 3)**.

After molding, the precision of PDMS structures is very good, reaching submicrometric values, between 5 and 500 μm (microchannel dimensions). Taking in account that occur unpredictable aging phenomena and that the PDMS have elastomeric properties. [53]

1.8.3. Instrumentation

1.8.3.1. Microsensors

Microsensors are used to measure and control physical properties. They can be electrochemical, thermal, magnetic sensors, among others. The electrochemical sensors are electrodes capable of detecting redox reactions in solution, through the oxidation and reduction of chemical species. This movement of charges is detected and measured by the electrodes. The electrochemical sensors are also able to measure impedance. The thermal sensors are used to evaluate the temperature variations. Finally, magnetic sensors consist of compounds made of magnetoresistive material that are sensitive to variations in the magnetic field. [65]

1.8.3.2. Microvalves

Microvalves are used to control gases or fluids and they consist of a flexible layer, above or below the channel of interest that is deformed in order to block the channel. Microvalves can be classified into passive and active valves. [65][66]

Active microvalves are controlled by an external parameter, that is the flow of a gas or a liquid, and this flow is controlled by the operator, and the microvalve behavior is almost independent of the flow direction. This type of microvalves demands an actuator that has to be powered from an external source. The active microvalves can be further divided into mechanical and non-mechanical. The active mechanical microvalves can be thermal, magnetic or a piezoelectric microactuator (**Figure 8**), for example. On the other hand, the active non-mechanical microvalves actuate due to changes occurring in the environment. [65][67]

The passive microvalves cannot be controlled by an external parameter and they depend on the direction of the through-flow. The passive microvalves can be further divided into mechanical and non-mechanical. The passive mechanical microvalves are flexible diaphragms or mechanical flap structures, for instance. Passive non-mechanical microvalves usually use surface properties in the microchannels to control the fluids inside, such as the hydrophobic microvalves. [67][66]

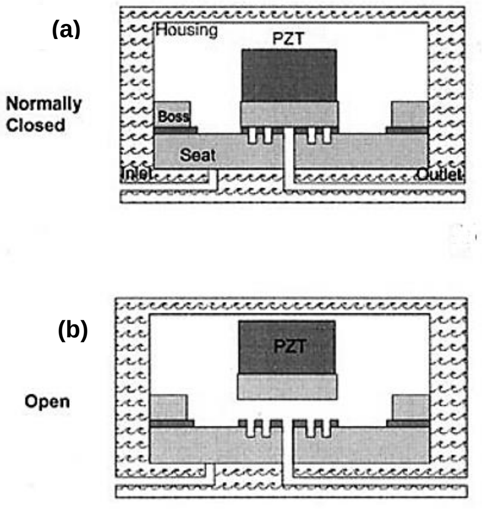

Figure 8: *Example of a piezoelectric actuated microvalve. (a) Microvalve closed; (b) Microvalve opened.* [68]

1.8.3.3. Micropumps

The micropump allows the pumping of the fluid along the microfluidic channels and it requires a microvalve unit for the one-way flow rate of the working fluid. Micropumps are also classified into the passive and active pumps. [69]

Active pumps need a physical actuator or a pumping mechanism. Examples of mechanical micropumps include piezoelectric, electrostatic, pneumatic (**Figure 9**) and electromagnetic micropumps. [70][66] Passive pumps don't need an external driving force or actuation, however they need to transform non-mechanical energy (electroosmotic, electrohydrodynamic, for example) into kinetic energy to drive the fluid through the microchannels. The passive micropumps can be further categorized as being chemical, electrical, magnetic and capillary micropumps. [70][66]

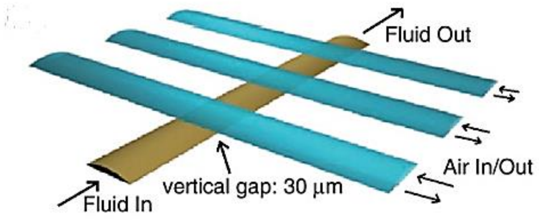

Figure 9. *A 3D scale diagram of pneumatic actuated valves in a peristaltic pump configuration. The channels are 100 μm wide and 10 μm high.* [66]

1.8.3.4. Heaters and Coolers

The majority of biotechnology applications require an optimal functioning of the enzymes, therefore a good temperature control is necessary. Due to this coolers or heaters are used, depending on the intended purpose. The heaters are composed of a resistance coupled with a thermocouple in order to measure and control the temperature of the system and the coolers are used to lower the temperature by using a second channel which is in contact with the channel of interest. In this second channel flows a colder liquid, allowing heat exchanges. [71][72]

1.9. Applications for Microfluidics

In this chapter microfluidics systems used for biotechnological applications will be discussed using examples found in the literature.

1.9.1. Screening Chip

The main goal of an enzymatic synthesis process is to have a high yield in the product of interest, whereby it is essential to optimize the reaction conditions, such as temperature, oxygen, pH, ionic strength and even the concentrations of the different constituents of the enzymatic reactions. [73]

Non-optimization of processes can lead to unnecessary waste of reagents and in this way makes an expensive process and with low productivity.

The use of microfluidics for screening allows for rapid analyzes using very small volumes, thereby reducing process costs. Unlike the lab-scale.

1.9.2. Microfluidic reactors

Some microfluidic devices serve as bioreactors or fermenters. And these two applications, besides allowing the synthesis of biomolecules of interest (such as the work done by Garza-García and co-workers that aimed at the synthesis of glycosylated pharmaceuticals [74]), as previously mentioned, also allow studies optimization of production conditions.

The use of miniaturized devices in biocatalysis is contributing to the evolution of processes in a more economical way. This is due to the great capacity of parallelization, allowing to evaluate at the same time a great variety of conditions, improving in this way the optimization of the process. The microfluidic reactors enjoy the aforementioned advantage, ruling out the necessity for elaborate scale-up procedures, which are not completely reproducible. In addition, microfluidic reactors have the advantage of high surface-to-volume ratio, ease of maintenance and high rates of heat and mass transfer. [75] This way the microfluidic reactors supply appropriate platforms for screening of biocatalytic activity.

An example is the work made by Boer and co-workers, in which using as model the protease cathepsin, integrated a chip-based microreactor with HPLC-electrospray ionization mass spectrometry (ESI-MS) and this way promoted the simultaneous detection of chemical and biological parameters. [76]

1.9.3. Immobilized Enzyme Microreactors

The immobilization promotes the control of the reaction by separation of the catalyst from the reaction solution and hence reducing contamination or inhibition, while improving the catalyst stability, durability and reusability. Moreover, the immobilization of enzymes provides a large interfacial area per unit volume and increase volumetric productivity. [75][77][78] Immobilization can be achieved by coating the wall of the microreactor, or by using a monolith structure or by packing the microchannels with small beads. [78]

There are several immobilization strategies at both the microscale and macroscale. Some of the microscale examples will then be presented below.

Filipe Carvalho and co-workers developed an immobilized enzyme microreactor that consisted in a microreactor with invertase covalently bound to silane-coated silica carriers, which was used for the hydrolysis of sucrose into invert sugar syrup. [79]

Another different microfluidic systems using immobilized enzymes was developed by Jones and co-workers using a chip type microreactor, made of PDMS, with the enzyme entrapped in the PDMS crosslinked matrix to hydrolyze of urea using urease as catalyzer. [80]

The work done by He and co-workers is also another example where they use immobilized enzymes, which consists of the immobilization of the glucose oxidase. This immobilization is made through the surface of the monolith coated with polyethylenimine with the goal to obtain D-gluconic acid from D-glucose. [81]

One of the objectives of my thesis is the development of a microfluidic reactor capable of producing L-DOPA with the enzyme of the reaction immobilized inside the microfluidic reactor, and porous micro beads are being considered as physical support for enzyme immobilization.

1.10. Objectives

Microfluidic systems are known to accelerate the development of bioprocesses, and in addition, it allows process optimization in a cost effective and rapid manner since it enables the use of small amounts of reagents in a very controlled form. Therefore this project aims to exploit the optimization chip for the production of biomolecules. In this way, the main objectives of the current project are the synthesis of L-DOPA and Dopamine individually using a microfluidic system with different configurations (i), the synthesis of dopamine from tyrosine substrate using the cascade reaction (ii) and the upscale of synthesis of L-DOPA (iii).

Chapter 2

2. Materials and Methods

This chapter will focus on the different methodologies used and developed for this project.

In the first part it will focus on the microfabrication techniques required to build the microfluidic structures for detection of the products and the microreactors used for production of products. In the second part of this chapter the setups used for the different types of experiments are explained as well as the protocols developed for enzymatic experiments, and consequently the protocols used for image analysis.

2.1. Microfluidic device fabrication

The fabrication of the microfluidic devices can be divided in several steps, namely hard mask fabrication, mold fabrication and the production of PDMS structures. These steps are explained below and the required equipment are listed in detail in **Table 2**.

Table 2. *Materials and equipment required for microfluidic device fabrication.*

Step of the Process	Reagents/ Materials	Equipments
Hard Mask Fabrication	- Acetone (99,6%), LabChem Inc. (Zelienople, PA/USA) - Deionized (DI) water - Alconox solution, Alconox Inc. (White Plains, NY/USA) - Isopropanol (IPA), (99,9%), LabChem Inc. (Zelienople, PA/USA) - Glass substrate, Corning Inc, (Corning, NY/USA) - Photoresist PFR 7790G, JSR (Sunnyvale, CA/USA) - Silicon wafer (150 mm diameter), University Wafer (South Boston, MA/USA) - TechniEtch A180 Aluminum etchant, Microchemicals (Ulm, DE)	- AutoCAD software (Autodesk Inc., Mill Valley, CA/USA) - Kerry Ultrasonic Cleaning Bath, Guyson (Skipton, North Yorkshire, UK) - Automatic Dicing SAW DAD-321, Disco Corporation, (Tokyo, JP) - Nordiko 7000 magnetron sputtering system, Nordiko Technical Services Ltd (Havant, Hampshire, UK) - SVG Resist coater and developer track, Silicon Valley Group Inc. (San Jose, CA/USA) - DWL lithograph, Heidelberg Instruments (Heidelberg, DE)

Mold Fabrication	- Silicon substrate, University Wafer (South Boston, MA/USA) - Alconox solution, Alconox Inc. (White Plains, NY/USA) - Acetone (99,6%), LabChem Inc. (Zelienople, PA/USA) - IPA, (99,9%), LabChem Inc. (Zelienople, PA/USA - SU-8 50 photoresist, Microchem Corp. (Newton, MA/USA) - SU8 2015 photoresist, Microchem Corp. (Newton, MA/USA) - AZ 40 XT photoresist, MicroChemicals Corp. (Ulm, Germany) - Propylene glycol ether acetate (PGMEA) (99,5%), SigmaAldrich (St. Louis, MO/USA) - AZ 400 K developer, MicroChemicals Corp. (Ulm, German) - DI water	- Vertical laminar airflow cabinet, FASTER-BSC-EN (Cornaredo, IT) - Spinner, Laurel Corp. - UVO cleaner 1444AX-220, Jelight Company, Inc. (Irvine, CA/USA) - Hotplate, Stuart (Stafforshine, UK) - UV light (254 nm, 400 W), UV Light Technology Limited (Birmingham, UK) - Stereo microscope, AmScope (Irvine, CA/USA) - Alpha-step 200 profilometer, Tencor Instruments
Fabrication of PDMS structures	- Sylgard 184 PDMS and curing agent, Dow Corning (Midland, MI/USA) - Micro slides 0.8 mm, Assistent (Sondheim, Germany) - Rounded syringes tips (20 and 18 Gauge), Instech Laboratories, Inc. (Plymouth Meeting, PA/USA)	- Analytical scale d=0.0001g, Scientech (Bradford, MA/USA) - Vacuum desiccator, Bel-Art Products (South Wayre, NJ/USA) - Spin coater, Laurel Corp. - Oven loading model 100-800, Memmert (Schwabach, DE) - Expanded oxygen plasma cleaner PDC-002-CE, Harrick Plasma (Ithaca, NY/USA)

2.1.1.Hard mask fabrication

First, the microfluidic structure was designed using Computer assisted design (CAD) software (AutoCAD) (**Figure 13. A**) and saved as dxf format for fabrication of the aluminum hard masks. The substrate used for mask fabrication was glass of 5x5 cm of Corning glass previously washed with isopropanol and deionized water and finally an immersion in an Alconox solution for 30 minutes at 65 °C. Then, the glass substrate was rinsed with DI water again, to remove the Alconox solution and remaining dirt, and blow dried with compressed air. Afterwards, a 200 nm aluminum layer was deposited over the clean substrate by magnetron sputtering using a Nordiko 7000 equipment. A 1.5 μm thick layer of positive photoresist (PFR 7790G) coating is done onto the recently deposited aluminum layer using a SVG resist coater. To achieve a 1.5 μm thickness, the substrate is spinned at 2000 rpm during 60 seconds. The CAD design is then transferred to a DWL laser direct write lithography system (diode laser: 405 nm, blue), where the pattern is photolithographically transfer to the photoresist. After exposure the substrate is transferred to the SVG track to perform the photoresist development, where a developer solution (TMA 238 WA) is poured onto the sample and left to react for 60 seconds, followed by a 15 second rinse with water and spinned for 30 seconds to dry. After the development step of the photoresist, since the photoresist is positive, the exposed regions of the aluminum layer will be removed by a wet chemical etching process with aluminum etchant. Once the etch is finished, confirmed through visual inspection in the microscope, the created pattern is revealed, as described in **Figure 10**.

All the microfabrication steps related with the mask fabrication were completed in class 100 cleanroom conditions (100 000 particles over 1 μm, per m^3) with exception of the photolithography step, which was performed in class 10 conditions (10 000 particles over 1 μm, per m^3).

In the present work, the required microfluidic structures needed two different channel heights, thus, two different aluminum hard masks were fabricated, as shown in the **Figure 13. L_1, L_2.**

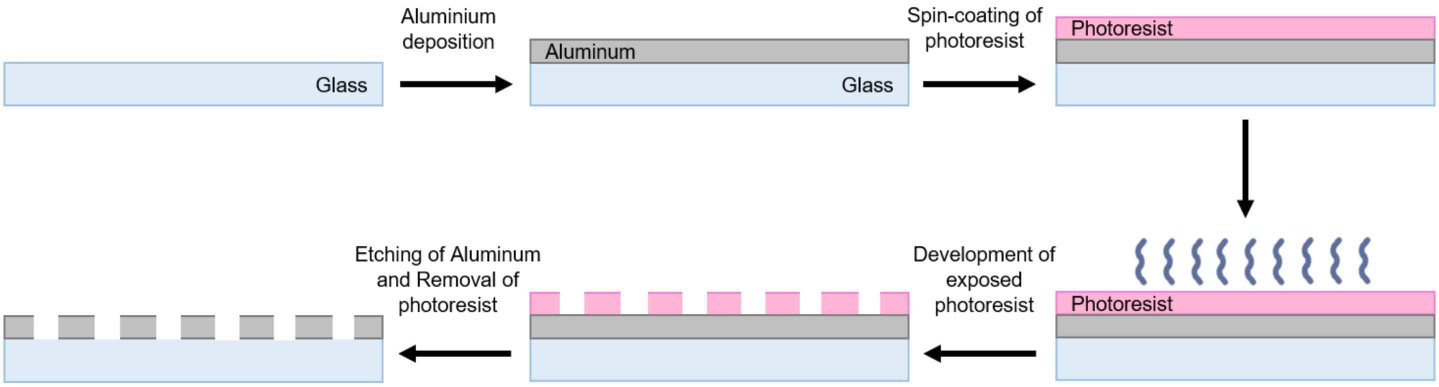
Glass
Aluminium deposition
Aluminum
Glass
Spin-coating of photoresist
Photoresist
Photoresist
Development of exposed photoresist
Etching of Aluminum and Removal of photoresist

Figure 10. *Sequence of steps involved in the fabrication of the aluminum hard masks.*

2.1.2. Mold fabrication

The two aluminum hard masks that were fabricated accordingly to the process described in **section 2.1.1** were then used to fabricate the two-layer master mold that allows the cast of PDMS microfluidic structures. The mold fabrication consisted in a set of stages of deposition and development of layers of different photoresists in order to create different heights, as described in **Figure 11**. In this work, molds with different layers heights were fabricated, 20 μm and 100 μm, which were based on previous work. [57] The mold fabrication is constituted for different steps, the silicon substrate cleaning, the spin-coating of 20 μm and 100 μm layer in height, and finally the hard bake.

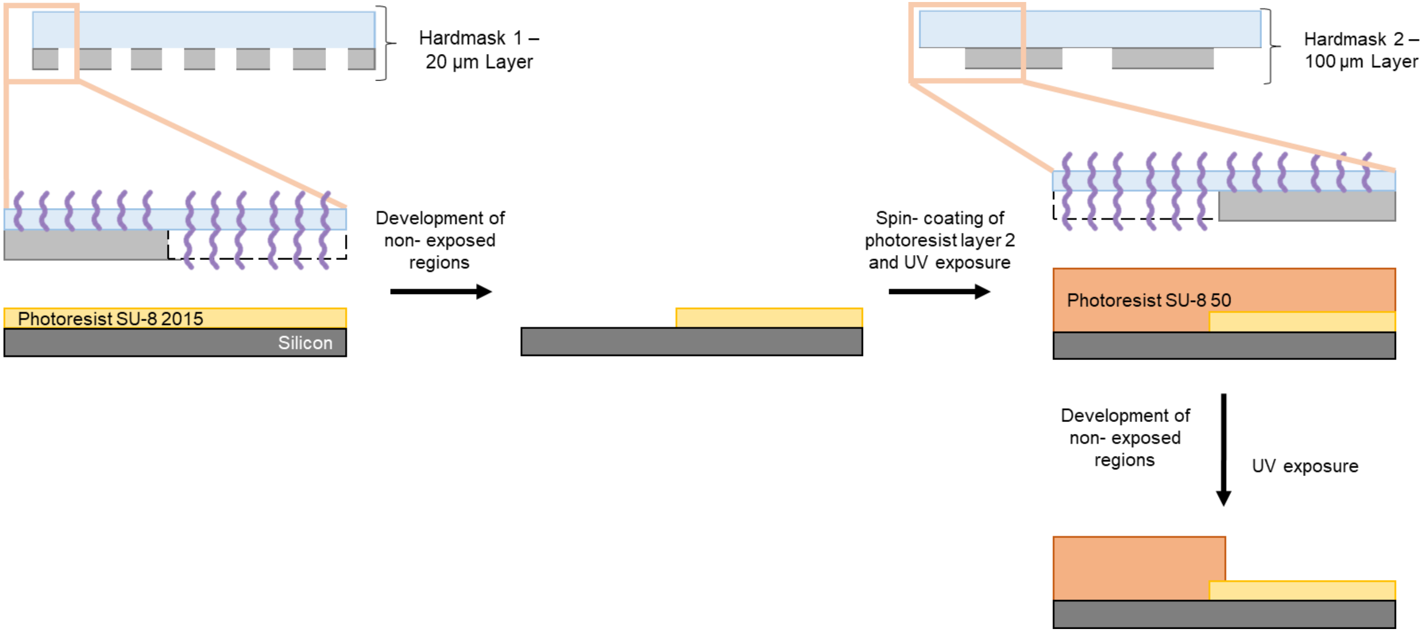
Hardmask 1 –
20 µm Layer
Hardmask 2 –
100 µm Layer
Development of
non- exposed
regions
Spin- coating of
photoresist layer 2
and UV exposure
Photoresist SU-8 2015
Silicon
Photoresist SU-8 50
Development of
non- exposed
regions
UV exposure

Figure 11. *Sequence of steps involved in the mold fabrication: 20 μm layer exposure, 20 μm layer development and 100 μm layer exposure, 100 μm layer development.*

a) Silicon substrate cleaning

To start the process, a silicon substrate 5×5 cm was cleaned by sequential rinsing, with acetone 99,6 %, isopropanol (IPA) and DI water, in order to remove any residues or other impurities on the surface,. After, this substrate was immersed in a heated AlconoxTM solution bath during 15 minutes at 65 °C, followed by cleaning with DI water and drying with compressed air.

b) 20 µm Layer

SU-8 2015 negative photoresist, was spin-coated on top of the substrate for 10 seconds at 500 rpm with an acceleration of 100 rpm/s, followed by a step of 34 seconds at 1700 rpm with an acceleration of 1300 rpm/s, originating a 20 µm thick layer. Then, a pre- exposure bake was done in a hot plate at 95 ºC during 4 minutes with a later step for cooling down of 1 minute. Afterwards, the hard mask with the 20 µm features was positioned over the recently deposited resist layer, carefully placing the aluminum surface facing down in order to prevent a loss in resolution due to scattering effects. The stack was exposed to UV light for 30 seconds, baked in hot plate at 95 ºC for 5 minutes and cooled for 2 minutes. After this, the substrate is ready for the development of the non-exposed photoresist, which consists in the immersion of the SU-8 in a PGMEA solution during 2 minutes with manual agitation. After the development, the substrate was cleaned with IPA followed by dried with compressed air. In **Figure 13. L$_2$** you can see the hard mask used for this process.

c) 100 μm Layer

SU-8 50 negative photoresist, was spin-coated on top of the substrate for 10 seconds at 500 rpm with an acceleration of 100 rpm/s, followed by a step of 30 seconds at 1000 rpm with an acceleration of 300 rpm/s, originating a 100 μm thick layer. The pre-exposure bake step in this stage included sequential baking by heating up to 65 ºC during 10 minutes, then further heating at 95 ºC for 30 minutes, and finally cooling down for 1 minute. The hard mask correspondent to the 100 μm design was positioned over the recently deposited resist layer, and manually aligned with the aluminum surface facing down. Afterwards, the stack was exposed to UV light during 70 seconds, and consequently baked in hot plate for 1 minute at 65°C, followed by 10 minutes of heating at 95 °C and, lastly, a step for cooling down for 2 minutes. Again, the photoresist layer was developed in PGMEA for about 10 minutes with manual agitation, washed with IPA, and dried. In **Figure 13. L_1** you can see the hard mask used for this process.

d) Hard Bake

Finally, the mold is hard baked at 150 ◦C for 45 min and left to slowly cool down on top of a hot plate until the temperature reaches 50 °C.

2.1.3. Fabrication of PDMS structures

The finished SU-8 molds were then used for the fabrication of the PDMS microchannels, as shown in **Figure 12**.

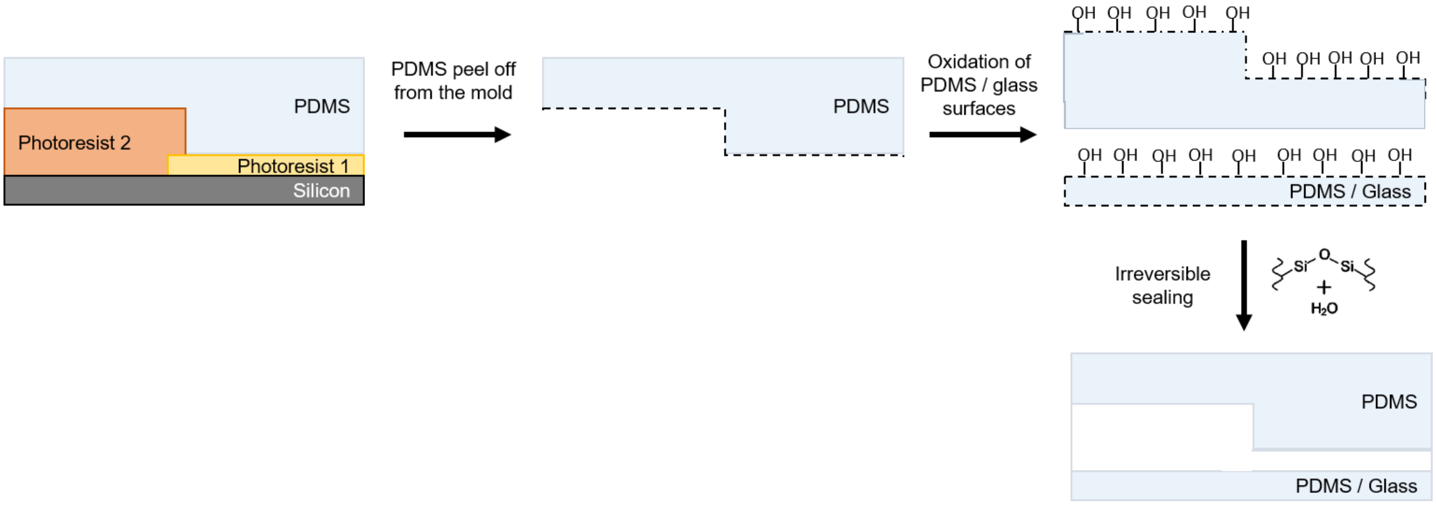
PDMS
Photoresist 2
Photoresist 1
Silicon
PDMS peel off from the mold
PDMS
Oxidation of PDMS / glass surfaces
OH OH OH OH OH
OH OH OH OH OH
OH OH OH OH OH OH OH OH OH
PDMS / Glass
Irreversible sealing
Si O Si
+
H_2O
PDMS
PDMS / Glass

Figure 12.*Sequence of steps involved in the fabrication of the PDMS structures.*

First, the fabricated mold was placed at the bottom of a petri dish with the patterned surface facing up and taped on each corner with Kapton tape. The PDMS elastomer was prepared in a plastic cup, using 10:1 weight ration of PDMS to curing agent, completely mixed originating a homogeneous solution, which was later degassed for 45 minutes. After this, the mixture was poured into the Petri dish that containing the mold, until it fills about half of the height of the Petri dish. The PDMS was left to cure for 90 minutes at 70 ◦C. The cured PDMS was afterwards cut with a scalpel and peeled off from the mold with appropriate tweezers. Then, the inlet and outlet holes were punched with a rounded 20 Gauge needle to allow the connection of the designed chambers to the outside, as you can see in **Figure 13. C**.

To seal the structures, it was prepared a 500 µm thick PDMS membrane. The membrane was produced by spin coating PDMS from the mixture previously prepared onto a silicon wafer at 250 rpm during 25 seconds with an acceleration of 100 rpm/s. Then, the membrane undergoes a baking step as described above and cut into pieces with a suitable size. Both structures were taken into an oxygen plasma cleaner for 1 minute with high intensity, in order to oxidize the contact surfaces to allow them to be irreversibly sealing against each other.

Surface treatment by oxygen plasma cleaner makes PDMS surfaces relatively hydrophilic and thus the final structures were stored for at least 24 hours before being used to allow PDMS to stabilize and regain its hydrophobicity.

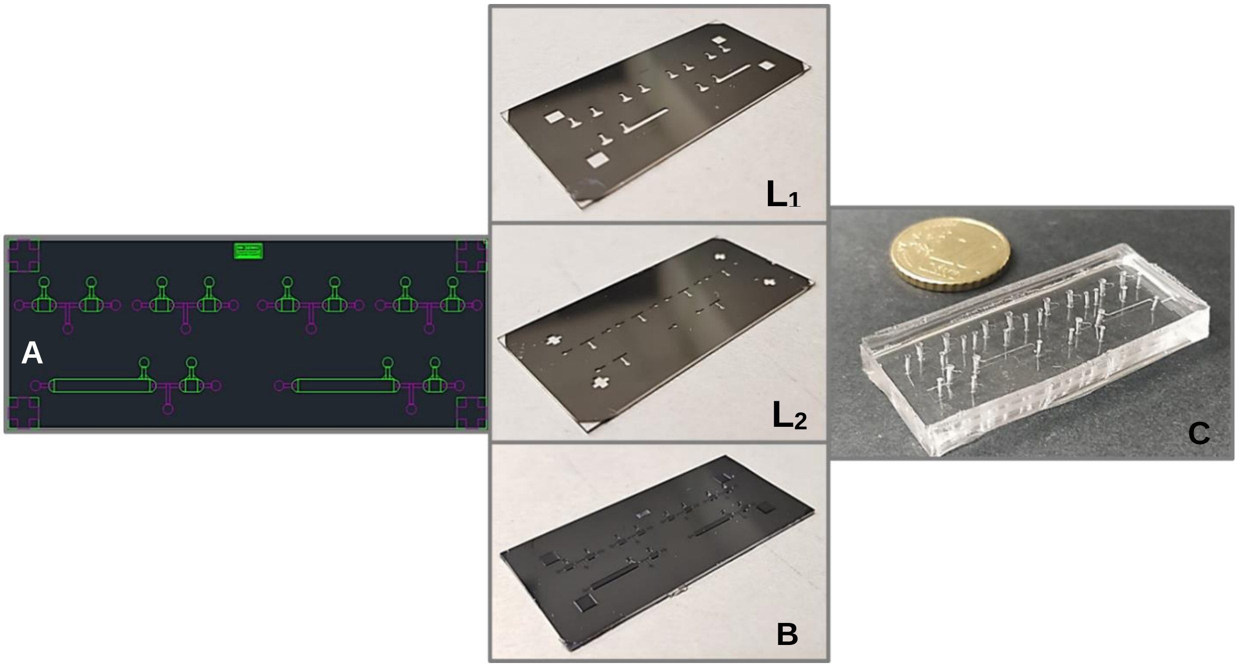

Figure 13. (**A**) Microfluidic structure designed using AutoCAD software with two layers: 20 µm (purple) and 100 µm (green); (**L1**) Hard Mask (aluminum) used to fabricate layer with 100 µm of height; (**L2**) Hard Mask used to fabricate layer with 20 µm of height; **(B)** Mold showing layers with different heights, 20 µm and 100 µm; **(C)** PDMS structure.

2.2. Enzymatic Experiments

The enzymatic synthesis performed at the microscale is divided into several steps: beads preparation protocol, packing method, enzyme Immobilization, product detection and production experiments. In **Table 3**, a list of the equipment, material and general reagents used throughout this experiments can be found.

Table 3. *Summary of the equipment, material and reagents needed for these experiments.*

Equipment	- CCD color camera XC30, Olympus (Shinjuku, Tokyo, JP) - Inverted Fluorescence Microscope CKX41, Olympus (Shinjuku, Tokyo, JP) - Fluorescence microscope (Leica DMLM), equipped with a DFC300FX camera - Syringe pump NE-1002X, New Era Pump Systems, Inc. (Farmingdale, NY/USA) - Hotplate, Stuart
Materials	- Syringe 1 mL U-100 Luer-Lock, Codan (Lensahn, DE) - Polyethylene tubing (BTPE-90), Instech Laboratories, Inc. (Plymouth Meeting, PA/USA) - Rounded syringes tips (20 Gauge), Instech Laboratories, Inc. (Plymouth Meeting, PA/USA) - PPA HyperCel (80-100 μm), HEA HyperCel (80-100 μm) and MEP HyperCel (80-100 μm), PALL - Spherical C18 bonded flash silica beads (45-75 μm), 97727-U Supelco Analytical (Bellefonte, PA) - CM Sepharose (90 μm), DEAE Sepharose (90 μm) and Q Sepharose (90 μm), GE Healthcare - Capto MMC (36–44 μm) and Capto Adhere (75 μm), GE Healthcare - Tubing adapters SC20/15, Instech Laboratories, Inc. (Plymouth Meeting, PA/USA)
Reagents	- Tyrosine, Sigma-Aldrich (USA) - Ascorbic Acid, Sigma-Aldrich (USA) - Levodopa (L-DOPA), Sigma-Aldrich (USA) - Dopamine, Sigma-Aldrich (USA) - Tyrosinase, Sigma-Aldrich (USA) - DOPA Decarboxylase, Antibodies online - Polyethylene glycol (PEG) 8000 MW, Sigma-Aldrich (USA) - Phosphate- Buffered Saline (PBS), Sigma-Aldrich (USA) - Milli-Q water 18 MΩ CM, Millipore

2.2.1. Beads preparation protocol

2.2.1.1. Detection (autofluorescence and detection)

Commercially available beads were supplied in an ethanol solution (20% v/v). For all beads used in this experiment – PPA / HEA / MEP HyperCel, Spherical C18, CM / DEAE / Q Sepharose, Capto MMC / Adhere, the first step was to homogenize the beads suspension and then transfer a certain volume of this suspension into a PEG 8000 20 % (w/w) solution in a proportion of 1:10 (1 being beads). PEG 20 %, being viscous, was used so that the beads remained dispersed throughout the solution, avoiding clogging of the channel with clumps of beads before an adequate packing was achieved.

2.2.1.2. Production (Enzyme Immobilization)

Through the process of silanization, silica beads become functionalized in-house with a primary amine, to electrostatically bind both the tyrosinase and DOPA-decarboxylase used. The silica beads were functionalized by exposing them to an oxygen plasma and incubating them in a solution of 2% (v/v) of (3-Aminopropyl) triethoxysilane (Sigma-Aldrich) in HPLC grade acetone, under constant mixing for 3h. The beads were than washed and stored using MilliQ-water. [82] Enzyme stock solutions were left overnight at room temperature with equal parts (v/v) of a suspension of the functionalized beads. Enzyme concentration per bead was determined by measuring the concentration of enzyme in the supernatant using the Bradford method and by weighing the dry mass of beads used.

2.2.2. Packing beads method

2.2.2.1. Detection (autofluorescence)

For these experiments, beads were packed, into the microfluidic structure, trough pulling. When is used a syringe pump on a pulling mode is applied a negative pressure at the outlet, through via capillary tubing pre-filled with PBS and connected to the microfluidic structure with a metal coupler inserted into the outlet. Already, into the inlet was inserted a pipette tip containing the bead suspension (section **2.2.1.1**.) and the packing was performed at a flow rate between 8 to 15 μL/min. The packing was always performed until all the column was packed, and no more beads could enter the column. After the packing step, the microfluidic structure was washed with 20 μL of PBS at a flow rate of 15 μL/min, to remove completely the PEG solution.

2.2.2.2. Detection (L-DOPA/Dopamine)

In this case, beads Q-Sepharose were packed through pulling mode. Where the bead suspension (prepared according to section **2.2.1.1**.), that is in pipette tip, enters the microfluidic structure by a negative pressure at the outlet, as explained above. The packing was performed at a flow rate of 7 μL/min and always performed until all the column was packed, and no more beads could enter the column. At that point the pipette tip that contained the packing solution would be removed and the column inlet was closed with a closed metallic adapter. After the packing step, the microfluidic structure was washed with 20 μL of PBS at a flow rate of 15 μL/min, to remove completely the PEG solution. In **Figure 14** is shown the schematics microbead used for detection.

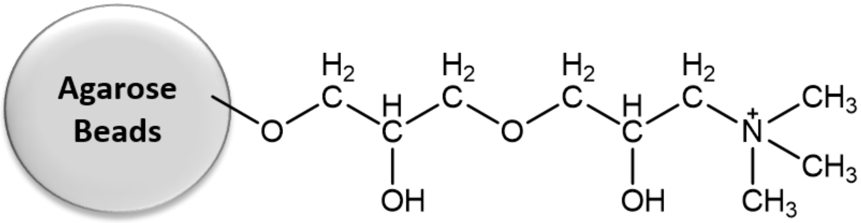

Figure 14. *Schematics of the nanoporous microbead used in this work for detection - Q Sepharose bead with strong ion exchange for ionic interactions. The matrix is agarose and these beads have a size of approximately 90 μm.*

2.2.2.3. Production (L-DOPA/Dopamine)

For production experiments, the tyrosinase – functionalized and DOPA – decarboxylase – functionalized beads (prepared according to section **2.2.1.2**.) were packed into the column through pulling mode, as explained above. The packing also performed at a flow rate of 7 μL/min, until all the column was packed. Then pipette tip that contained the packing solution is removed and the column inlet is sealed off with a closed metallic adapter. After the packing step, the microfluidic structure is not washed with PBS.

2.2.3. Bradford Method

Protein quantification analysis were performed according to the Bradford protein method. The process was performed according to the Instructions guide for a microplate procedure, provided by Coomassie (Bradford) Protein Assay Kit, from Thermo Scientific. [83] Two protocols were used depending on the working range. Through the standard microplate protocol (working range = 100-1500 µg/mL), were pipetted 5 μL of each unknown sample into the appropriate wells. Then 250 μL of the Coomassie Reagent was added to each well with agitation for 30 seconds. For the most consistent results the plate was incubated for 10 minutes at room temperature. The absorbance at 595 nm was then measured with a plate reader. Already through the micro microplate protocol (working range = 1-25 µg/mL), instead of 5 µL and 250 µL of unknown sample and the Coomassie Reagent as the previous protocol were pipetted 150 µL and 150 µL, respectively.

2.2.4. Product Detection

For these experiments, the microfluidic structure was packed with Q-Sepharose, as described in section **2.2.2.2**. The microfluidic structure used for detection is in the **Figure 15**.

L-DOPA detection is achieved thanks to the polymerization reaction that occurs when exposed to alkaline conditions, as described in the work of Hormozi-Nezhad and co-workers.[84] The addition of NaOH to L-DOPA leads to the formation of nanoparticles with fluorescent properties. These nanoparticles can be detected using an inverted fluorescence microscope coupled to a CCD color camera. For the L-DOPA detection, the sample under analysis was mixed with a 1 M solution of NaOH at a 1:4 ratio (1 being NaOH). The resulting mixture was then injected into a microfluidic column packed with Q-Sepharose beads and the fluorescence shift was measured using UV excitation ($\lambda_{excitation}$ = 365 nm, $\lambda_{emission}$ = 420 nm). The rate of fluorescence increase of pure L-DOPA solutions was monitored during 10 minutes (the images were captured every minute using specific acquisition conditions) and used as a calibration curve. This calibration curve was used to determine the amount of L-DOPA that came out of the reactor and the amount of L-DOPA that is consumed. The detection was always done with a flow rate of 1 µL/ min.

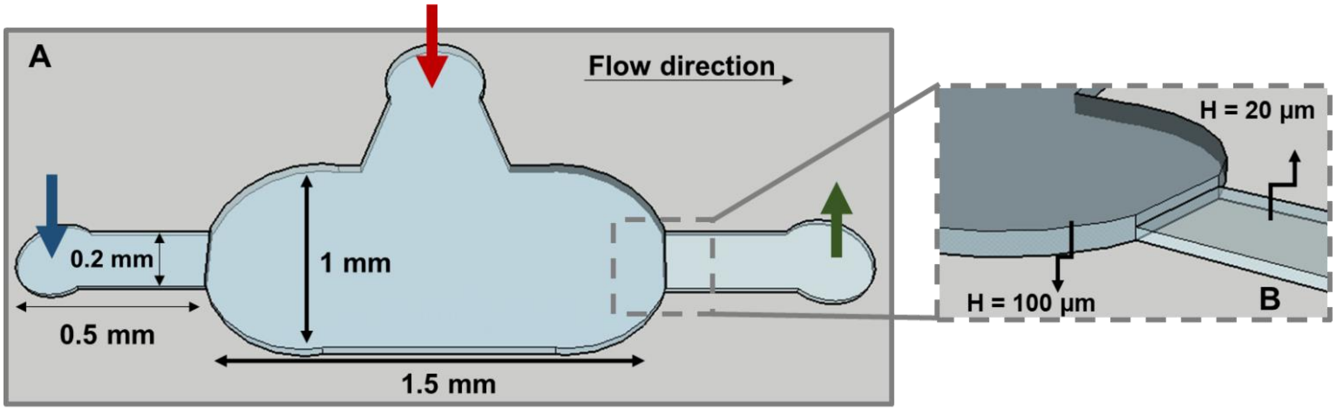

Figure 15. *Microfluidic structure used for product detection:* ***(A)*** *The Q-Sepharose beads are packed through the side inlet (Red arrow), which is then closed with a closed metallic adapter. The mixture between L-DOPA and NaOH (pipette tip) is then pulling (Blue arrow). The mixture solution was pulling through the column using the polyethylene tubing coupled to an open metallic adapter with an PBS syringe controlled by a syringe pump (Green Arrow), applying a negative pressure at the outlet and* ***(B)*** *Bead trapping feature used to trap the beads.*

2.2.5. Image Analysis

For the quantification of produced and consumed L-DOPA, the obtained micrographs were then analyzed using the ImageJ software from National Institutes of Health, USA. [85] These images were split into their 3 color channels, Red, Green and Blue. In the case of L-DOPA as the resulting fluorescent nanoparticles are not pure blue, they are cyan blue, only the green channel was considered. After converting the source image to green channel, it is considered an inner area of the channel and then an equal outer area (background), as shown in **Figure 16**. The value obtained from the outer area is subtracted from the value obtained from the inner area.

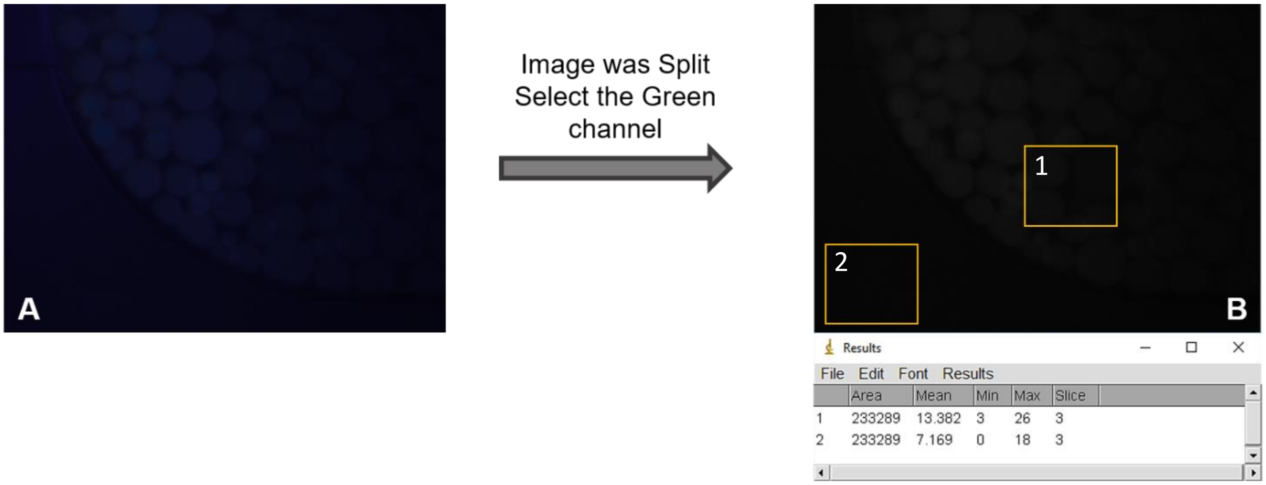

	Area	Mean	Min	Max	Slice
1	233289	13.382	3	26	3
2	233289	7.169	0	18	3

Figure 16. *Image Analysis:* ***(A)*** *Source image and* ***(B)*** *Conversion to a green channel, then the value obtained from the outer area is subtracted from the value obtained from the inner area.*

2.2.6. Production Experiments – Microscale

The microfluidic bioreactors were packed with the enzyme functionalized beads using a syringe pump on a pulling mode, as explained in section **2.2.2.3.** After packing, the microfluidic bioreactors were placed on top of a hotplate in order to ensure a working temperature of 32.5ºC throughout the experiments, while the reaction substrate was injected at the appropriate flowrate using a syringe pump on a pushing mode. The output of the microreactor was collected in intervals of at least 10 min in order to provide enough volume for both product detection (section **2.2.4.**) and enzyme content analysis. The optimization experiments focused on the aspect of flow rate (0.5 µL/min, 1 µL/min and 2 µL/min), concentration of ascorbic acid in the reaction medium (100 µM and 200 µM) and also reactor geometry. The step-up of production as shown in **Figure 17**. In this figure is possible to see two microreactors with different geometries used for optimization of production of L-DOPA, in **Figure 17.A** is represented the "Short Reactor", which has a volume of 0.13 μL and **Figure 17.B** is represented the "Long Reactor", which has a volume of 1 μL. Finally, in **Figure 17.C** is represented the microreactor used for cascade reaction, in order to produce L-DOPA and dopamine.

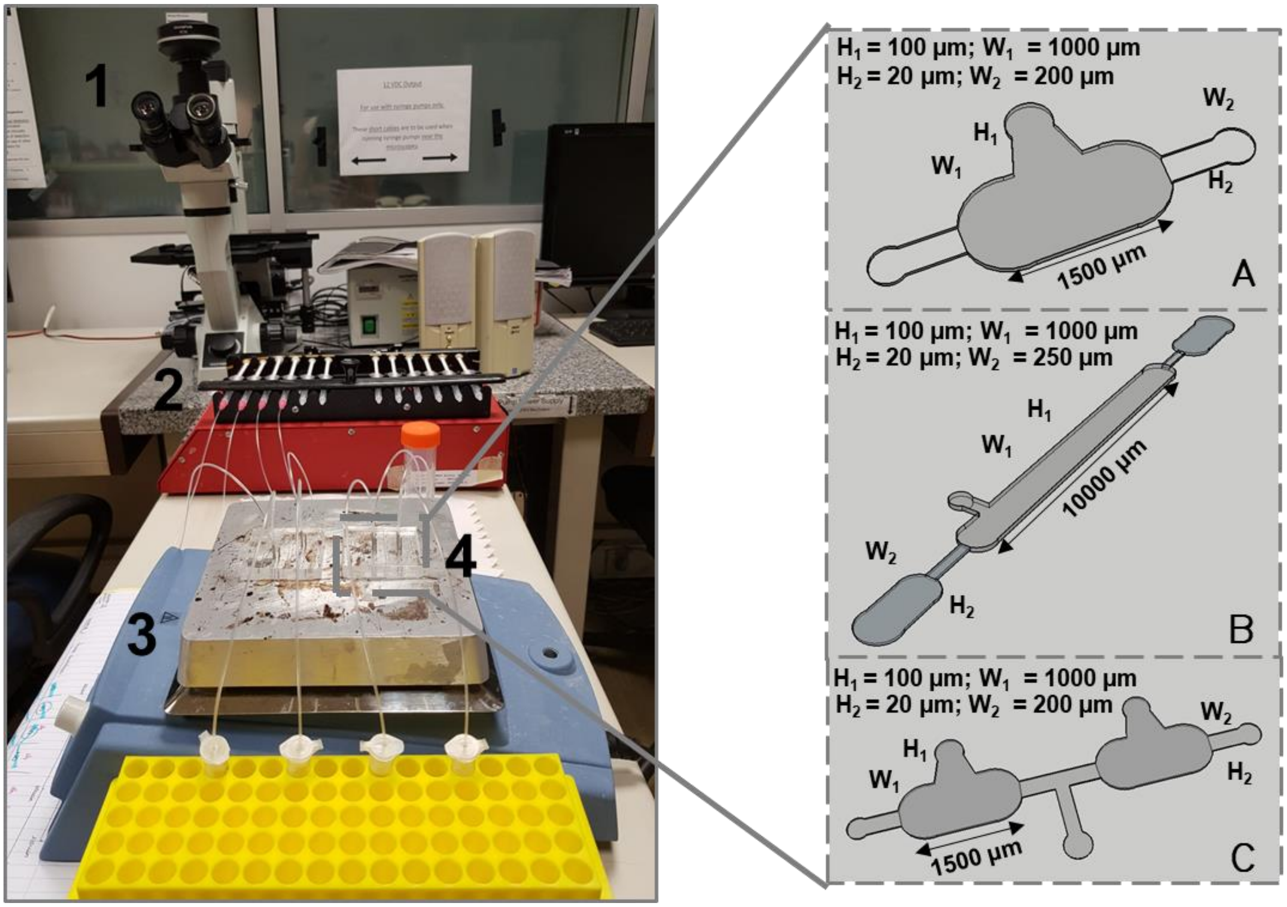
1
2
3
4
H_1 = 100 μm; W_1 = 1000 μm
H_2 = 20 μm; W_2 = 200 μm
H_1
W_1
W_2
H_2
1500 μm
A
H_1 = 100 μm; W_1 = 1000 μm
H_2 = 20 μm; W_2 = 250 μm
H_1
W_1
10000 μm
W_2
H_2
B
H_1 = 100 μm; W_1 = 1000 μm
H_2 = 20 μm; W_2 = 200 μm
W_2
H_1
W_1
H_2
1500 μm
C

Figure 17. *Step-up of microscale production experiments:* ***(1)*** *Inverted fluorescence microscope coupled to a CCD color camera;* ***(2)*** *Syringe Pump (Multi-channel) on a pulling mode;* ***(3)*** *Hotplate in temperature of 32.5ºC;* ***(4)*** *Microreactors (**A**, **B** and **C** – Different microreactors with different geometries used for production of L-DOPA and Dopamine), are not drawn to scale.*

2.2.7. Production Experiments - Macroscale

The macroscale version of the packed-bed reactor was a stainless steel pre-column typically used for HPLC with an inner diameter of 1 cm and a total length 2.5 cm (**Figure 18**). The column was connected to an AKTA pumping system to provide adequate pumping at the desired flowrate. Both the bioreactor and the reservoir for the reaction substrate were heated at 32˚C by immersion in a hot bath (VWR). Beads were packed manually into the columns and samples were collected at regular intervals for quantification of product output and free-enzyme.

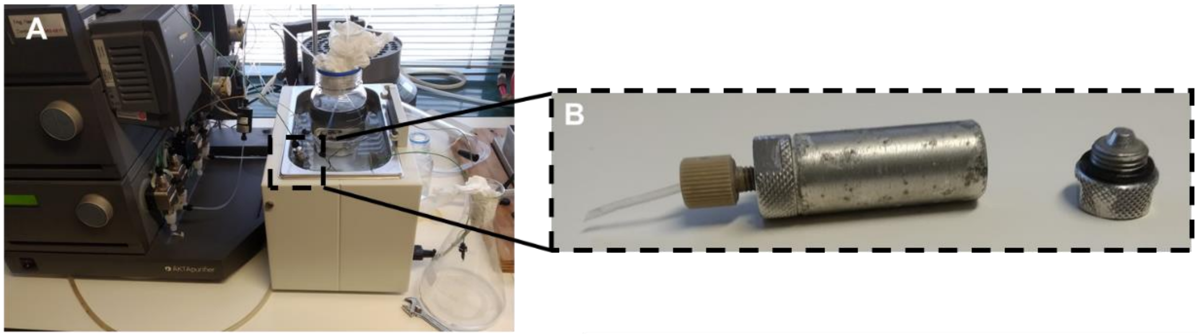

Figure 18. *Step-up of macroscale production experiments:* ***(A)*** *An AKTA system for pumping, a hot bath, substrate reservoir which is also in the bath and a collection flask and* ***(B)*** *The beads are packed into a stainless steel pre-column holder typically used for HPLC.*

2.2.8. Reverse phase High Performance Liquid Chromatography (rp-HPLC)

The production of dopamine was confirmed through rp-HPLC. It was performed using a similar method to C. Muzzi and co-workers. [86] Where the stationary phase is C18 and mobile phase is 6.9 g/L NaH_2PO_4; 800 mg/L EDTA; 250 mg/L Phenol-4-Sulfonic Acid (97%); Methanol (3%), pH 3.6; Q= 1.2mL/min. the detection was made in 280nm. Both L-DOPA and Dopamine standards were prepared with concentrations ranging from 100 μM to 1 μM in a potassium phosphate solution (pH= 2.5; 20 mM), which was also used as the mobile phase of the HPLC. The HPLC system was 20 μL, while the flowrate was 1 mL/min, resulting in an average retention time for L-DOPA of 3.18 minutes and 3.74 minutes for dopamine.

Chapter 3

3. Results and Discussion

This chapter focuses on the results obtained during the detection and production of L-DOPA and dopamine. As well as the upscale results of L-DOPA production. The results obtained in the production of dopamine individually, as well as through the cascade of reactions will also be presented.

3.1. L-DOPA detection method

3.1.1. Fluorescence Nanoparticles

Under alkaline conditions, L-DOPA is oxidized to its quinone derivative, which in turn is rapidly oxidized to dopachrome and spontaneously polymerized by covalent binding and aggregation, as described in work by Hormozi-Nezhad and co-workers.[84] The resulting polymers are nanoparticles, which due to their conjugated structures exhibit fluorescence properties, as seen in **Figure 19**. Therefore, the addition of NaOH to L-DOPA leads to the formation of fluorescent polylevodopa nanoparticles, which can be detected using a fluorescence microscope.

With this in mind, the idea will be to capture the nanoparticles with beads to be able to detect them under a microscope.

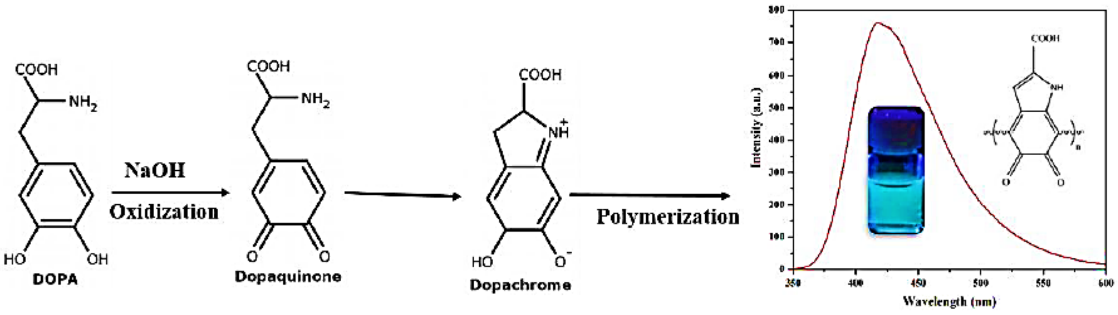
COOH
NH2
HO
OH
DOPA
NaOH
Oxidization
COOH
NH2
O
O
Dopaquinone
COOH
NH+
HO
O-
Dopachrome
Polymerization
800
700
600
500
400
300
200
100
0
Intensity (a.u.)
350
400
450
500
550
600
Wavelength (nm)
COOH
NH
O
O
n

Figure 19. Fluorescence spectrum. Resulting polymers exhibiting fluorescent properties. [84]

This section will show the results obtained to determine which beads can be used to capture L-DOPA. Once the ideal bead for detection is determined, this will be used for detection in future work. The results will also be shown which will allow to conclude in which ascorbic acid concentrations it is possible to work.

3.1.2. Autofluorescence

The first goal is to detect L-DOPA in order to monitor the reactor output. The approach used relies on the use of beads typically used in chromatographic processes. Therefore, the first step was to determine which beads you can use to capture L-DOPA, using a pre-existing column design available at INESC-MN. [57] These columns used were 1 cm long, had a width of 0.1 cm and a height of 100 µm, additionally they had a smaller channel with 200 µm of width and a height of 20 µm (**Figure 20. A** and **Figure 20. B**), designed to trap beads with diameters superior to 20 µm. So, different screen studies were done for different types of beads.

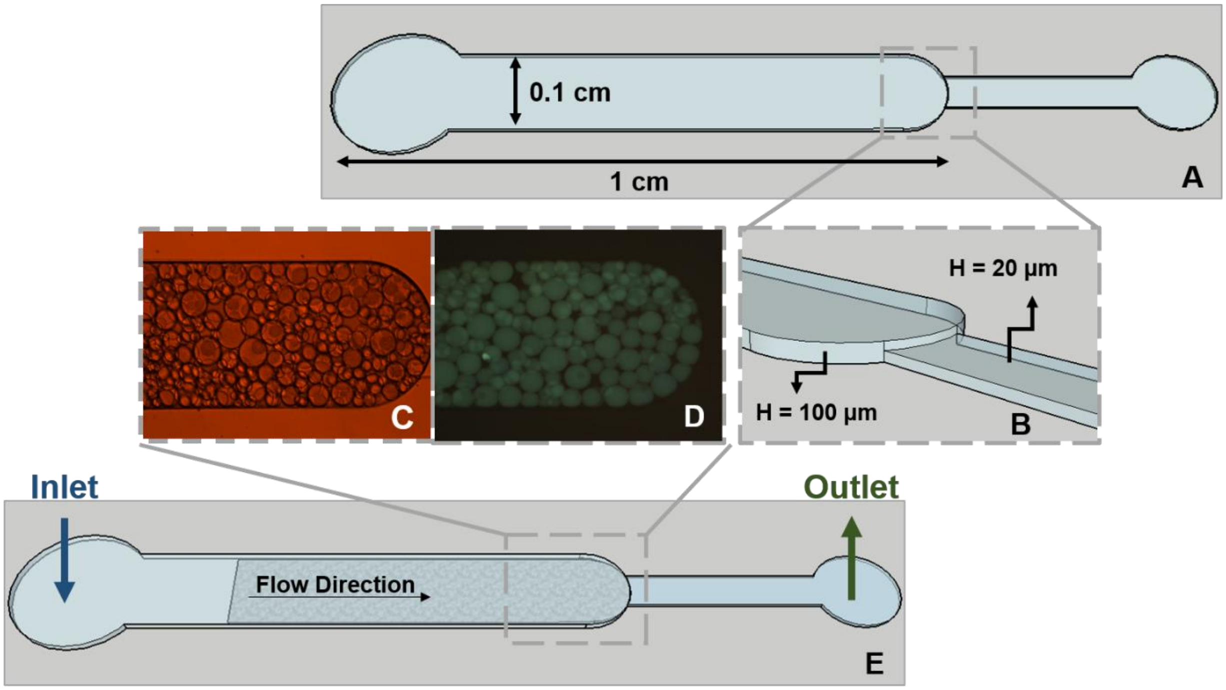

Figure 20. *Pre-existing column design available at INESC-MN:* ***(A)*** *Schematics of the columns used for the screen experiments and dimensions;* ***(B)*** *Bead trapping feature used to trap the beads;* ***(C)*** *Packed column (brightfield);* ***(D)*** *Packed column (UV filter);* ***(E)*** *Detail of an only column showing the inlet (pipette tip with containing the bead suspension - blue arrow) and outlet (metal adapter - green arrow) through which the liquid was flowed by applying a negative pressure at the outlet. The accumulated negative pressure would then force the packing solution to enter the column through the column inlet.*

In **Table 4** shows the beads with different sizes and functionalizations used in this step. In this table, for anion exchanger and cation exchanger, respectively, it means that the bead is positively and negatively charged to the surface due to their specific ligands.

The ideal beads are those that don’t have autofluorescence (because we want to detect L-DOPA through fluorescence) and those that can interact with L-DOPA.

Table 4. *Different types of beads and their interactions used in this project for to determine which beads can be used to capture L-DOPA.* [87]

Beads	Average Size	Ion Exchanger	Ligands	Interactions
Capto Adhere	~75 μm	Strong Anion	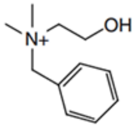	Ionic interaction, hydrogen bonding and hydrophobic interaction
Capto MMC	~36 - 44 μm	Weak Cation	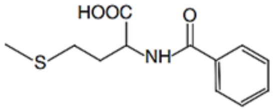	
CM - Sepharose	~90 μm		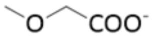	Ionic interaction and hydrophobic interaction
DEAE - Sepharose		Weak Anion	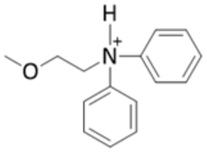	
Q - Sepharose		Strong Anion	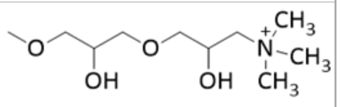	
PPA HyperCel	~80 – 100 μm	Anion	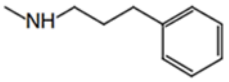	Hydrophobic interaction and ionic interaction
HEA HyperCel		Anion	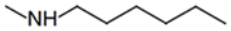	
MEP HyperCel		Anion	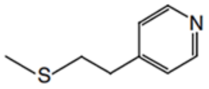	Hydrophobic Interaction, affinity interaction and ionic interaction
Silica	~45 – 75 μm	---	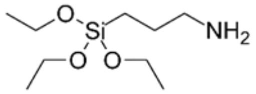	Hydrophilic interaction

Therefore, the beads referred to in table 4 were prepared according to the protocol in section **2.2.1.1.** and the screening studies were performed where the column was packed. The packing solution containing beads was pulled through the column as described in section **2.2.2.1**, as shown in **Figure 20. E**. Then, images for different types of beads with an exposure time of 2*s* and a 2x gain were captured (**Figure 20.D**), thus enabling to see which beads had not autofluorescence.

In **Figure 21** some captured images can be observed. With the images captured it was possible to conclude which beads to exclude to continue the screen study. The beads chosen to continue the study were DEAE Sepharose (**Figure 21.B**), Q – Sepharose (**Figure 21.D**), HEA HyperCel (**Figure 21.F**), CM –Sepharose (**Figure 21.E**) and Silica (**Figure 21. H**). These beads were chosen because they displayed very low values of autofluorescence.

The previously selected beads - DEAE Sepharose, Q – Sepharose, HEA HyperCel, CM – Sepharose and Silica, were then subjected to a new screening study, which consisted of check the capture efficiency of each microbead by flowing a known solution of the L-DOPA nanoparticles (100 μM) against the beads. The results obtained are shown in **Figure 22**. Where it can be seen that the Silica and CM-Sepharose beads do not fluoresce when a pure 100 μM L-DOPA solution was passed for 10 minutes. Concluding that these beads are not able to capture L-DOPA nanoparticles.

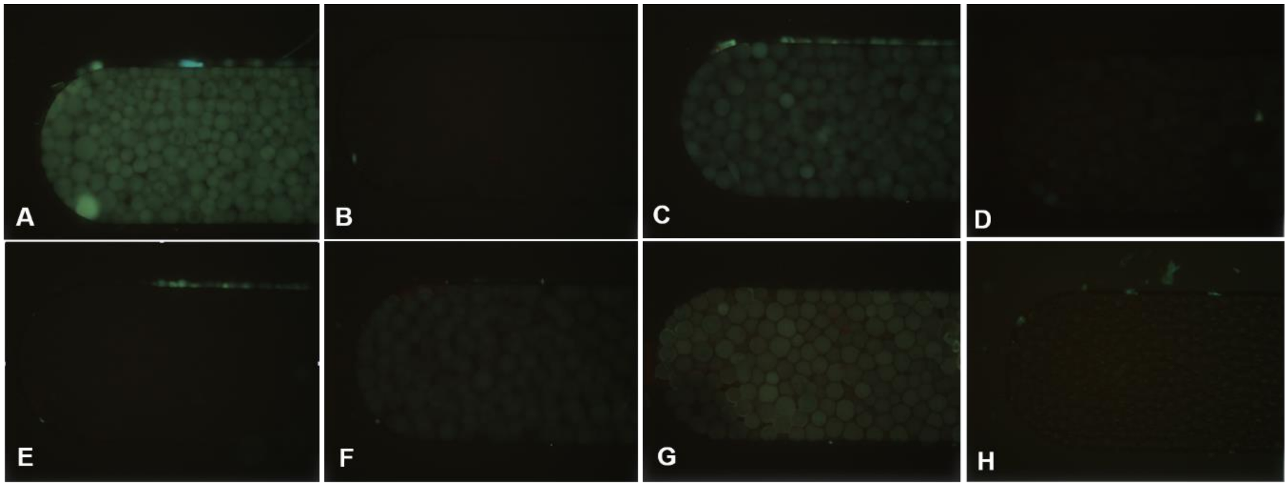

Figure 21. *Autofluorescence:* ***(A)*** *Capto Adhere;* ***(B)*** *DEAE- Sepharose;* ***(C)*** *PPA;* ***(D)*** *Q – Sepharose;* ***(E)*** *CM – Sepharose;* ***(F)*** *HEA HyperCel;* ***(G)*** *MEP HyperCel and* ***(H)*** *Silica. The conditions of acquisition using Leica DMLM Microscope were exposure time of 2s and gain of 2x. Objective lens: 10x.*

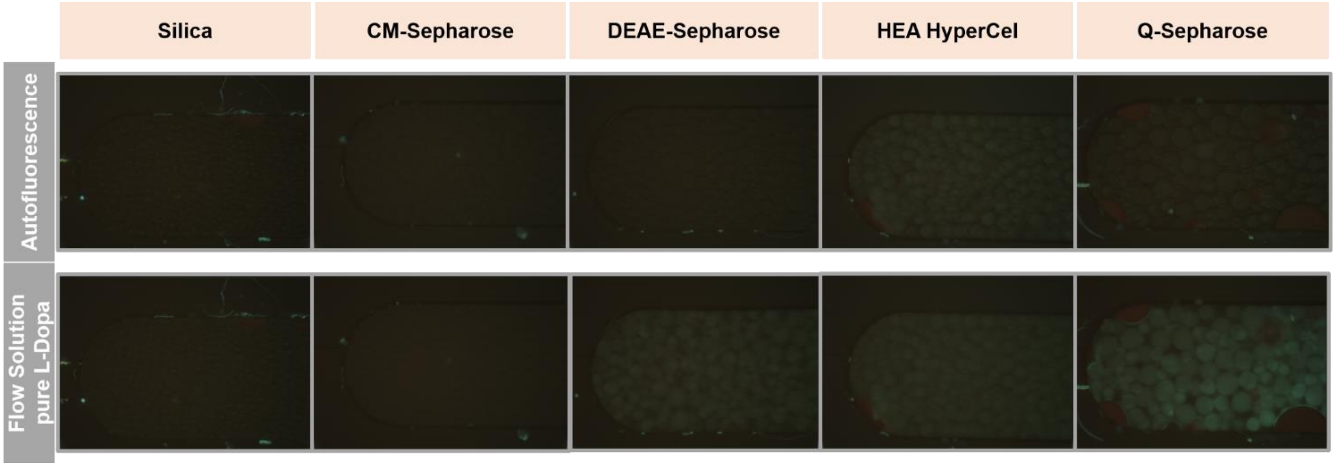

Figure 22. *Detection of L-DOPA. 5 beads were used for this studies: Silica, CM Sepharose, DEAE-Sepharose, HEA HyperCel and Q-Sepharose. First was study the autofluorescence of beads and then was flowed one solution of pure L-DOPA at 100 μM to know if any beads capture the fluorescence nanoparticles of L-DOPA. Using [NaOH]* $_{reaction\ medium}$ *= 0.2 M. The conditions of acquisition using Leica DMLM Microscope were exposure time of 2s and gain of 2x. Objective lens: 10x.*

3.1.3. With PEG vs without PEG

After knowing which beads to use in order to detect L-DOPA, the screen studies were done using the microfluidic structure shown in **Figure 20.A**. for two different methods, Method A and Method B, which, respectively, correspond to no washing or washing the columns with PBS after the column is packed with the beads (section **2.2.2.1**).

A pure solution of L-DOPA at 100 μM was flow into the column following the packing with beads (**section 2.2.1.1**) using both methods. From **Figure 23** it is possible to see that Method A and Method B have different behaviors.

In Method A, where there was no column washing, the signal was found to decrease over time. Perhaps because the PEG binds electrostatically to the beads and shields the charges that would grab the L-DOPA. On the other hand, Method B (where column washing occurs with PBS), is in accordance with the supposed, increased fluorescence over time. Because as the fluorescent nanoparticles get into the column, they become clinging to the beads. So the correct method is to wash the column after packing the beads to remove the PEG, as described in section **2.2.2.1** and **2.2.2.2**.

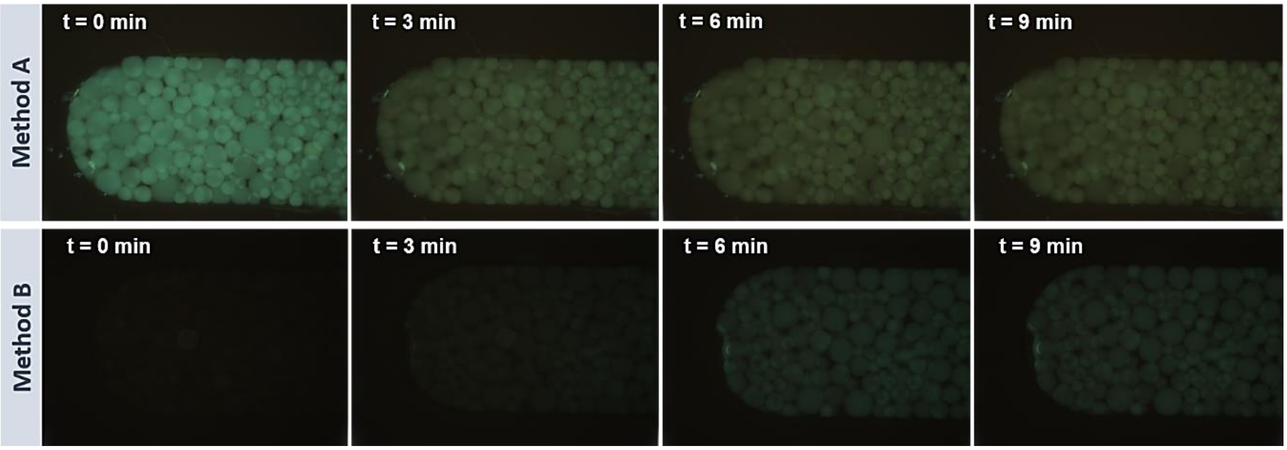

Figure 23. *Detection of L-DOPA at 100 μM using two methods:* ***Method A*** *- Without washing the columns with PBS and* ***Method B*** *– With washing the columns with PBS. Images captured for 0, 3, 6 and 9 minutes for a pure solution of L-DOPA at 100 μM flow of 1 μL/min using Q-Sepharose beads. Using* $[NaOH]_{reaction\ medium}$ *= 0.2 M. The time 0 min corresponds to the beginning of the entry of the mixture solution (L-DOPA + NaOH). The conditions of acquisition using Leica DMLM Microscope were exposure time of 2s and gain of 2x. Objective lens: 10x.*

Now knowing the correct method - Method B, screen studies were done to check which of the beads previously selected (HEA Hypercel, Q and DEAE Sepharose) have the highest fluorescence, when the pure solution of L-DOPA at 100 μM is passed in the column. This way, the beads were prepared and packaged, according to sections **2.2.1.1.** and **2.2.2.1.**, respectively. Based on **Figure 24.A** it can be verified that the beads that promote the largest signal, are Q-Sepharose beads.

T**able 4** shows that the three beads mentioned above, besides being anionic exchanger, have the same interactions. What distinguishes them is the fact that Q-Sepharose beads are a strong anionic exchanger. Which is somehow related to that observed in **Figure 24. A**. Because although all beads are anionic exchanger, that is, the bead is positively charged on the surface, the Q-Sepharose beads being a strong anionic exchanger, this indicates that these beads are strong positively charged on the surface, and therefore interact more with L-DOPA fluorescent nanoparticles and consequently show the greatest intensity of fluorescence. Thus, it is believed that the resulting fluorescent nanoparticles are negatively charged. HEA Hypercel beads, through the image is possible to see that the beads initially interact with L-DOPA. But over time the beads are not able to capture the product.

Concluding that Q-Sepharose beads exhibit higher fluorescence, this means that these beads better capture the fluorescent nanoparticles formed. Therefore the Q-Sepharose beads were the only beads selected to continue the screen studies. Knowing that the ideal beads for detecting L-DOPA are Q-Sepharose, so all future work has been done with these beads. Fluorescence emission curves were plotted over time for increasing concentrations of pure L- DOPA (0-100 μM). As can be seen in **Figure 24.B,** where fluorescence intensity in addition to increasing as L-DOPA concentration increases, it increases over time of residence in the column.

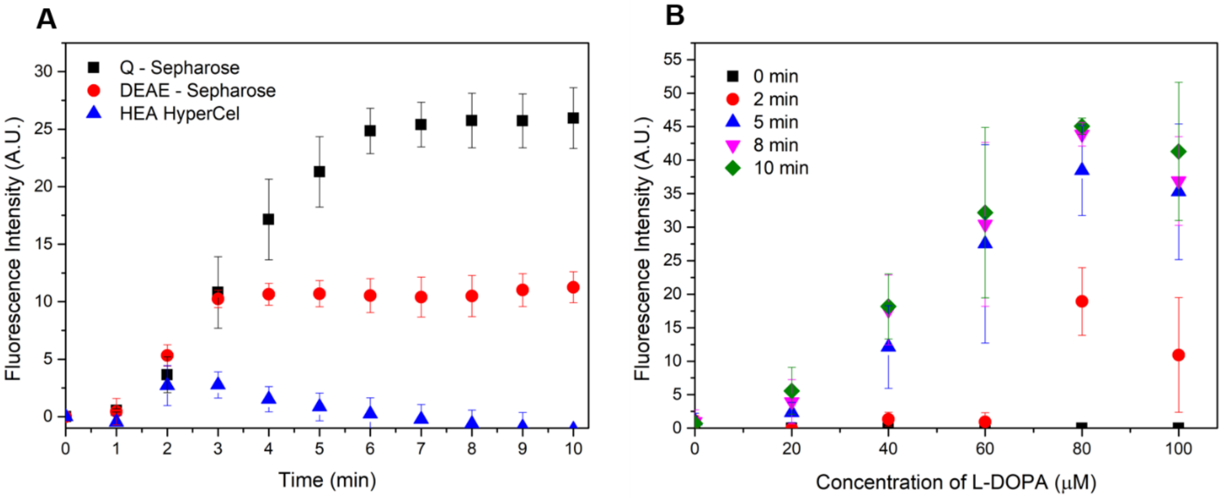

Figure 24. *Screen studies:* ***(A)*** *The fluorescence increase over time for different types of beads: HEA beads Hypercel, Q and DEAE Sepharose when the mixture solution (pure L-DOPA at 100 μM and NaOH) is passed in the column; and* ***(B)*** *The fluorescence increase over time for increasing concentrations of pure L- DOPA, using Q-Sepharose beads. [NaOH] reaction medium = 0.2 M. The measurements were performed at a flow rate of 1 μL/min. The conditions of acquisition using Leica DMLM Microscope were exposure time of 2s and gain of 2x. n=2*

3.1.4. Reducing agent optimization

For the production of L-DOPA, it is possible to use the enzyme tyrosinase and L-tyrosine as a substrate. However, tyrosinase participates in several oxidation reactions up until the production of melanin. In order to avoid further oxidation of L-DOPA there is a need to add a reducing agent to the reaction medium. [10] The reducing agent of choice for this work was ascorbic acid as it does not produce a toxic by-product and does not interfere with the enzymatic activity of the DOPA-decarboxylase needed for the second step of the reaction. Therefore, in the presence of ascorbic acid the dopaquinone is reduced to L-DOPA while ascorbic acid is oxidized to dehydroascorbic acid (**Figure 25**).

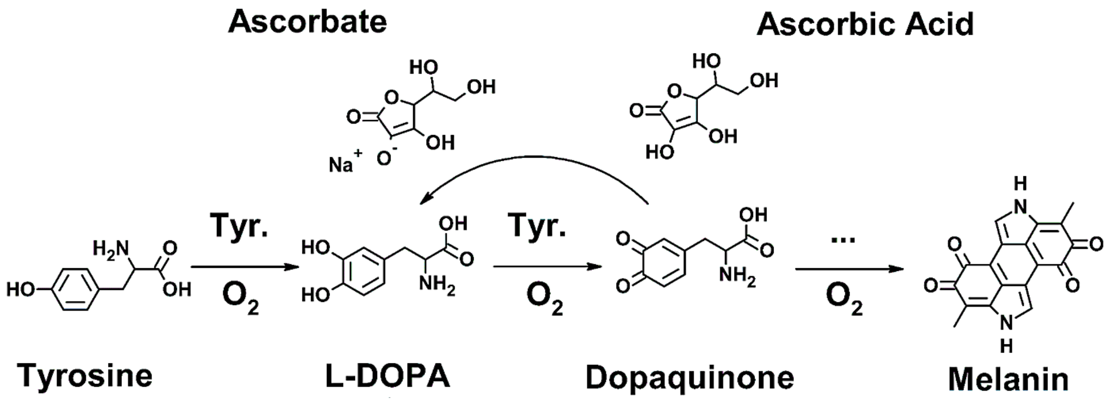

Figure 25. *L-DOPA reaction pathway using L- tyrosine as a substrate. Tyrosinase plays a part in several of the reactions that take place, which eventually culminate with the production of melanin. Ascorbic acid is added to the reaction as the reducing agent of choice, to prevent the further oxidation of L-DOPA. Adapted from E.J.S. Brás and co-workers, in peer review.*

Thus, different amounts of ascorbic acid were tested for the same concentration of pure L-DOPA at 100 μM, in order to check for possible interferences, as it is a possible contaminant during the production experiments. Thus it was determined what the range of ascorbic acid concentrations where it is possible to work that is the range where it is possible to see fluorescence. With this in mind, the microfluidic structure of **Figure 20. A** was packed with Q-Sepharose beads according to section **2.2.2.1.** and then several screening studies were done. Where the mixture solution consists of pure solution of L-DOPA at 100 μM, ascorbic acid with a certain concentration (0 μM – 2 mM) and finally NaOH, was flowed into the column packed, as described in **Figure 20.E**.

The results are shown in **Figure 26**, where it can be concluded that the range of ascorbic acid concentrations where it is possible to work is 10-200 μM. Above the range of these concentrations, the fluorescence decreases, since ascorbic acid interferes with the assay, forming a salt (sodium ascorbate), there being not enough NaOH to provide the formation of fluorescent nanoparticles.

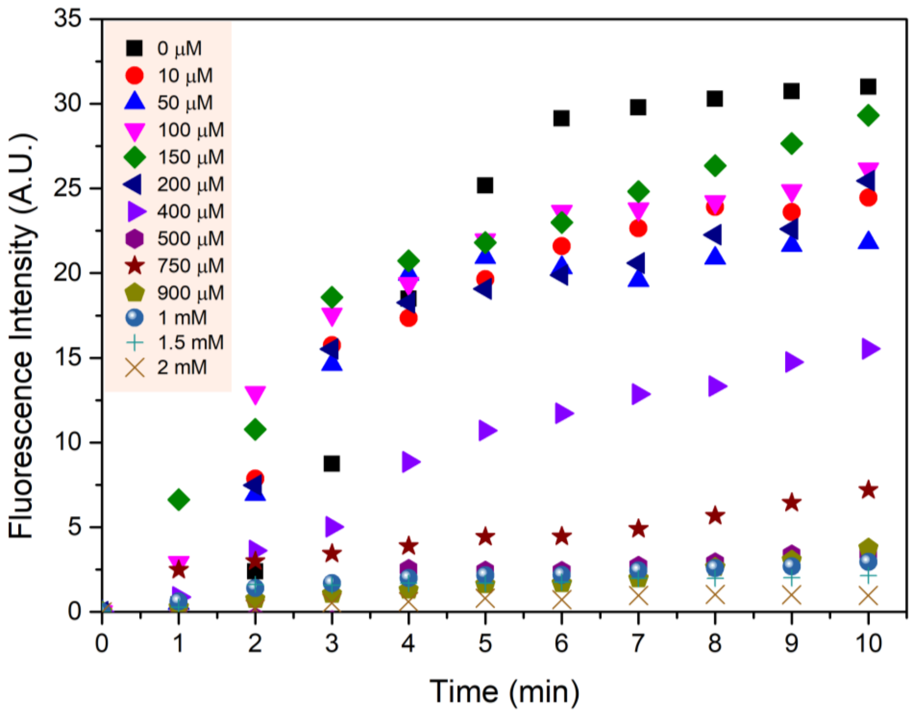

Figure 26. *Representation of the fluorescence emission as a function of time, for different concentrations of ascorbic acid in reaction medium. The [L-DOPA] is fixed, 100 μM. Using [NaOH] reaction medium = 0.2 M. The measurements were performed at a flow rate of 1 μL/min. The conditions of acquisition using Leica DMLM Microscope were exposure time of 2s and gain of 2x. n=1*

According to M. Hormozi-Nezhad and co-workers [84], it is reported that the formation of fluorescent nanoparticles of L-DOPA was dependent on the concentration of NaOH used. Therefore, a simple screening study was performed, where the NaOH concentration was varied and the pure L-DOPA concentration at 100 μM as well as the ascorbic acid concentration at 2 mM remained constant. This concentration of ascorbic acid was chosen because, as shown in **Figure 26**, it is one of the concentrations that shows virtually no fluorescence. Therefore, in order to verify that at higher NaOH concentrations fluorescent nanoparticles could be formed, this study was performed. The results are shown in **Figure 27**. Where it is possible to verify that the photos captured did not show fluorescence, believing that, the added NaOH is only sufficient to form a salt, not allowing the fluorescent nanoparticles to form. This way, it can be concluded that for nanoparticle formation to occur, it would be necessary to further increase the NaOH concentration using the 2 mM acid concentration, in order to obtain measurable fluorescence. Given that the NaOH solution is exothermic, it was dangerous to further increase the NaOH concentration. This way, this study stayed here.

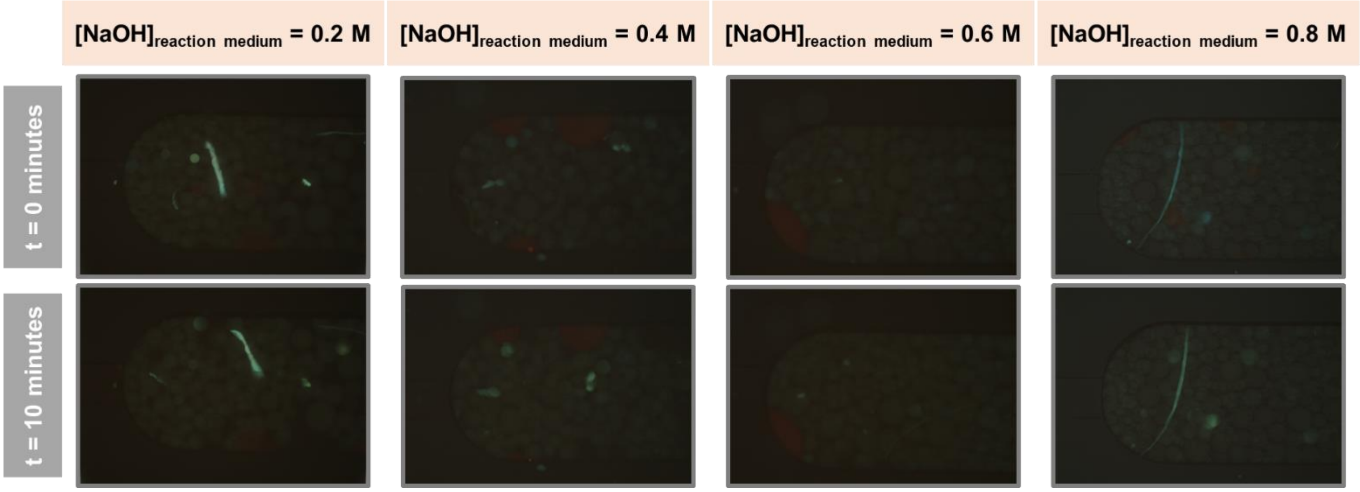
$[NaOH]_{reaction\ medium}$ = 0.2 M
$[NaOH]_{reaction\ medium}$ = 0.4 M
$[NaOH]_{reaction\ medium}$ = 0.6 M
$[NaOH]_{reaction\ medium}$ = 0.8 M
t = 0 minutes
t = 10 minutes

Figure 27. *Representation of the fluorescence emission as a function of time, for different concentrations of NaOH in reaction medium. The [L-DOPA] and the [Ascorbic acid] are fixed, 100 µM and 2 mM, respectively. The measurements were performed at a flow rate of 1 µL.min*$^{-1}$*. The conditions of acquisition using Leica DMLM Microscope were exposure time of 2s and gain of 2x. Objective lens: 10x.*

Further assays were always performed using the NaOH concentration in reaction medium at 0.2 M, and the range of concentrations of ascorbic acid considered was 10-200 µM.

So far the microscope used was Leica DMLM Microscope. In further experiments, due to logistical reasons, the experiments were performed using a microscope CKX41 Olympus.

3.2. Calibration Curve of pure L-DOPA solutions. Monitor the amount at reactor output

Once established that the beads that can be used to detect L-DOPA and the range of concentrations of ascorbic acid where it is possible to work, the next step was to make a calibration curve for each concentration of ascorbic acid, so one can monitor the amount of L-DOPA at reactor output. For the range of ascorbic acid concentration where it is possible to work, three concentrations of acid 0, 100 and 200 µM were selected for which calibration curves were made.

First a calibration curve was made using the microfluidic structure shown in **Figure 20.A**. This curve was made for 3 different concentrations of ascorbic acid, and for each acid concentration, the pure L-DOPA concentration was varied 5 times. The calibration curve obtained is shown in **Annex 1**. However, this curve has not been considered because the microfluidic structure considered has a negative impact of air bubbles and disturbance to package integrity may lead to irregular flow rates, noise at the detection site and reproducibility analysis failures. Apart from this the conditions of image acquisition were not ideal either (exposure time of 2s and a gain of 1).

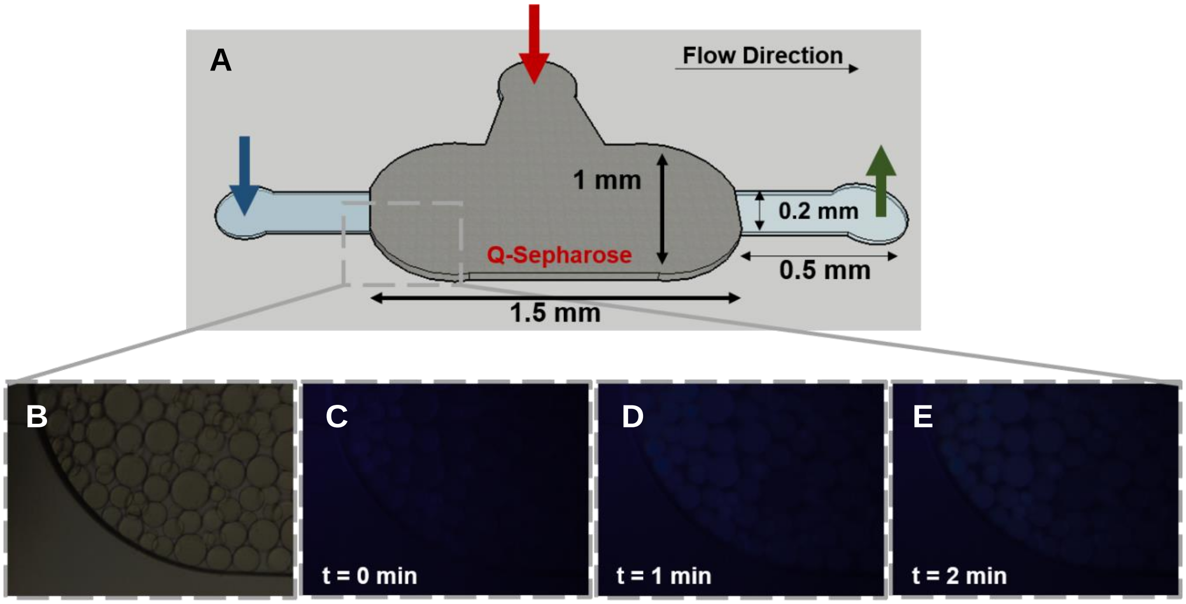

Figure 28. ***(A)*** *Schematics of the microfluidic structure used for the calibration curves experiments and dimensions. The Q-Sepharose beads are packed through the side inlet (Red arrow), which is then closed with a closed metallic adapter, as described in section* ***2.2.2.2****. The mixture between L-DOPA, ascorbic acid and NaOH (pipette tip) is then pulling (Blue arrow). The mixture solution was pulling through the column using the polyethylene tubing coupled to an open metallic adapter with a PBS syringe controlled by a syringe pump (Green Arrow), applying a negative pressure at the outlet.* ***(B)*** *Brightfield (column packed).* ***(C) - (E)*** *Image captured at a long time (UV filter). The conditions of acquisition using Olympus (UV filter) were exposure time of 1s and a gain of 0x. Objective lens: 10x.*

With this in mind, a new microfluidic structure was designed and optimal acquisition conditions were screened. The exposure time and the gain that respectively, corresponds to the period of time for which the sensor of a digital camera is actually exposed to the light so as to capture a picture and to the number of electron-hole pairs generated per incident photon in a photo-detector were screened. The new microfluidic structure it has 1.5 mm long, had a width of 1 mm and a height of 100 μm, additionally they had a smaller channel with 0.2 mm of width and a height of 20 μm, as shown in **Figure 28.A.**

Thus, a second calibration curve was made using the new microfluidic structure and capturing images with an exposure time of 1s and a gain of 0x. This curve was also made for 3 different concentrations of ascorbic acid, and for each acid concentration, the pure L-DOPA concentration was varied 6 times - 0, 1, 3, 10, 30, 100 and 300 μM. Then, these solutions were flowed into the columns, at a flowrate of 1 μL/min. Where these columns were packed with Q-sepharose beads, as shown in **Figure 28.A**. Photos were taken every minute for 6 minutes. The images acquired through the Olympus microscope are analyzed as described in **section 2.2.5.,** where only the channel green was considered, because the fluorescent nanoparticles of L-DOPA are not pure blue, they are cyan blue, but also because looking at **Figure 29** it is possible to observe that a better signal to noise ratio is obtained than when full image is considered.

Then the slope of the first three points corresponding to the first 2 minutes (0, 1 and 2 minutes) for each L-DOPA concentration and for each ascorbic acid concentration were considered, as described in **Annex 2**. Only the first two were considered because they are the points that best represent the fluorescence increment. Since over time there is a darkening of the beads, and therefore the fluorescence tends to decrease, as shown in **Figure 30**. Then, with the slopes previously obtained, the calibration curves were made as a function of L-DOPA concentration.

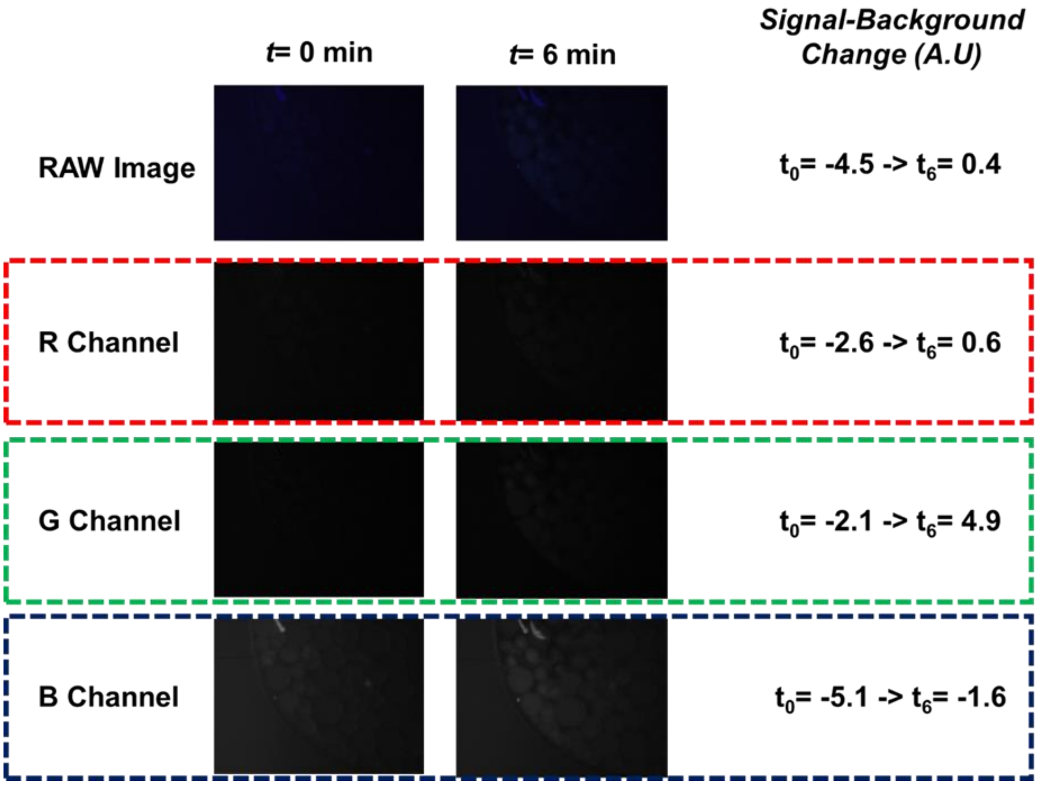
t= 0 min
t= 6 min
Signal-Background Change (A.U)
RAW Image
t_0= -4.5 -> t_6= 0.4
R Channel
t_0= -2.6 -> t_6= 0.6
G Channel
t_0= -2.1 -> t_6= 4.9
B Channel
t_0= -5.1 -> t_6= -1.6

Figure 29. *Experimental Image analysis method. By splitting the full image (RAW Image) in RGB color channels a better signal to ratio is obtained, especially for low concentrations of L-DOPA. Adapted from E.J.S. Brás and co-workers, in peer review.*

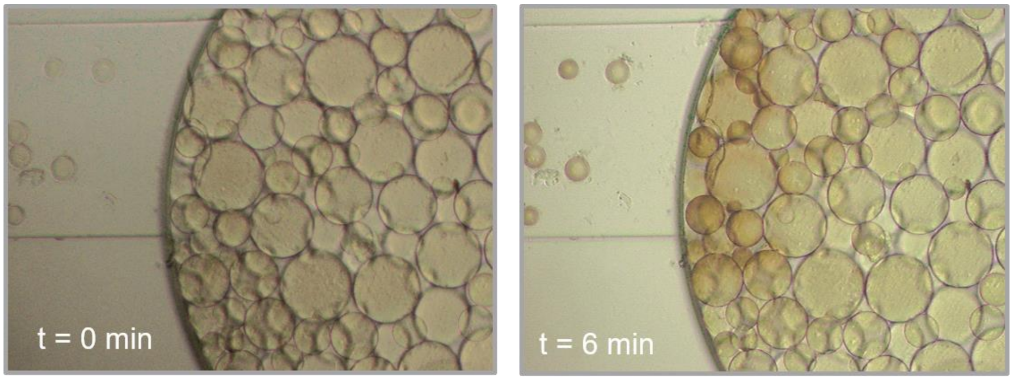

Figure 30. *Q-Sepharose beads darkening over the detection time, using brightfield.*

The set of calibration curves considered, is shown in **Figure 31**. For each calibration curve it was considered the trend line to intersect zero. These equations were used to monitor the productivity of the microreactor, which will be addressed in the next sections.

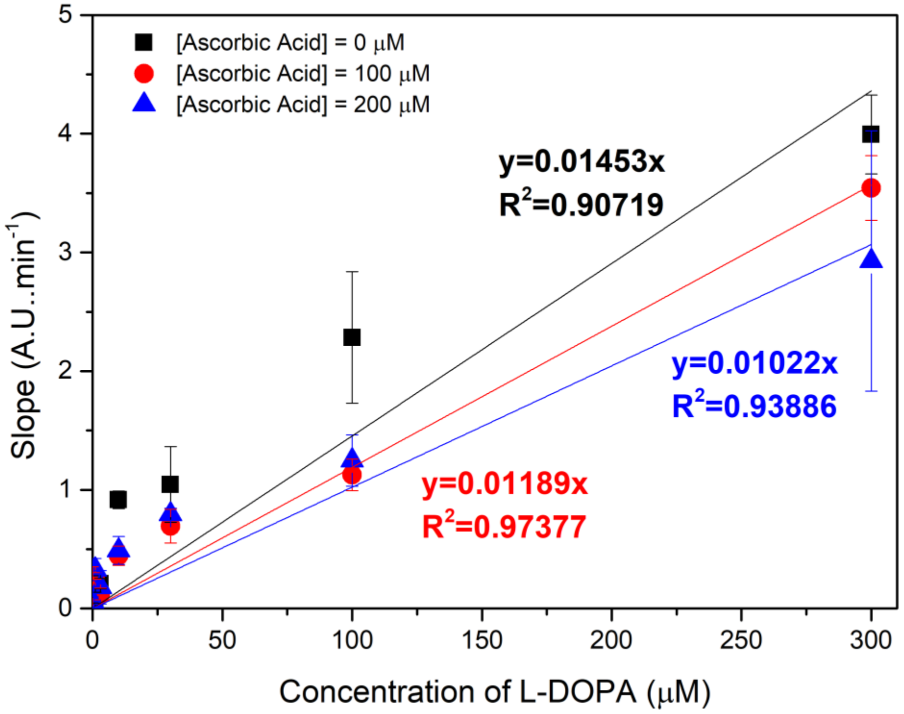

Figure 31. *Calibration Curve for each concentration of ascorbic acid, 0 μM (black), 100 μM (red), 200 μM (blue). Was made with an exposure time of 1s and a gain of 0, microscope CKX41 Olympus. n=4*

3.3. Microscale Production of L-DOPA. Screening Conditions

For the L-DOPA production tyrosine and ascorbic acid were used as substrate and the tyrosinase as enzyme (**Figure 25**).

The production of L-DOPA in microscale (**section 2.2.6.**) consists of injecting a substrate solution (tyrosine and ascorbic acid) into a microfluidic structure that is packaged with tyrosinase functionalized beads prepared according to the protocol in section **2.2.1.2**. Tyrosinase immobilization occurs because at pH 7 the enzyme is negatively charged (the isoelectric point, 4.7, is below 7) and the functionalized silica beads have a positive charge. With this in mind the enzyme electrostatically binds to the beads. After the tyrosinase functionalized beads are prepared they are packed in the column as described in section **2.2.2.3**. Then the overall structure of the optimization experiments for the production conditions of L-DOPA consists in retrieving the output of the chosen reactor, which is called the sample under analysis (S.U.A) and detecting the L-DOPA content using a smaller microfluidic structure, as described in section **2.2.4**. **Figure 32** describes the entire procedure performed.

For the optimization of the reaction conditions, parameters of interest include, but are not limited to, temperature, pH, flowrate, residence time, substrate concentration etc. It has been reported that the optimal temperature for tyrosinase activity is approximately 30ºC as well as that the optimal pH being between 6 and 8. [88] Thus, temperature and pH were maintained at 32.5ºC and 7, respectively.

The optimization experiments focused on the aspect of flow rate, substrate ratio in the reaction medium and also reactor geometry. The metric used for the optimization of the microreactor was the substrate conversion (%), defined as the concentration of L-DOPA divided by the concentration of the respective substrate being injected into the system. The results are summarized in **Figure 32**.

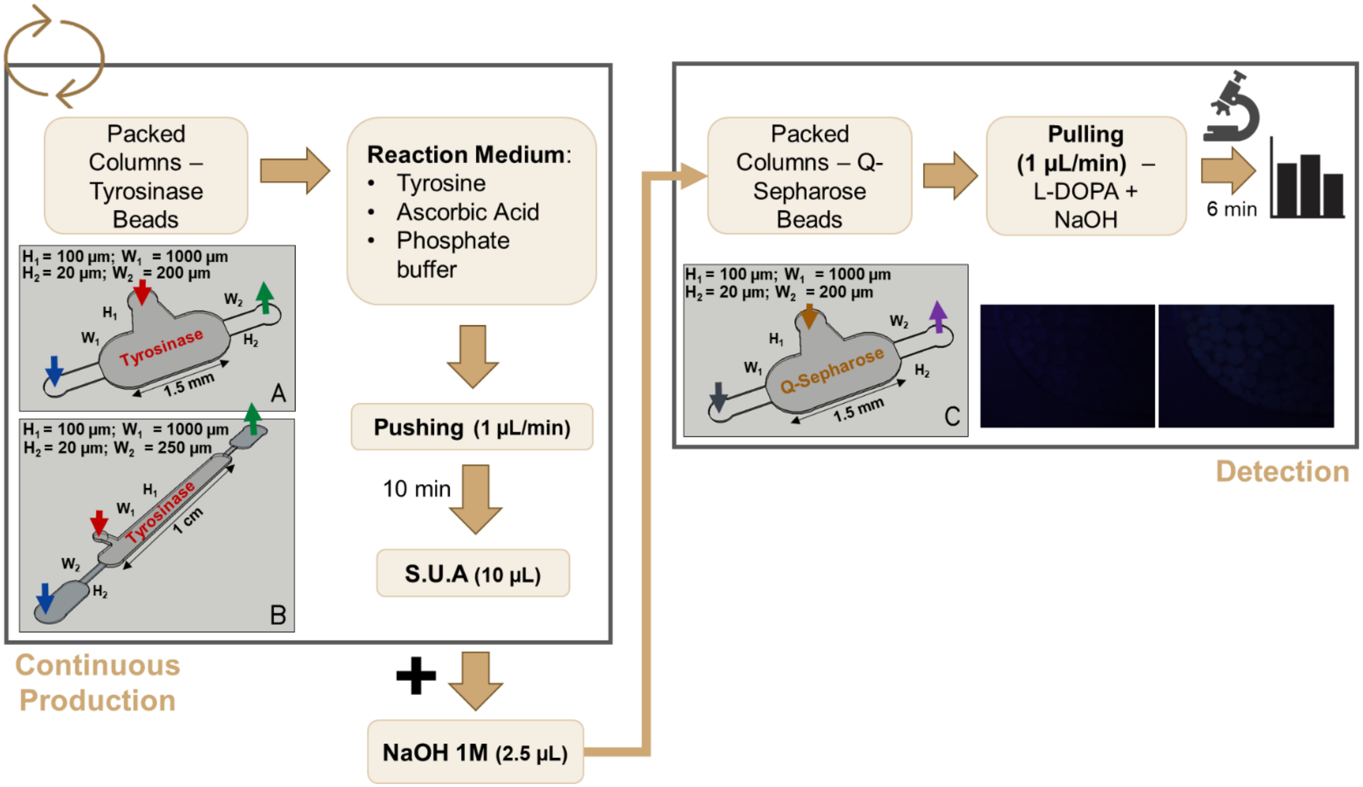
Packed Columns – Tyrosinase Beads
Reaction Medium:
Tyrosine
Ascorbic Acid
Phosphate buffer
H₁ = 100 μm; W₁ = 1000 μm
H₂ = 20 μm; W₂ = 200 μm
W₂
H₁
W₁
Tyrosinase
H₂
1.5 mm
A
H₁ = 100 μm; W₁ = 1000 μm
H₂ = 20 μm; W₂ = 250 μm
H₁
W₁
Tyrosinase
1 cm
W₂
H₂
B
Pushing (1 μL/min)
10 min
S.U.A (10 μL)
Continuous Production
NaOH 1M (2.5 μL)
Packed Columns – Q-Sepharose Beads
Pulling (1 μL/min) – L-DOPA + NaOH
6 min
H₁ = 100 μm; W₁ = 1000 μm
H₂ = 20 μm; W₂ = 200 μm
W₂
H₁
W₁
Q-Sepharose
H₂
1.5 mm
C
Detection

Figure 32. *Production using 1 μL/min as example and Detection of L-DOPA. Two reactor geometries was used for optimization experiments of production:* ***(A)*** *"Short Reactor" (V = 0.13 μL) and* ***(B)*** *"Long Reactor" (V = 1 μL). The columns were packed with tyrosinase-functionalized beads through the side inlet (Red arrow), which is then closed with a closed metallic adapter (as described in section* ***2.2.2.3****). The substrate solution (tyrosine and ascorbic acid) is then pushing through the column inlet using the polyethylene tubing coupled to an open metallic adapter with a substrate solution controlled by a syringe pump (Blue arrow). Then the sample for analysis (S.U.A) was recovered at the reactor outlet (Green arrow).* ***(C)*** *The microfluidic structure used for the detection protocol, section* ***2.2.4.*** *This microfluidic column used for the detection protocol has the same dimensions the column used for production (Short Reactor).*

In relation to the optimization made with different flow rates, in **Figure 33. A** it is possible to see that the working flowrate has a significant impact on the initial moments of the reaction, however eventually reaches a steady state (around 35 minutes) which is independent of the flow rate. This was not expected, because for lower flowrates, the residence time inside the reactor will be longer, and therefore, in addition to increasing the chances of the substrate finding the enzyme over the entire reactor length, should increase the probability of the reaction reaching a post-L-DOPA stage, due to the catecholase activity (conversion of L-DOPA to dopaquinone) of the enzyme. [10] However, changes in flow rates and consequently in residence times may not be sufficient to cause a significant difference in the output of the reactor. Since the behavior is basically identical regardless of the flow rate used, the flow rate chosen for following experiments was 1 μL/min.

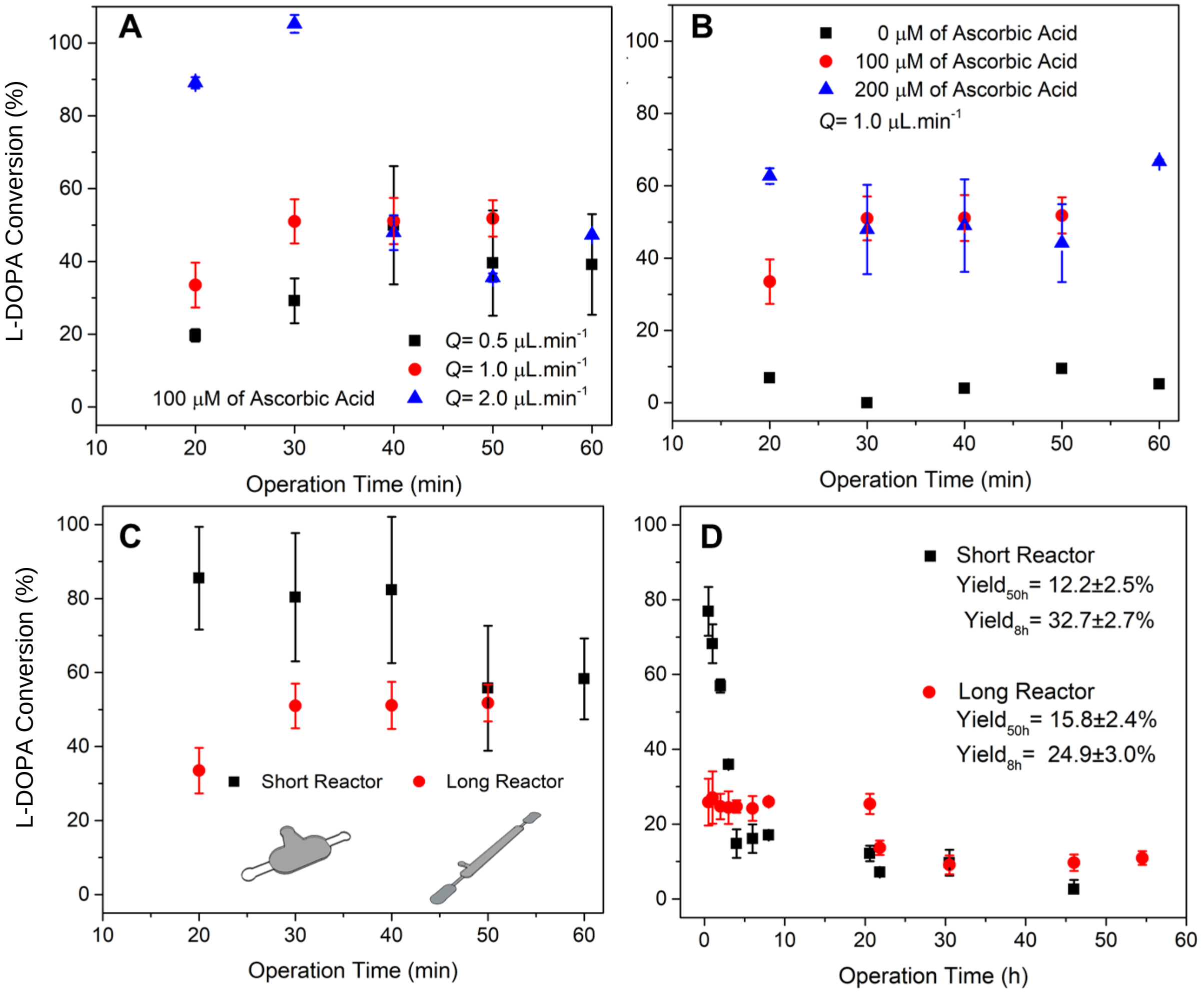

Figure 33. *Optimization experiments for the production of L-DOPA using tyrosine as a substrate:* ***(A)*** *Flowrate (n=3),* ***(B)*** *Reducing agent concentration (n=3) and* ***(C)*** *Reactor geometry (n=3) was studied.* ***(D)*** *Using the optimal conditions, both reactor geometries were checked for long term viability (n=4). In* ***(B)***, ***(C)*** *and* ***(D)*** *was considered flowrate of 1 μL/min. Adapted from E.J.S. Brás and co-workers, in peer review.*

The next optimization was to verify the impact of the reducing agent, in the form of ascorbic acid. As mentioned earlier, the presence of ascorbic acid is crucial to allow the reaction to produce L-DOPA, the results are shown in **Figure 33.B**. In this figure it is possible to observe that in the absence of ascorbic acid the reaction output is very close to zero. However, there seems to be an upper limit to the amount of ascorbic acid that will improve the reaction conditions. But increasing the amount of acid from 100 μM to 200 μM did not further improve the conversion, so the concentration of ascorbic acid chosen for following experiments was 100 μM.

The lack of impact of flow rates on microreactor productivity led to the optimization of reactor geometry. For these optimization experiments, two reactor geometries were considered, the “Long Reactor”, which has a 1 cm long, had a width of 0.1 cm and a height of 100 μm, while the “Short Reactor” differs only by having a 1.5 mm long (**Figure 32**). The results obtained are shown in **Figure 33.C**. In this figure it is possible to observe that the short reactor largely outperforms the long reactor. This is due to the low residence time of the substrate inside the short reactor and to the fact that each substrate molecule will find less enzymes when compared to the long reactor, decreasing the possibility of side reactions and further product degradation. In this way, the reactor chosen for to produce L-DOPA in cascade reaction, which will be talk later, was the short reactor.

With this optimization performed there was still the issue of operational stability over longer periods of time, these results are presented in **Figure 33.D**. It can be observed that in both cases there is an initial loss of enzymatic activity in the system, which had not previously been recorded. The reasons for this may be reactor fouling, which prevents the newer substrates from reaching the enzyme (**Figure 34**); suicidal nature of tyrosine substrate for tyrosinase activity [89][90]; or enzyme wash-out of the system due to poor interaction between APTES functionalized beads and the enzyme. In order to know if occurred enzyme washout, the Bradford method (described in section **2.2.3**) was used, and it was concluded that no enzyme was detected at the reactor outflow. However, washout may have occurred at concentrations not detectable by this test.

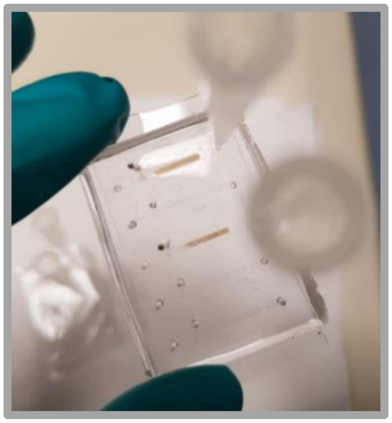

Figure 34. *Microfluidic structure of Long Reactor after production of L-DOPA. Column darkening throughout production. Byproducts tend to deposit themselves on the microbeads, which leads to mass transport limitations in longer assays. Impossible that new substrates reach the enzyme.*

The Bradford assay was performed on the reactor output, in order to assess the possibility of enzyme washout. Due to volume constraints this was only performed for the long term productions. **Figure 35** shows the calibration curve obtained using tyrosinase solutions as a standard and **Table**

5 summarizes all the measured absorbance's, showing there is no measurable enzyme in the reactor outflow.

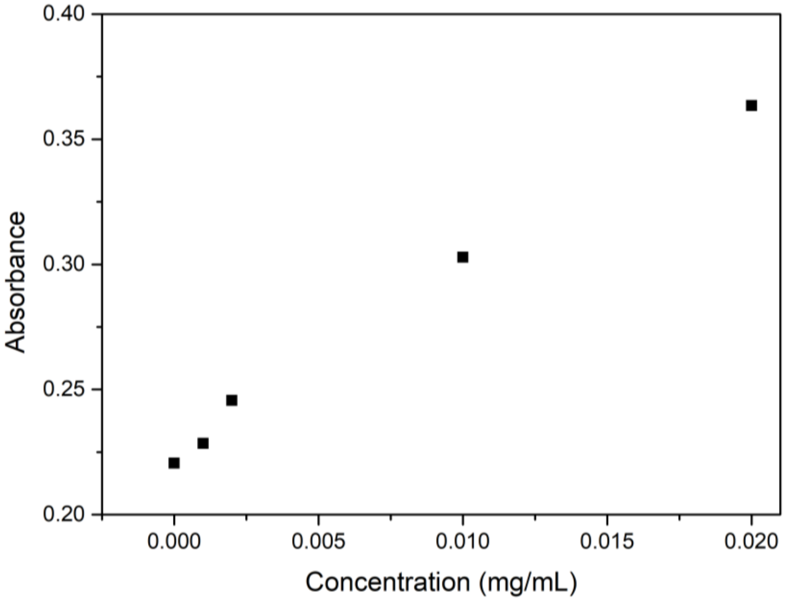

Figure 35. *Calibration curve obtained using tyrosinase solutions as a standard – Bradford method.*

Table 5. Summarizes all absorbance's obtained throughout production.

Sample	**Abs $_{595\ nm}$ (reactor 1)**	**Abs $_{595\ nm}$ (reactor 2)**	**Abs $_{595\ nm}$ (reactor 3)**	**Abs $_{595\ nm}$ (reactor 4)**
Micro Short Reactor (8-24h)	0.2428	0.2468	0.242	0.235
Micro Long Reactor (8-24h)	0.2395	0.2327	0.2085	0.2404

3.4. Dopamine Detection Method

Dopamine production is another major goal of this work. The dopamine is obtained through the decarboxylation of L-DOPA using the enzyme DOPA-decarboxylase, as shown is **Figure 36**. So, it is necessary to detect dopamine to be able to quantify it later.

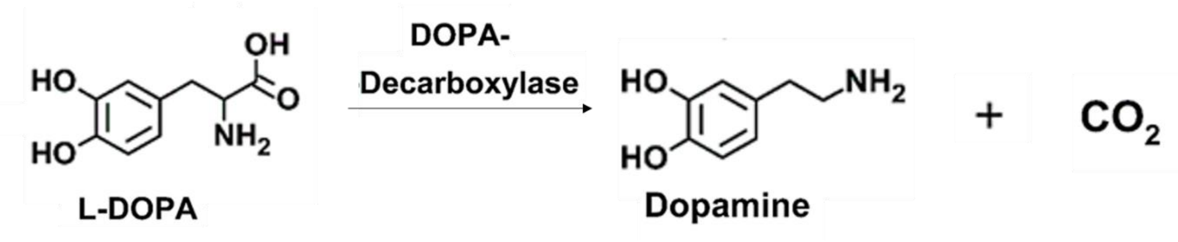

Figure 36. *Dopamine reaction pathway using L-DOPA as a substrate and DOPA-decarboxylase as am enzyme.*

First is necessary to know if L-DOPA interferes with dopamine detection. The detection of dopamine is made through of the addition of NaOH, that participate in polymerization reactions as described by Adem Yildirim and co-workers [91], forming red fluorescent nanoparticles, that are observed in green filter. By capturing the resulting fluorescent nanoparticles, using a smaller microfluidic column, as shown in **Figure 28.A**, packed with Q-Sepharose microbeads, is to possible monitoring the fluorescence increase over time.

In order to determine whether L-DOPA interferes with the direct detection of dopamine, two calibration curves were made. One for 6 different pure dopamine concentrations, and another calibration curve where the 100 μM pure L-DOPA concentration remained constant and the dopamine concentration varied 6 times. In this last curve, images were acquired using the UV filter (to detect L-DOPA) and the green filter (to detect Dopamine). For both calibration curve the microfluidic column was packed with Q-Sepharose, as described in section **2.2.2.2.** and then the different solution previously prepared was flowed.

The two curves obtained are shown in **Figure 37**. The results shown in the figure allow us to conclude that L-DOPA interferes with the direct detection of dopamine. Taking the pure Dopamine concentration at 100 μM as an example, in **Figure 37.A** it is possible to verify that the fluorescence intensity is lower than in **Figure 37.B**. If there was no interference there would be no such difference. However from **Figure 37.B**, it can be also observe that regardless of the dopamine concentration, the fluorescence intensity of L-DOPA remains relatively constant, concluding that dopamine has a small interference in the detection of L-DOPA when using the UV filter. This last observation is a point in favor of quantifying dopamine through the consumption of L-DOPA.

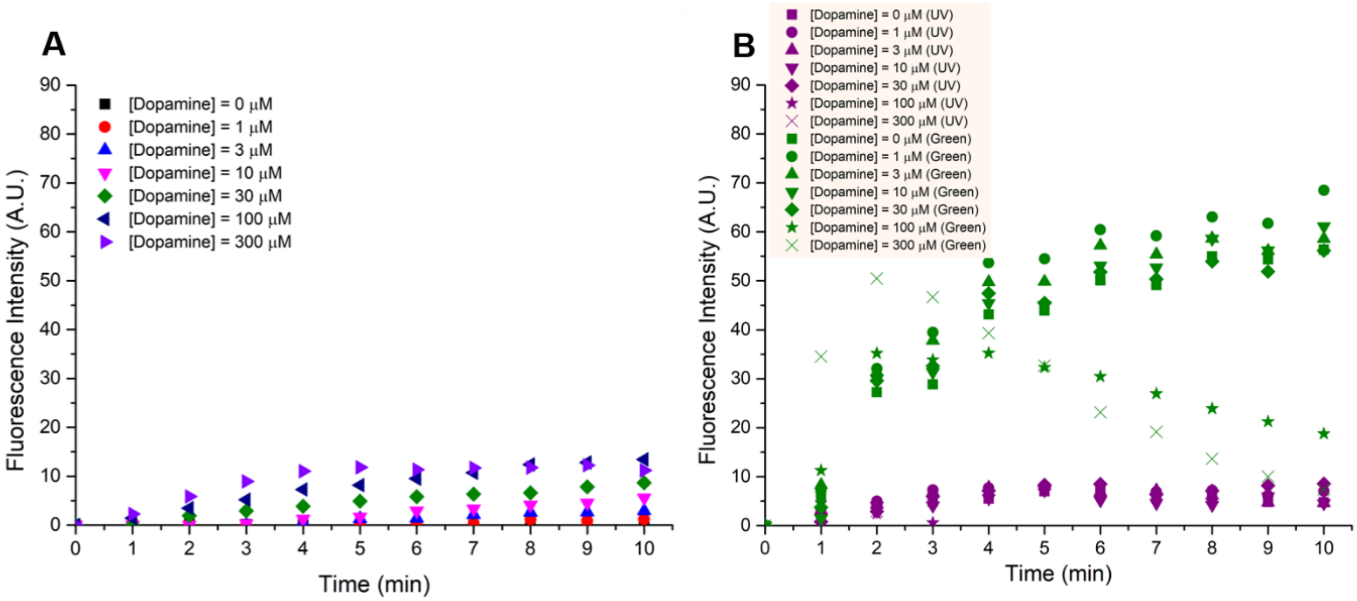

Figure 37. *Calibration Curves monitoring the fluorescence increase over time:* ***(A)*** *Pure dopamine concentrations varied 6 times, using green filter and* ***(B)*** *Pure solution of L-DOPA at 100 μM concentration remained constant and the dopamine concentration varied 6 times (n=1).*

But still unsatisfied with these results, because the ideal would be to do direct detection of dopamine rather than through the consumption of L-DOPA, several screening studies have been done for different types of beads (**Table 4**) using a pre-existing column design available from INESC-MN (**Figure 20.A**). [57] Screening was performed in order to find beads that, without autofluorescence, capture only Dopamine fluorescent nanoparticles and ultimately do not capture L-DOPA fluorescent nanoparticles. In **Figure 38** are some of the beads studied, and it can be concluded that none of the beads studied could be used because beads that lack autofluorescence did not capture fluorescent dopamine nanoparticles (CM Sepharose, PPA and MEP HyperCel) and beads that had some autofluorescence captured fluorescent dopamine nanoparticles, but also capture up L-DOPA particles (Capto Adhere).

With this, it was concluded that it is not possible to detect dopamine. Thus dopamine was quantified through the consumption of L-DOPA. Using the calibration curve determined in section **3.2.** This way it is possible to monitor dopamine production from the consumption of L-DOPA.

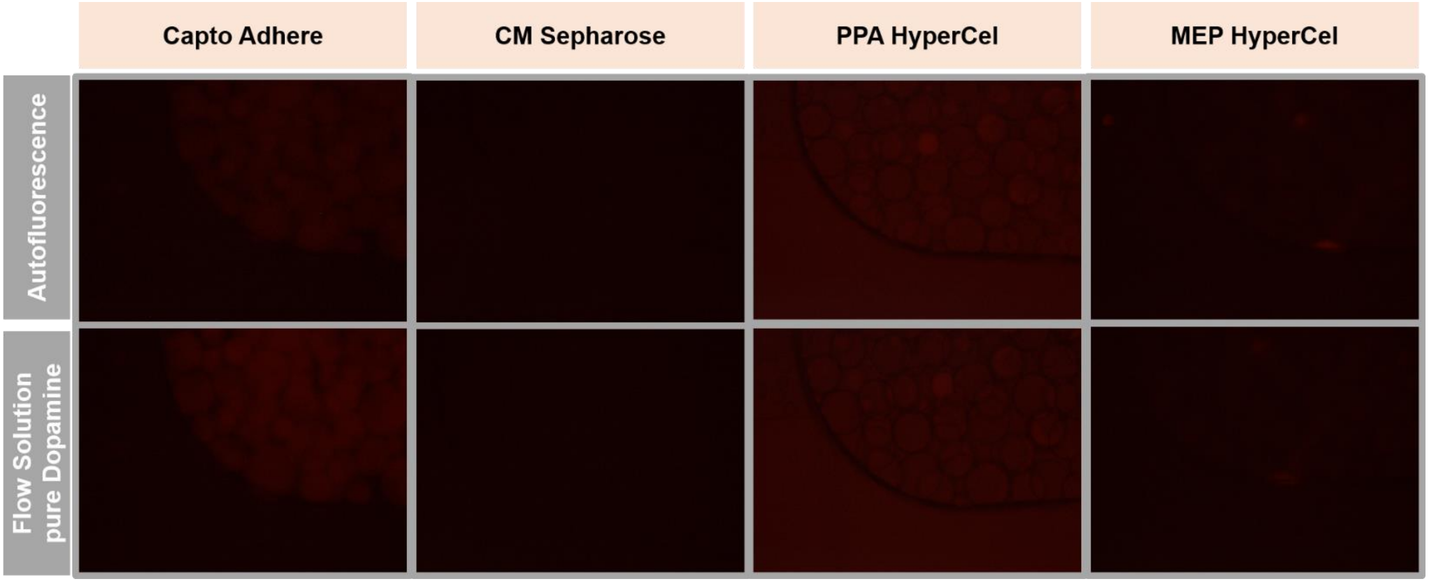

Figure 38. *Detection of Dopamine. 4 typed of beads were used for these studies: Capto Adhere, CM Sepharose, PPA and MEP HyperCel. The autofluorescence of beads was initially assessed, then a solution of pure Dopamine at 100 μM was flowed to establish if any beads capture the fluorescence nanoparticles of Dopamine. Using [NaOH]* $_{\text{reaction medium}}$ *= 0.2 M. The conditions of acquisition using Olympus Microscope were exposure time of 1s and a gain of 0x. Objective lens: 10x.*

3.5. Microscale Production of Dopamine. Screening Conditions

For the dopamine production pure L-DOPA was used as substrate and the DOPA decarboxylase as enzyme (**Figure 36**).

As mentioned above, the monitoring of production of dopamine occurs through L-DOPA consumption, due to the impossibility of direct detection of dopamine.

The production of dopamine in microscale (**section 2.2.6.)** consists of injecting a substrate solution (pure L-DOPA) into a microfluidic structure that is packaged with Dopa-decarboxylase functionalized beads prepared according to the protocol in section **2.2.1.2.** Dopa-decarboxylase immobilization occurs because at pH 7 the enzyme is negatively charged (isoelectric point, 5.7, is below 7) and the functionalized silica beads have a positive charge. With this in mind the enzyme electrostatically binds to the beads. After the Dopa-decarboxylase functionalized beads are prepared they are packed in the column as described in section **2.2.2.3**. Then the overall structure of the optimization experiments for the production conditions of L-DOPA consists in retrieving the output of the chosen reactor, which is called the sample under analysis (S.U.A) and detecting the L-DOPA content using a smaller microfluidic structure. As is shown in **Figure 39**.

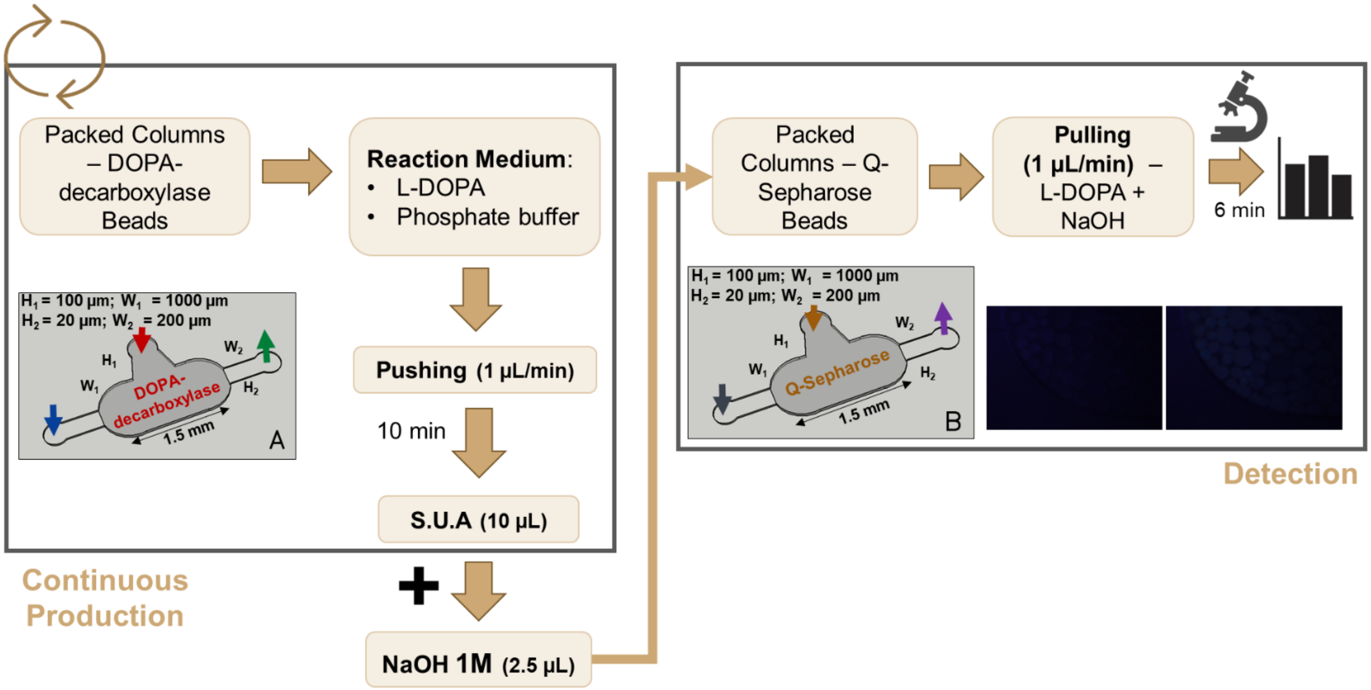
Packed Columns – DOPA-decarboxylase Beads
Reaction Medium:
L-DOPA
Phosphate buffer
H_1 = 100 µm; W_1 = 1000 µm
H_2 = 20 µm; W_2 = 200 µm
W_2
H_1
W_1
DOPA-decarboxylase
H_2
1.5 mm
A
Pushing (1 µL/min)
10 min
S.U.A (10 µL)
Continuous Production
NaOH 1M (2.5 µL)
Packed Columns – Q-Sepharose Beads
Pulling (1 µL/min) – L-DOPA + NaOH
6 min
H_1 = 100 µm; W_1 = 1000 µm
H_2 = 20 µm; W_2 = 200 µm
W_2
H_1
W_1
Q-Sepharose
H_2
1.5 mm
B
Detection

Figure 39. *Consumption of L-DOPA using 1 µL/min as example and Detection of L-DOPA and Detection of L-DOPA. A reactor used for optimization experiments of production:* ***(A)*** *"Short Reactor". The columns were packed with Dopa-Decarboxylase-functionalized beads through the side inlet (Red arrow), which is then closed with a closed metallic adapter (as described in section* ***2.2.2.3.****). The substrate solution (pure L-DOPA) is then pushing through the column inlet using the polyethylene tubing coupled to an open metallic adapter with a substrate solution controlled by a syringe pump (Blue arrow). Then the sample for analysis (S.U.A) was recovered at the reactor outlet (Green arrow).* ***(B)*** *The microfluidic structure used for the detection protocol, section* ***2.2.4.*** *This microfluidic column used for the detection protocol has the same dimensions the column used for production (Short Reactor).*

The detection of L-DOPA occurs through mixing the S.U.A with NaOH L-DOPA participate in polymerization reactions as described above. Through capturing the resulting fluorescent nanoparticles, using a smaller microfluidic column packed with Q-Sepharose microbeads (section **2.2.4.**) is possible to monitor the consumption of L-DOPA (**Figure 39.B**).

The ideal temperature for DOPA decarboxylase activity is approximately 30 ° C and the ideal pH is between 6 and 8. [88] Therefore, for dopamine production conditions similar to those for L-DOPA production were tested. With this in mind, the temperature and pH were kept at 32.5ºC and 7, respectively. The same conditions were also maintained to avoid problems integrating the two stages of production.

The optimization experiments focused on the aspect of flow rate. Only flowrate has been optimized because dopamine has more complex reaction schemes and so fewer optimizations have been made compared to the optimizations made for L-DOPA production.

The metric used for the optimization of the microreactor was the substrate conversion (%), defined as the concentration of L-DOPA divided by the concentration of the respective substrate being injected into the system, then this result obtained is subtracted at 100, in order to determine the yield of L-DOPA consumed. Knowing the yield of L-DOPA consumed, it is possible determine the yield of dopamine produced, the results are summarized in **Figure 40**.

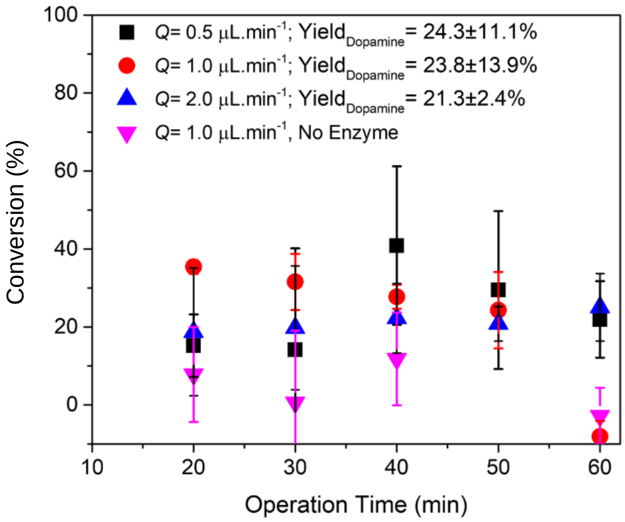

Figure 40. *Flow rate optimization of the dopamine production. A pure L-DOPA solution was used as a substrate and its consumption was monitored using the aforementioned described method (n=4). Adapted from E.J.S. Brás and co-workers, in peer review.*

The yield of dopamine production was determined by the consumption of L-DOPA in the system. Thus, a control assay without DOPA decarboxylase was performed to account for any loss of L-DOPA due to bead adsorption or spontaneous oxidation, which was determined to be between 5 and 10% of the initial amount of L-DOPA.

In relation to the optimization made with different flow rates, in **Figure 40**. It is possible to see that the working flow rate does not have a dramatic impact on system output, similar to that observed for L-DOPA production. Dopamine productivity appears to be very low, with an average yield of approximately 22%. With that in mind, leading us to continue the work using a flow rate of 1 μL/min.

In order to know if enzyme washout occurred during dopamine production experiments a separate reactor was used to pool samples for 30 min intervals. The Bradford method (described in **section 2.2.3**) was used. The Bradford assay was performed on the reactor output. **Figure 41** shows the calibration curve obtained using DOPA-decarboxylase solutions as a standard and **Table 6** summarizes all the measured absorbance's, showing that there is some washout of the enzyme, which may be poorly attached to the beads.

The fact that the enzyme wash-out occurs leads us to believe that this is why the conversion is low, with an average yield of approximately 22%. And for this same reason, the production has not been optimized for long periods of time as for L-DOPA production.

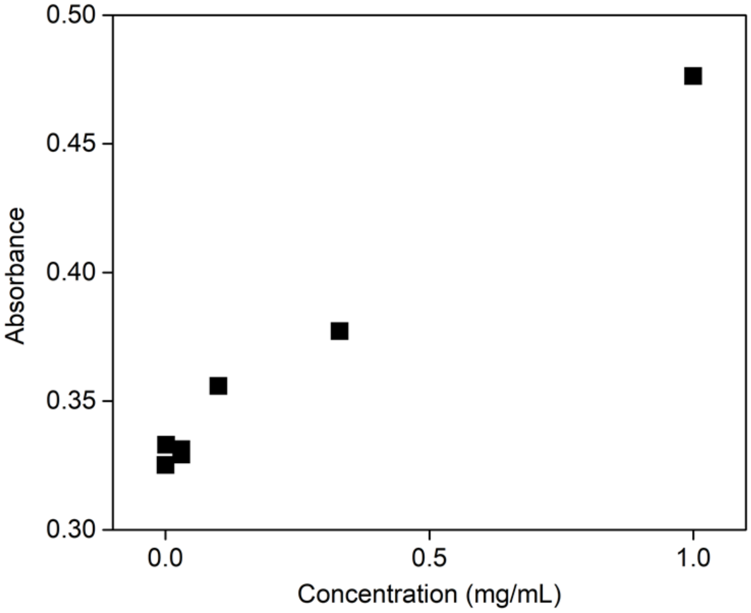

Figure 41. *Calibration curve using DOPA-decarboxylase solutions as a standard – Bradford method. Adapted from E.J.S. Brás and co-workers, in peer review.*

Table 6. *Results obtained for DOPA-decarboxylase wash-out studies* at microscale experiments*.*

Sample	**Abs $_{595\ nm}$ (reactor 1)**
Micro Short Reactor (0-30min)	0.3408
Micro Short Reactor (30-60min)	0.3356

3.6. Cascade Production

Now that optimizations of individual L-DOPA and Dopamine productions were performed, the cascade reaction was tested. For this a new microfluidic system consisting of two sequential chambers was fabricated as shown in **Figure 42.A**. The first chamber was packed with tyrosinase functionalized beads, and the second chamber was packed with Dopa- Decarboxylase functionalized beads, as described in section **2.2.2.3**. There is a small outlet between the two chambers that was used to retrieve samples for assessment of L-DOPA production.

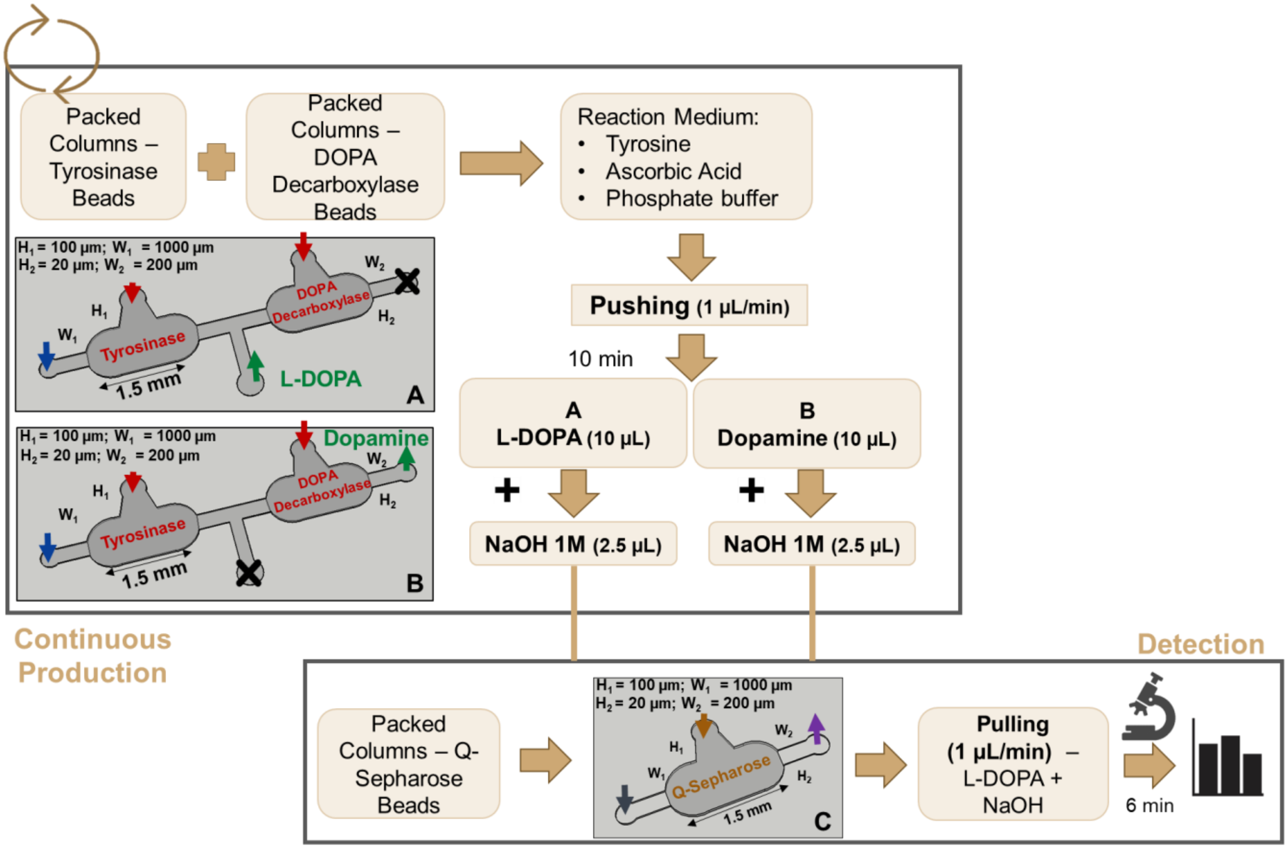

Packed Columns – Tyrosinase Beads
Packed Columns – DOPA Decarboxylase Beads
Reaction Medium:
• Tyrosine
• Ascorbic Acid
• Phosphate buffer
H_1 = 100 μm; W_1 = 1000 μm
H_2 = 20 μm; W_2 = 200 μm
H_1
W_1
H_2
W_2
Tyrosinase
DOPA Decarboxylase
1.5 mm
L-DOPA
A
Dopamine
B
Pushing (1 μL/min)
10 min
A
L-DOPA (10 μL)
B
Dopamine (10 μL)
+
NaOH 1M (2.5 μL)
+
NaOH 1M (2.5 μL)
Continuous Production
Detection
Packed Columns – Q-Sepharose Beads
Q-Sepharose
C
Pulling (1 μL/min) – L-DOPA + NaOH
6 min

Figure 42. *Sequential production of both L-DOPA and dopamine in a single microfluidic system and detection of L-DOPA. The chambers were packed, with respectively enzymes, through the side inlet (Red arrow), which is then closed with a closed metallic adapter (as described in section* ***2.2.2.3.****). The substrate solution (tyrosine and ascorbic acid) is then pushing through the column inlet using the polyethylene tubing coupled to an open metallic adapter with a substrate solution controlled by a syringe pump (Blue arrow). Then the sample for analysis (S.U.A) was recovered at the reactor outlet (Green arrow):* ***(A)*** *For the monitoring of L-DOPA production, the outlet is sealed off and the middle outlet is used for sample retrieval and* ***(B)*** *For the detection of dopamine through of the consumption of L-DOPA, the middle outlet is sealed off and the sample is collected at the outlet.* ***(C)*** *Microfluidic structure packed with beads Q-Sepharose, as described in section* ***2.2.2.2.****, used for detection of L-DOPA, as described in section* ***2.2.4****.*

A total of 4 systems were used simultaneously for these experiments, where samples from the first column were retrieved from 2 of them for L-DOPA assessment (**Figure 42.A**), while the other 2 structures were used for dopamine assessment at the outlet (**Figure 42.B**). For detection, these samples are mixed with NaOH, resulting in fluorescent nanoparticles which will be captured using a smaller microfluidic column packed with Q-Sepharose microbeads (**Figure 42.C**).

Figure 43 shows the results obtained using cascade reactions. It can be observed that the yield of dopamine is 70 %, relative to the amount of L-DOPA being produced in the first stage, which is approximately 45 %. This productivity is much higher than that recorded when was used pure L-DOPA at 100 μM (single-step reaction). This leads to believe that the Dopa- Decarboxylase chamber is being injected with higher concentrations of L-DOPA that it is capable of converting, or that the produced L-DOPA is purer than the injected L-DOPA stock for production of Dopamine, referred to above, in section **3.5**.

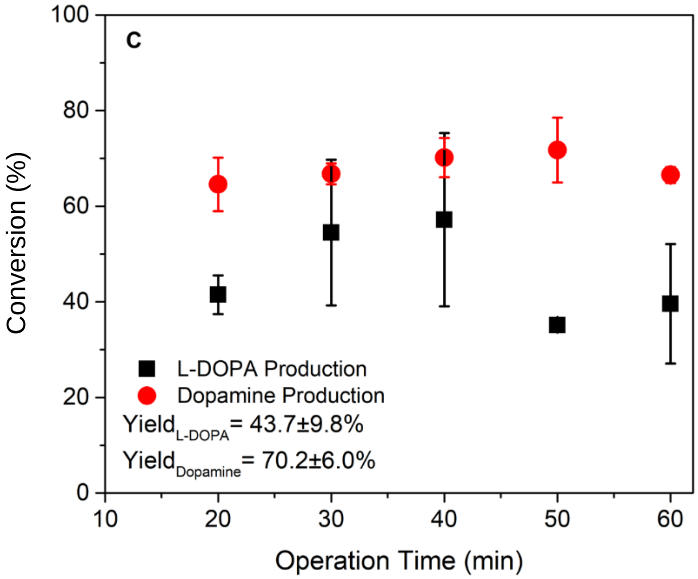

Figure 43. *Productivity for the sequential production of both L-DOPA and dopamine in a single microfluidic system, from of tyrosine as substrate. The flowrate used was 1 μL/min (n=2). Adapted from E.J.S. Brás and co-workers, in peer review.*

The results demonstrate the feasibility of packed-bed reactors, not only for single-step reactions but also for multi-step reaction sequences. One can argue the use of these types of microreactors for largescale production through the use of complex scaling-out methods. However, it is believed that the best use of these microreactors is for the screening of process conditions/enzymes, but for this to be true, it is necessary to perform an adequate upscale of the system. This topic is further discussed in the next section.

3.7. Macroscale Production of L-DOPA

The macroscale production was made as described in section **2.2.7**.

Only the synthesis of L-DOPA was up-scaled. In order to upscale the production system correctly, there are certain physical characteristics that must be maintained, such as the proportion of the system and the behavior of flow and mass transport. In order to maintain the mass and heat transport behavior in both systems, it is first necessary to characterize the microfluidic system by calculating the Reynolds (Re) number and the Péclet (Pe) number. In the case of the Pe, two variants were calculated, one that is dependent on the particles that compose the packed-bed (Pe_P), the other relates to the axial dispersion throughout the length of the reactor (Pe_L). The method of calculating these dimensionless numbers is presented and the results are summarized in **Table 7**.

$$Re_{Packed\ Bed} = \frac{2Rp \times v \times \rho}{\mu(1-\epsilon)} \qquad \text{(Equation 10)}$$

$$\frac{1}{Pe_P} = \frac{0.7D}{2Rp \times v} + \frac{\epsilon}{0.18 + Re_{Packed\ Bed}^{0.59}} \qquad \text{(Equation 11)}$$

$$Pe_L = Pe_P \frac{L}{2Rp} \qquad \text{(Equation 12)}$$

From the empirical equations (**Equations 10, 11** and **12**) where *Rp* is particle radius, *v* the velocity of the fluid, *ρ* the density, *μ* the viscosity of the fluid, ε the reactor void volume, *D* the diffusion coefficient and *L* the characteristic dimension, can be verified that by maintaining the same flow characteristics as the microfluidic system in terms of Pe and Re numbers, it is possible to upscale packed-bed reactors. Because the behavior of the flow will be dominated only by the bead packing. Unlike other reactors, such as plug flow reactors and tank reactors, where flow behavior will be dominated by reactor geometry.

Table 7. *Flow properties and resulting working flow rates for both micro and macroscale.*

System	Hydraulic Diameter (m)	Flow rate (µL/min)	Re	Pe_P	Pe_L
Short (micro)	1.8×10^{-4}	1	1.74×10^{-3}	1.8×10^{-5}	5.4×10^{-3}
Long (micro)					3.6×10^{-2}
Short (macro)	1×10^{-2}	780			5.4×10^{-3}
Long (macro)					3.6×10^{-2}

The macroscale version of the bioreactor consists of a chromatography pre-column packed with tyrosinase functionalized beads, as shown in section **2.2.7.** In order to prevent the washout of the beads through the reactor outlet, a small piece of cotton was placed at the bottom of the bed, the bed height was fixed using an appropriate volume of beads. Production experiments were carried on for 8h and compared to their microscale counterparts. This comparison can be found in **Figure 44**.

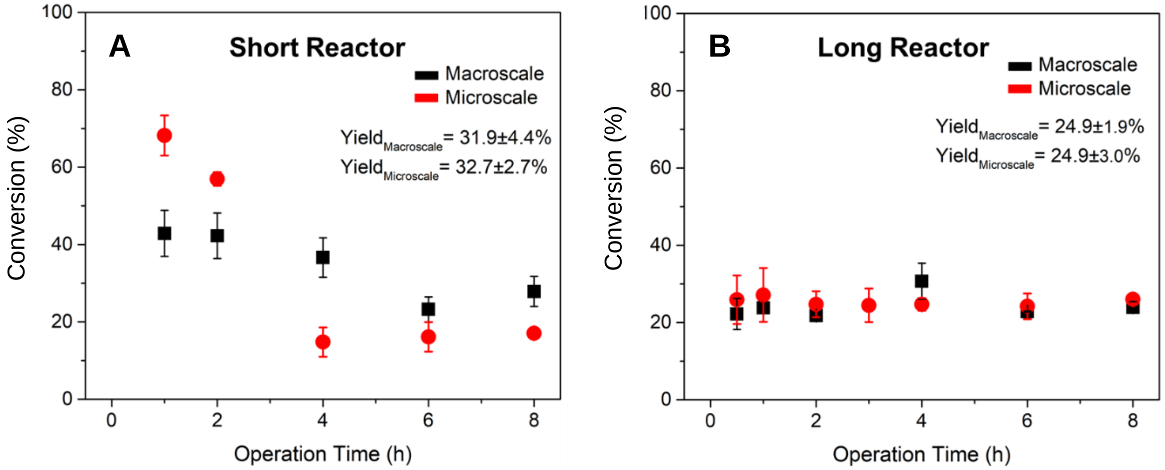

Figure 44. *Comparison between macroscale and microscale production:* ***(A)*** *The experiment lasted for 8h for both the Short reactor and* ***(B)*** *The experiment lasted for 8h for both the Long reactor. For the macroscale experiments (n=2). Adapted from E.J.S. Brás and co-workers, in peer review.*

Looking the results for short reactor **Figure 44.A**, it can be concluded that there is a good correlation between the substrate conversions at both scales. Similar losses of enzymatic activity occurring on both scales. These activity losses are probably due to the accumulation of reaction byproducts (**Figure 45**) or the enzyme washout, as previously mentioned.

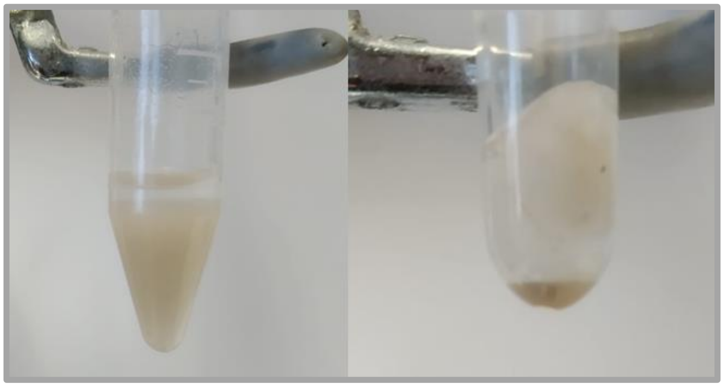

Figure 45. *Comparison between the original bead stock (left) and the beads used for 8 h at the macroscale (right). The white substance above the beads in right picture is the cotton used to prevent bead washout from the column.*

In order to know if occurred enzyme washout, the Bradford method (described in **section 2.2.3**) was used. The Bradford assay was performed on the reactor output. **Figure 46** shows the calibration curve obtained using tyrosinase solutions as a standard and **Table 8** summarizes all the measured absorbance's, showing that no enzyme was detected at the reactor outflow.

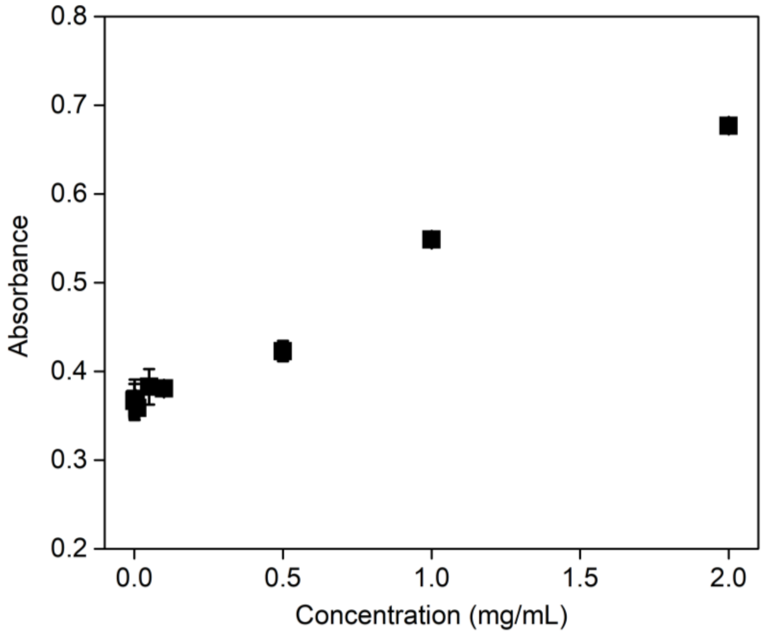

Figure 46. *Calibration curve obtained using tyrosinase solutions as a standard – Bradford method (n=2). Adapted from E.J.S. Brás and co-workers, in peer review.*

Table 8. *Results obtained for tyrosinase wash-out studies at macroscale experiments.*

Sample	Abs $_{595\ nm}$ (reactor 1)	Abs $_{595\ nm}$ (reactor 2)
Macro Short Reactor (1h)	0.3495	0.3558
Macro Short Reactor (2h)	0.3397	0.3387
Macro Short Reactor (4h)	0.353	0.3484
Macro Short Reactor (6h)	0.3573	0.3608
Macro Short Reactor (8h)	0.3816	0.3692
Macro Long Reactor (1h)	0.3475	0.3496
Macro Long Reactor (2h)	0.3413	0.3487
Macro Long Reactor (4h)	0.3617	0.3493
Macro Long Reactor (6h)	0.3363	0.3455
Macro Long Reactor (8h)	0.3308	0.3426

As for the Long reactor, **Figure 44. B**, the results obtained for the microscale are identical to the results obtained for the macroscale throughout the experiment. With this in mind, it can be concluded that by using a microfluidic system and maintaining similar mass transport conditions, it is possible to accurately predict the result of the macroscale process for packed-bed reactors.

The results obtained from the microscale and macroscale were then compared with results obtained from other enzymatic reactors reported in the literature (**Table 9**). Using the substrate conversion as a means of comparison, it is possible to observe that the system presented in this work has a similar output to other systems reported in the literature. Therefore, this similarity shows that the system used in this work has the same performance as traditional optimizations performed by other groups using other reactors, further validating this microfluidic approach to process optimization.

Table 9. *Substrate conversion comparison to literature reports. Conversions marked with "*" refer to the initial 8h working period. CSTR – Continuous Stirred Tank Reactor*

System	Conversion (%)	Mode of operation
Microscale (Short)	12.2 (32.7*)	Packed Bed
Macroscale (Short)	31.9	Packed Bed
Microscale (Long)	15.7 (24.9*)	Packed Bed
Macroscale (Long)	24.9	Packed Bed
Yang and co-workers [20]	53.0	Batch Reactor
Yang and co-workers [20]	28.5	CSTR
Yang and co-workers [20]	13.5	Packed Bed
Chao and co-workers [92]	44.1	Batch Reactor

3.8. HPLC

In order to prove that dopamine production occurred in the previous procedures, was used the technique of HPLC (High-Performance Liquid Chromatography), as described in section **2.2.8**. HPLC is an analytical technique to separate, identify, and quantify components in a mixture. HPLC used in this work was reverse phase (RP-HPLC), which means it has a nonpolar stationary phase and a moderately polar aqueous mobile phase, so the polar compounds are eluted first and the most nonpolar eluted later.

3.8.1. L-DOPA and dopamine standards

First, in order to perform quantitative analysis of samples containing L-DOPA and dopamine in their composition, it is necessary to draw the chromatograms of the standards used for both L-DOPA and dopamine. The standards used are dilutions made from their respective stock, which was at a concentration of 200 μM.

The peaks and their compounds (L-DOPA and dopamine) were identified by separately injecting into the system under the same conditions, obtaining chromatograms. These chromatograms are plotted by the recorder that is directly connected to the computer, and the detector through which the sample passes is a UV radiation detector. Thus, the computer directly provides the absorbance chromatograms given in arbitrary units for the respective area (A.U.), as a function of the respective retention time of each substance, which is given in minutes. These chromatograms are shown in **Figure 47,** in **(A)** L-DOPA and **(B)** Dopamine.

For each standard used, regardless of the compound analyzed, different retention times and respective peak areas were obtained because the standards have different concentrations.

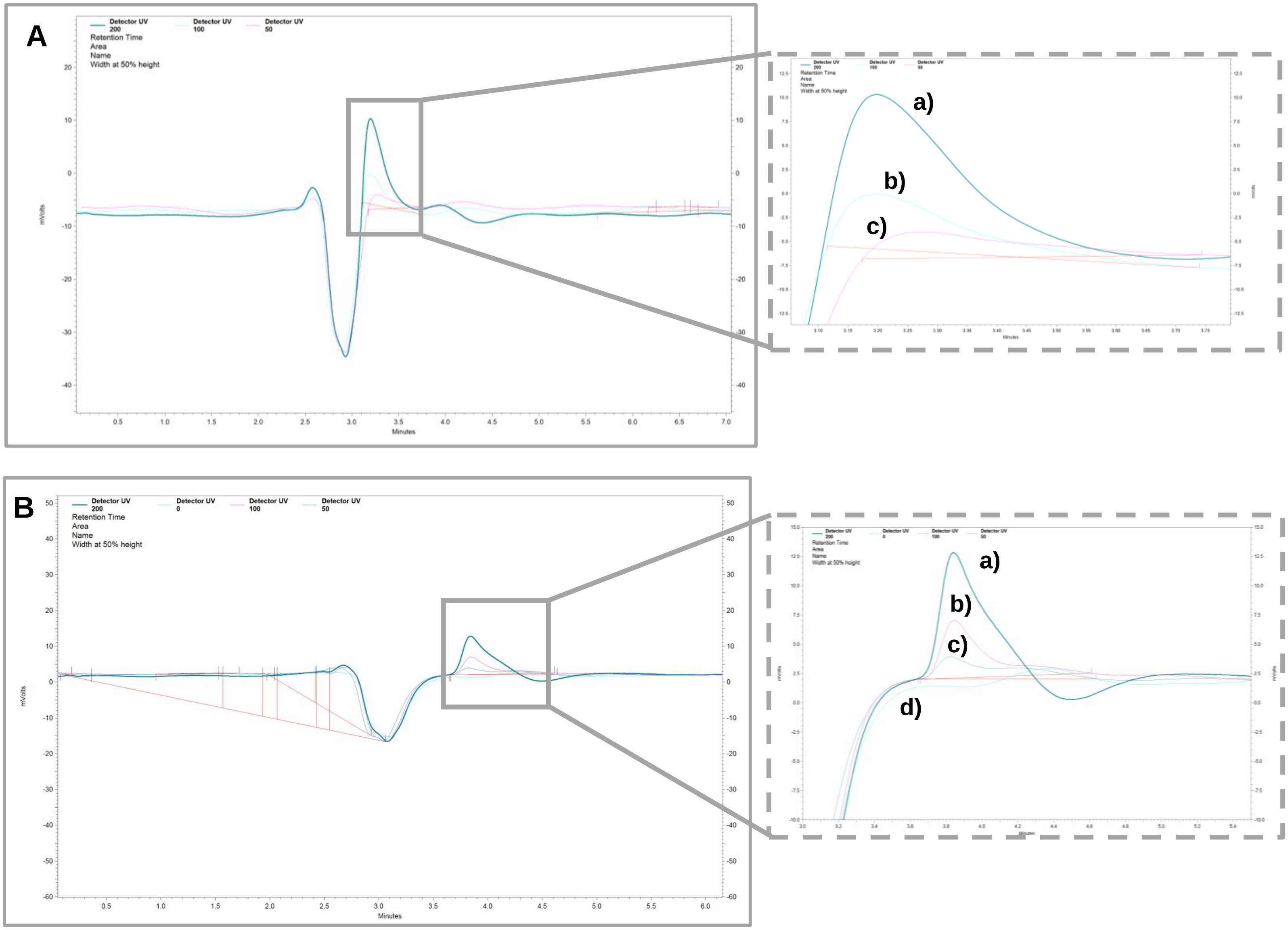

Figure 47. *Chromatogram of different standard solutions with different concentrations:* ***(A)*** *L-DOPA and* ***(B)*** *Dopamine. In chromatogram of L-DOPA:* ***a)*** *[L-DOPA] = 200 μM;* ***b)*** *[L-DOPA] = 100 μM and* ***c)*** *[L-DOPA] = 50 μM. In chromatogram of L-Dopamine:* ***a)*** *[L-DOPA] = 200 μM;* ***b)*** *[L-DOPA] = 100 μM,* ***c)*** *[L-DOPA] = 50 μM and* ***d)*** *[L-DOPA] = 0 μM. For each standard has its retention time, which will be shown in* ***Table 10*** *and* ***Table 11****, respectively for compound L-DOPA and dopamine.*

In **Table 10** and **Table 11** summarize the retention time (min) collected based on the chromatograms for the L-DOPA and Dopamine standards, respectively. It was concluded that, for L-DOPA and Dopamine the retention time, is respectively, 3.18 and 3.74 minutes.

Table 10. *Summarize the retention time (min) and the peak area (A.U) collected based on the chromatograms for the L-DOPA.*

[Standard]	**Retention Time$_1$ (min)**	**Retention Time$_2$ (min)**	**Peak Area$_1$ (A.U)**	**Peak Area$_2$ (A.U)**
12.5 μM	3.3	3.42	2409	1764
25 μM	3.185	---	11685	---
50 μM	3.166	---	44836	---
100 μM	3.13	3.06	78925	95913
200 μM (stock)	3.145	3.05	184736	220328
Average	3.182			

Table 11. *Summarize the retention time (min) and the peak area (A.U) collected based on the chromatograms for the Dopamine.*

[Standard]	**Retention Time$_1$ (min)**	**Retention Time$_2$ (min)**	**Peak Area$_1$ (A.U)**	**Peak Area$_2$ (A.U)**
12.5 μM	3.581	3.851	5388	883
25 μM	4.06	---	12312	---
50 μM	3.603	3.52	42186	48528
100 μM	3.78	---	86111	---
200 μM (stock)	3.718	3.785	250483	219812
Average	3.737			

The determination of linearity was performed by constructing the calibration curve with standard L-DOPA and Dopamine solutions of various concentrations: 12.5, 25, 50, 100 and 200 μM for L-DOPA (**Figure 48.A**) and 12.5, 25, 50, 100 and 200 μM for Dopamine (**Figure 48.B**). This calibration curve correlates peak area values with their respective L-DOPA and Dopamine concentrations for the different standards. In both calibration curves an R^2 was obtained around 0.99, which is close to 1, it can be predicted that there is linearity between peak area and concentration. These curves can be used to determine the concentration of L-DOPA and Dopamine compounds in samples.

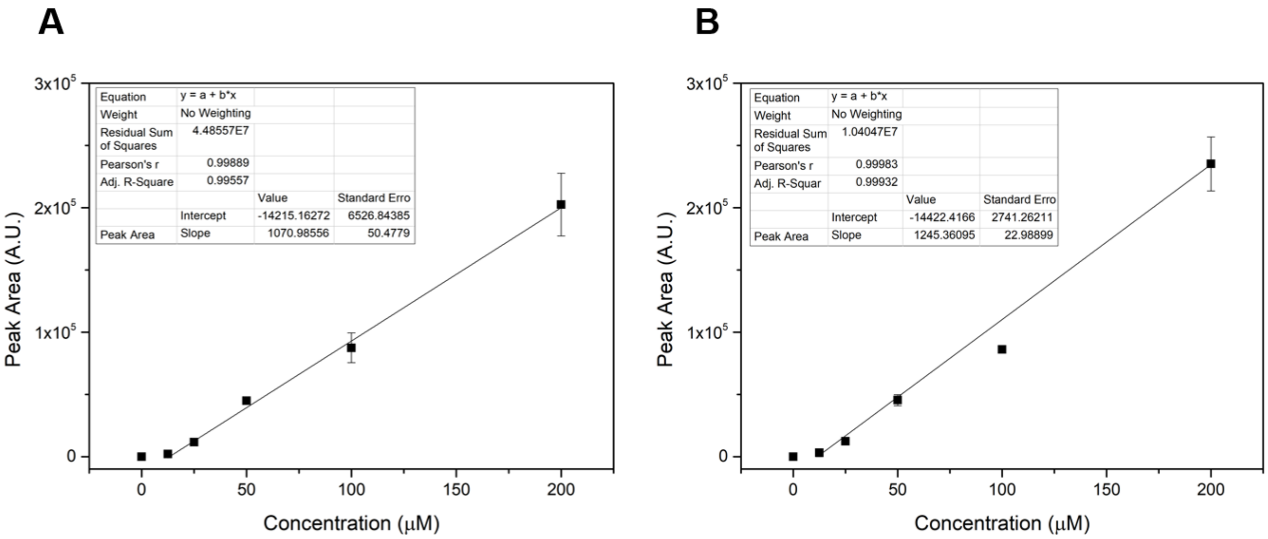

Equation	y = a + b*x		
Weight	No Weighting		
Residual Sum of Squares	4.48557E7		
Pearson's r	0.99889		
Adj. R-Square	0.99557		
		Value	Standard Erro
	Intercept	-14215.16272	6526.84385
Peak Area	Slope	1070.98556	50.4779

Equation	y = a + b*x		
Weight	No Weighting		
Residual Sum of Squares	1.04047E7		
Pearson's r	0.99983		
Adj. R-Squar	0.99932		
		Value	Standard Erro
	Intercept	-14422.4166	2741.26211
Peak Area	Slope	1245.36095	22.98899

Figure 48. *Calibration Curves:* ***(A)*** *L-DOPA and* ***(B)*** *Dopamine for different concentrations of standard solutions: 12.5, 25, 50, 100 and 200 μM. These curves can be used to determine the concentration of L-DOPA and Dopamine compounds in samples (n=2).*

3.8.2. Artificial mixtures

Artificial mixtures of different proportions were made between L-DOPA and dopamine in order to know what the peaks were when the two components were in reaction, as shown in **Figure 49. B**, where it can be seen that for different proportions the behavior is relatively the same compared to the separate samples as shown in **Figure 47**. The method presents selectivity, since it is verified that the retention time of the test compounds maintained its baseline, showing no interferences. However an ideal chromatogram when the mixture of the two compounds is used would be two individualized peaks, not two overlapping peaks like the one in **Figure 49. B**.

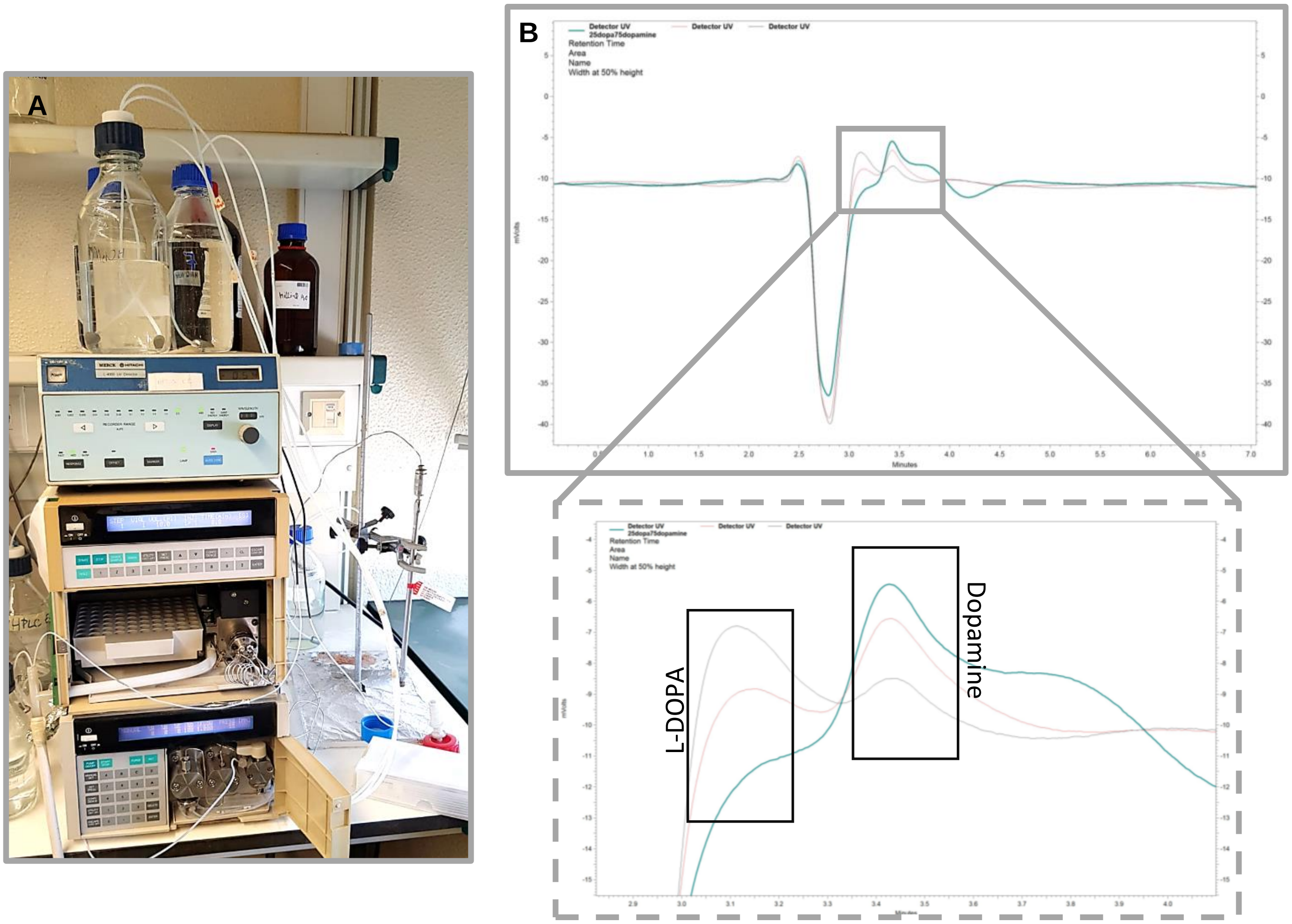

Figure 49. HPLC: **(A)** Step-up and **(B)** Chromatogram obtained for artificial mixtures of different proportions between L-DOPA and dopamine: **Grey** – 75 µM of L-DOPA + 25 µM of dopamine, **Pink** - 50 µM of L-DOPA + 50 µM of dopamine and **Blue** – 25 µM of L-DOPA + 75 µM of dopamine. The retention time for L-DOPA and Dopamine, is approximately, 3.13 and 3.45 minutes, respectively.

3.8.3. Determination of compounds in samples

Following the standard curves of the individual samples and the mixed samples, the dopamine production was performed, using the short reactor, from the pure L-DOPA substrate at a concentration of 100 µM for 2 hours (to have sufficient volume to perform HPLC analysis) at a flow rate of 1 µm/min. The reactor output obtained from this production was analyzed on HPLC. The results obtained are shown in **Figure 50**.

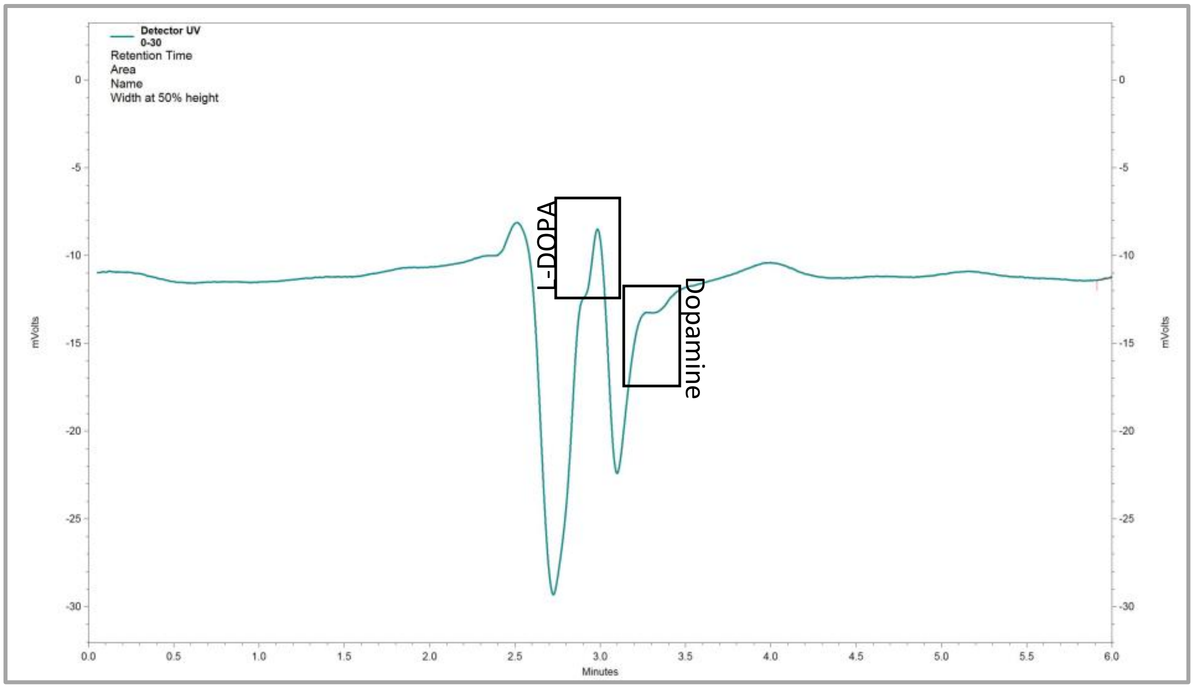

Figure 50. *Chromatogram obtained for real sample. Peaks of L-DOPA and Dopamine compounds are highlighted, depending on retention times, 3.1 minutes for L-DOPA, and 3.45 minutes for Dopamine.*

In **Figure 50** it is possible to see the chromatogram obtained for real sample. It can be concluded that it is not a perfect chromatogram, but comparing with the chromatogram and retention times obtained for the artificial mixture (**Figure 49.B**) it can be deduced that probably the real sample contains dopamine. With this in mind it follows that dopamine production occurs. But anyway, in order to better the results it will be necessary to make some optimizations, so that the compounds L-DOPA and Dopamine have more different retention times in order to have more individualized peak, to increase method resolution.

Chapter 4

4. Conclusions and Future Works

In this work was demonstrated, a microfluidic approach to enzymatic production optimization. Optimization of both upstream and downstream processing steps is often very burdensome, therefore it is essential to optimize the reaction conditions through screening studies in order to obtain the best conditions for the continuous productions of these high value biomolecules. Microfluidic bioreactors present an efficient and inexpensive alternative, allowing for multiple experiments to be performed rapidly while consuming a minimal amount of reagents in a very controlled form, in terms of both mass and heat transfer, in addition to the reduced reaction times, imposed by small diffusion lengths within the microfluidic device.

The objectives defined at the beginning of this project were achieved since it was possible to:

- Screen and optimize conditions in order to detect L-DOPA;
- Optimize conditions in order to produce L-DOPA and dopamine with the use of microfluidic bioreactors: for the individual production of L-DOPA through the tyrosine substrate; individual production of dopamine through the pure L-DOPA substrate; and finally the production of L-DOPA and dopamine using cascade reactions, using tyrosine as substrate;
- Demonstrate feasibility of using this type of system for a multi-step production scheme was demonstrated by converting tyrosine into dopamine in a continuous mode;
- Upscale of the system of production of L-DOPA, obtaining similar conversions of substrate to those obtained in the microscale and also in the literature.

In order to detect L-DOPA several screening studies were performed with different types of beads, and it was concluded that the only beads that could be used would be Q-Sepharose beads. With this, it was also possible to conclude that following packing the beads, there would have to be a washing step to remove the PEG used to aid the packing of the beads.

Knowing that the addition of a reducing agent - ascorbic acid is essential for the synthesis of L-DOPA, several assays were carried out with different acid concentrations, keeping the L-DOPA concentration constant in order to determine if there was interference in the detection of L-DOPA and it was possible to conclude that the range of ascorbic acid concentrations where it was possible to work was between 10-200 μM. After the detection method of L-DOPA was complete, it was started to produce L-DOPA.

In the production of L-DOPA, optimizations were made regarding flowrate, reactor geometry and substrate ratio in the reaction medium. In relation to flowrate it was found that there is an impact in the initial moments of the reaction, but eventually reaches a steady state. Later in relation to reactor geometry it was concluded that the short reactor far outperforms the long reactor, this is due to the low substrate residence time within the short reactor and the fact that each substrate molecule will find fewer enzymes when compared to the reactor long. and finally, in relation substrate ratio in the reaction medium it was concluded that in the absence of ascorbic acid, the reaction output is very close to zero and there seems to be a higher limit to the amount of ascorbic acid that will improve the reaction conditions. In long L-DOPA productions, in order to study operational stability, initial losses in enzyme activity were observed, perhaps due to reactor fouling, suicidal nature of tyrosine substrate for tyrosinase activity or enzyme wash-out of the system due to the weak interaction between the APTES functionalized spheres and the enzyme.

Regarding the detection of dopamine, it was concluded that it was only achieved from the consumption of L-DOPA. Therefore dopamine productivity was followed by detection of L-DOPA. Dopamine production has been optimized for flow rates and has been found not to have a dramatic impact on system output.

In cascade reaction experiments it was found that productivity here is much higher when 100 μM pure L-DOPA (single-step reaction) is used, believing that the Dopa-Decarboxylase chamber is being injected with higher concentrations of L DOPA that is capable of converting.

In addition, the results obtained in macroscale are identical to those obtained for the microscale throughout the experiment. It can be concluded that by maintaining similar mass transport conditions, it is possible to accurately predict the result of the macroscale process for Packed- bed reactors.

Finally, with the HPLC results, although the chromatogram obtained for the real sample is not perfect, it can be deduced that dopamine production occurs.

As a final observation, microfluidic structures are a versatile and powerful tool both to obtain the screening results in a rapid manner.

As future prospects, it seems that this type of approach could be very useful mainly to screen enzymatic conditions, since it is possible to apply a set of different conditions and the conversions of substrate for each one of them. In any case it would be necessary to:

- Implement downstream processing in order to obtain the desired product without any contaminant;
- Screening studies of some solutions to elute the detection column so that they can be reused;
- Develop a lab-on-chip system where biomolecules could be produced and simultaneously detected. For detection to occur, the addition of NaOH is essential, so it was added to the system through a valve system. Such as the solution that would be used to elute the column containing the Q-Sepharose beads. This system should also include downstream processing, to reuse some reagents and purify the product obtained;
- Develop a heater to put on the chip so that the temperature is always constant.

Chapter 5

5. References

[1] J. M. Choi, S. S. Han, and H. S. Kim, “Industrial applications of enzyme biocatalysis: Current status and future aspects,” Biotechnology Advances. 2015. **33**(7): p. 1443–1454.

[2] R. den Haan, E. van Rensburg, S. H. Rose, J. F. Görgens, and W. H. van Zyl, “Progress and challenges in the engineering of non-cellulolytic microorganisms for consolidated bioprocessing,” *Current Opinion in Biotechnology*. 2015. **33**: p. 32–38.

[3] H. Sun, H. Zhang, E. L. Ang, and H. Zhao, “Biocatalysis for the synthesis of pharmaceuticals and pharmaceutical intermediates,” *Bioorganic and Medicinal Chemistry*. 2018. **26**(7), 1275–1284.

[4] P. A. Lewitt, “Levodopa therapy for Parkinson’s disease: Pharmacokinetics and pharmacodynamics,” *Movement Disorders*. 2015. **30**(1): p. 64–72.

[5] I. Beaulieu-Boire and A. E. Lang, “Behavioral effects of levodopa,” *Movement Disorders*. 2015. **30**(1): p. 90–102.

[6] N. D. Volkow, R. A. Wise, and R. Baler, “The dopamine motive system: Implications for drug and food addiction,” *Nature Reviews Neuroscience*. 2017. **18**(12): p. 741–752.

[7] W. Schultz, “Dopamine reward prediction-error signalling: A two-component response,” *Nature Reviews Neuroscience*. 2016. **17**(3): p. 183–195.

[8] V. Ruonala, E. Pekkonen, O. Airaksinen, M. Kankaanpää, P. A. Karjalainen, and S. M. Rissanen, “Levodopa-induced changes in electromyographic patterns in patients with advanced Parkinson’s disease,” *Front. Neurol.*, 2018. **9**(35).

[9] A. J. Reyes, K. Ramcharan, P. Harnarayan, and J. Mooteeram, “Symmetrical digital gangrene after a high dose intravenous infusion of epinephrine and dopamine following resuscitation from cardiac arrest,” *BMJ Case Reports*. 2016. doi:10.1136/bcr-2016-217977.

[10] K. Min, K. Park, D. H. Park, and Y. J. Yoo, “Overview on the biotechnological production of l-DOPA,” *Applied Microbiology and Biotechnology*. 2014. **99**(2): p. 575–584.

[11] A. Demirci, G. Izmirlioglu, and D. Ercan, “Fermentation and Enzyme Technologies in Food

Processing," in *Food Processing: Principles and Applications: Second Edition*, 2014, John Wiley & Sons, Ltd., Pennsylvania, p. 107–136.

[12] J. E. Leresche and H. P. Meyer, "Chemocatalysis and biocatalysis (biotransformation): Some thoughts of a chemist and of a biotechnologist," *Organic Process Research and Development*. 2006. **10**(3): p. 572–580.

[13] P. Fernandes, F. Carvalho, and M. P.C. Marques, "Miniaturization in Biotechnology: Speeding up the Development of Bioprocesses," *Recent Pat. Biotechnol.*, 2011. **5**(3): p. 160–173.

[14] K. S. Elvira, X. C. I Solvas, R. C. R. Wootton, and A. J. Demello, "The past, present and potential for microfluidic reactor technology in chemical synthesis," *Nature Chemistry*. 2013. **5**(11): p. 905–915.

[15] D. L. Nelson and M. M. Cox, *Lehninger Principles of Biochemistry*: *Fourth Edition*, 2005, W.H. Freeman & Co., New York, p. 190-237.

[16] S. Tuncagil, S. K. Kayahan, G. Bayramoglu, M. Y. Arica, and L. Toppare, "l-Dopa synthesis using tyrosinase immobilized on magnetic beads," *J. Mol. Catal. B Enzym.*, 2009. **58**(1-4): p. 187–193.

[17] A. Bijelic, M. Pretzler, C. Molitor, F. Zekiri, and A. Rompel, "The structure of a plant tyrosinase from Walnut leaves reveals the importance of 'substrate-guiding residues' for enzymatic specificity," *Angew. Chemie - Int. Ed.*, 2015. **54**(49): p. 14677–14680.

[18] M. Kanteev, M. Goldfeder, and A. Fishman, "Structure-function correlations in tyrosinases," *Protein Science*. 2015. **24**(9): p. 1360–1369.

[19] C. W. G. Van Gelder, W. H. Flurkey, and H. J. Wichers, "Sequence and structural features of plant and fungal tyrosinases," *Phytochemistry*. 1997. **45**(7): p. 1309–1323.

[20] D. Y. Xu, J. Y. Chen, and Z. Yang, "Use of cross-linked tyrosinase aggregates as catalyst for synthesis of l-DOPA," *Biochem. Eng. J.*, 2012. **63**: p. 88–94.

[21] J. Berg, J. Tymoczko, and L. Stryer, *Biochemistry, 5th edition*, 2002, W.H. Freeman & Co., New York, Chapter 8.

[22] N. M. F. Carvalho *et al.*, "Uso de equações lineares na determinação dos parâmetros de Michaelis-Menten," *Quim. Nova*, 2010. **33**(7), 1607–1611.

[23] T. Jesionowski, J. Zdarta, and B. Krajewska, "Enzyme immobilization by adsorption: A review," *Adsorption*. 2014. **20**(5-6): p. 801–821.

[24] B. Krajewska, "Application of chitin- and chitosan-based materials for enzyme immobilizations: A review," *Enzyme and Microbial Technology*. 2004. **35**(2-3): p. 126–139.

[25] P. Fernandes, “Enzymes in food processing: A condensed overview on strategies for better biocatalysts,” *Enzyme Research*. 2010. p. 1-19.

[26] L. Hajba and A. Guttman, “Continuous-flow biochemical reactors: Biocatalysis, bioconversion, and bioanalytical applications utilizing immobilized microfluidic enzyme reactors,” *J. Flow Chem.*, 2016. **6**(1): p. 8–12.

[27] P. K. Robinson, “Enzymes: principles and biotechnological applications,” *Essays Biochem.*, 2015. **59**(0): p. 1–41.

[28] N. R. Mohamad, N. H. C. Marzuki, N. A. Buang, F. Huyop, and R. A. Wahab, “An overview of technologies for immobilization of enzymes and surface analysis techniques for immobilized enzymes,” *Biotechnology and Biotechnological Equipment*. 2015. **29**(2): p. 205–220.

[29] S. N. Doble, M. & Gummadi, *BIOCHEMICAL ENGINEERING: First Edition,* 2007, PHI Learning Pvt. Ltd., p. 159-160.

[30] A. Coker, *Modeling of chemical kinetics and reactor design: First Edition*, 2001, Gulf Professional Pub., p. 218-259.

[31] A. Illanes, *Enzyme biocatalysis: Principles and applications*: *First Edition*, 2008, Springer Netherlands., p. 205-245.

[32] A. Illanes, L. Wilson, and C. Vera, *Problem solving in enzyme biocatalysis*, 2013, John Wiley and Sons Ltd., p. 141–180.

[33] H. S. Fogler, *Essentials of chemical reaction engineering*, 2011, Prentice-Hall, p. 33-59.

[34] A. M. Ribiero, P. Neto, and C. Pinho, “Mean porosity and pressure drop measurements in packed beds of monosized spheres.pdf,” *Int. Rev. Chem. Eng.*, 2010. **2**(1): p. 40-46.

[35] R. Subramanian, “Flow through Packed Beds and Fluidized Beds,” *Clarkson Univ.,* 2004.

[36] Dinheirovivo. "Aumento da despesa em medicamentos rondou os 500 milhões em três anos". Available in: <https://www.dinheirovivo.pt/economia/aumento-da-despesa-em-medicamentos-rondou-os-500-milhoes-em-tres-anos/ >. 2018. Accessed: 15.October.2019 .

[37] D. J. Pollard and J. M. Woodley, “Biocatalysis for pharmaceutical intermediates: the future is now,” *Trends in Biotechnology*. 2007. **25**(2): p. 66–73.

[38] P. Gupta and A. Mahajan, “Green chemistry approaches as sustainable alternatives to conventional strategies in the pharmaceutical industry,” *RSC Advances*. 2015. **5**(34): p. 26686–26705.

[39] S. K. Ma *et al.*, “A green-by-design biocatalytic process for atorvastatin intermediate,” *Green*

Chem., 2010. **12**(1): p. 81–86.

[40] A. A. Desai, “Sitagliptin manufacture: A compelling tale of green chemistry, process intensification, and industrial asymmetric catalysis,” *Angew. Chemie - Int. Ed.*, 2011. **50**(9): p. 1974–1976.

[41] T. Li *et al.*, “Efficient, chemoenzymatic process for manufacture of the boceprevir bicyclic [3.1.0]proline intermediate based on amine oxidase-catalyzed desymmetrization,” *J. Am. Chem. Soc.*, 2012. **134**(14): p. 6467–6472.

[42] J. M. Woodley, “New opportunities for biocatalysis: making pharmaceutical processes greener,” *Trends in Biotechnology*. 2008. **26**(6): p. 321–327.

[43] S. Saqib, A. Akram, S. A. Halim, and R. Tassaduq, “Sources of β-galactosidase and its applications in food industry,” *3 Biotech*. 2017. **7**(1): p. 79.

[44] C. Pezzella, L. Guarino, and A. Piscitelli, “How to enjoy laccases,” *Cellular and Molecular Life Sciences*. 2015. **72**(5): p. 923–940.

[45] A. K. Patel, R. R. Singhania, and A. Pandey, “Novel enzymatic processes applied to the food industry,” *Current Opinion in Food Science*. 2016. **7**: p. 64–72.

[46] N. S. Neta, J. A. Teixeira, and L. R. Rodrigues, “Sugar Ester Surfactants: Enzymatic Synthesis and Applications in Food Industry,” *Crit. Rev. Food Sci. Nutr.*, 2015. **55**(5): p. 595–610.

[47] J. Trbojević Ivić *et al.*, “Design of biocompatible immobilized Candida rugosa lipase with potential application in food industry,” *J. Sci. Food Agric.*, 2016. **96**(12): p. 4281–4287.

[48] J. Staroń, J. M. Dąbrowski, E. Cichoń, and M. Guzik, “Lactose esters: synthesis and biotechnological applications,” *Critical Reviews in Biotechnology*. 2018. **38**(2): p. 245–258.

[49] M. A. Sanromán and F. J. Deive, “Food Enzymes,” in *Current Developments in Biotechnology and Bioengineering: Food and Beverages Industry*, 2016. p. *119–120.*

[50] S. Wu *et al.*, “Protein engineering of nitrilase for chemoenzymatic production of glycolic acid,” *Biotechnol. Bioeng.*, 2008. **99**(3): p. 717–720.

[51] Y. Cui, W. Cui, Z. Liu, L. Zhou, M. Kobayashi, and Z. Zhou, “Improvement of stability of nitrile hydratase via protein fragment swapping,” *Biochem. Biophys. Res. Commun.*, 2014. **450**(1): p. 401–408.

[52] A. Panova *et al.*, “Chemoenzymatic synthesis of glycolic acid,” *Adv. Synth. Catal.*, 2007. **349**(8-9): p. 1462–1474.

[53] P. Tabeling, *Introduction to Microfluidics*. New York: Oxford University Press, 2005.

[54] C. Hansen and S. R. Quake, “Microfluidics in structural biology: Smaller, faster... better,” *Current Opinion in Structural Biology*. 2003. **13**(5): p. 538–544.

[55] E. R. Choban, L. J. Markoski, A. Wieckowski, and P. J. A. Kenis, “Microfluidic fuel cell based on laminar flow,” *J. Power Sources*, 2004. **128**(1): p. 54–60.

[56] A. Naillon, P. Joseph, and M. Prat, “Sodium chloride precipitation reaction coefficient from crystallization experiment in a microfluidic device,” *J. Cryst. Growth*, 2017. **463**: p. 201–210.

[57] I. F. Pinto *et al.*, “The application of microbeads to microfluidic systems for enhanced detection and purification of biomolecules,” *Methods*, 2017. **116**: p. 112–124.

[58] D. J. Beebe, G. A. Mensing, and G. M. Walker, “Physics and Applications of Microfluidics in Biology,” *Annu. Rev. Biomed. Eng.*, 2002. **4**(1): p. 261–286.

[59] Y. XIA and G. M. WHITESIDES, “ChemInform Abstract: Soft Lithography,” *ChemInform*, 2010. **37**(5): p. 550–575.

[60] Y. Sun and J. A. Rogers, “Structural forms of single crystal semiconductor nanoribbons for high-performance stretchable electronics,” *Journal of Materials Chemistry*. 2007. **17**(9): p. 832.

[61] P. Kim, K. W. Kwon, M. C. Park, S. H. Lee, S. M. Kim, and K. Y. Suh, “Soft lithography for microfluidics: A Review,” *Biochip Journal*. 2008. **2**(1): p. 1-11.

[62] J. Kuncová-Kallio and P. J. Kallio, “PDMS and its suitability for analytical microfluidic devices,” in *Annual International Conference of the IEEE Engineering in Medicine and Biology - Proceedings*, 2006. p. 2486–2489.

[63] J. Zhou, D. A. Khodakov, A. V. Ellis, and N. H. Voelcker, “Surface modification for PDMS-based microfluidic devices,” *Electrophoresis*. 2012. **33**(1): p. 89–104.

[64] R. S. Kane, S. Takayama, E. Ostuni, D. E. Ingber, and G. M. Whitesides, “Patterning proteins and cells using soft lithography,” in *The Biomaterials: Silver Jubilee Compendium*, 1999. p. 161–174.

[65] J. W. Judy, “Microelectromechanical systems (MEMS): Fabrication, design and applications,” *Smart Mater. Struct.*, 2001. **10**(6): p. 1115–1134.

[66] C. Zhang, D. Xing, and Y. Li, “Micropumps, microvalves, and micromixers within PCR microfluidic chips: Advances and trends,” *Biotechnology Advances*. 2007. **25**(5): p. 483–514.

[67] A. Doll, M. Wischke, H. J. Schrag, A. Geipel, F. Goldschmidtboeing, and P. Woias, “Characterization of active silicon microvalves with piezoelectric membrane actuators,” *Microelectron. Eng.*, 2007. **84**(5-8): p. 1202–1206.

[68] E.-H. Yang, C. Lee, and J. M. Khodadadi, “Development of MEMS-Based Piezoelectric Microvalve Technologies,” *Sensors Mater. Sensors Mater. Sensors Mater.*, 2007. **19**(1): p. 1-18.

[69] O. C. Jeong, S. W. Park, S. S. Yang, and J. J. Pak, “Fabrication of a peristaltic PDMS micropump,” in *Sensors and Actuators, A: Physical*, 2005. **123-124**: p. 453–458.

[70] F. Abhari, H. Jaafar, and N. A. Md Yunus, “A comprehensive study of micropumps technologies,” *International Journal of Electrochemical Science*. 2012. **7**(10): p. 9765-9780.

[71] S. Wang, Y. Yin, C. Hu, and P. Rezai, “3D integrated circuit cooling with microfluidics,” *Micromachines*. 2018. **9**(6): p. 287.

[72] Y. H. Chang, G. Bin Lee, F. C. Huang, Y. Y. Chen, and J. L. Lin, “Integrated polymerase chain reaction chips utilizing digital microfluidics,” *Biomed. Microdevices*, 2006. **8**(3): p. 215–225.

[73] L. A. Lerin *et al.*, “Enzymatic synthesis of ascorbyl palmitate in ultrasound-assisted system: Process optimization and kinetic evaluation,” *Ultrason. Sonochem.*, 2011. **18**(5): p. 988–996.

[74] L. D. Garza-García *et al.*, “Continuous flow micro-bioreactors for the production of biopharmaceuticals: The effect of geometry, surface texture, and flow rate,” *Lab Chip*, 2014. **14**(7): p. 1320–1329.

[75] P. Fernandes, “Miniaturization in biocatalysis,” *International Journal of Molecular Sciences*. 2010. **11**(3): p. 858–879.

[76] A. R. De Boer, B. Bruyneel, J. G. Krabbe, H. Lingeman, W. M. A. Niessen, and H. Irth, “A microfluidic-based enzymatic assay for bioactivity screening combined with capillary liquid chromatography and mass spectrometry,” *Lab Chip*, 2005. **5**(11): p. 1286-1292.

[77] S. Matosevic, N. Szita, and F. Baganz, “Fundamentals and applications of immobilized microfluidic enzymatic reactors,” *J. Chem. Technol. Biotechnol.*, 2011. **86**(3): p. 325–334.

[78] M. P. C. Marques and P. Fernandes, “Microfluidic devices: Useful tools for bioprocess intensification,” *Molecules*. 2011. **16**(10): p. 8368–8401.

[79] F. Carvalho and P. Fernandes, “Packed bed enzyme microreactor: Application in sucrose hydrolysis as proof-of-concept,” *Biochem. Eng. J.*, 2015. **104**: p. 74–81.

[80] F. Jones, Z. Lu, and B. B. Elmore, “Development of novel microscale system as immobilized enzyme bioreactor,” *Appl. Biochem. Biotechnol. - Part A Enzym. Eng. Biotechnol.*, 2002. ***98-100****(1-9): p. 627–640.*

[81] P. He, G. Greenway, and S. J. Haswell, “Development of enzyme immobilized monolith micro-reactors integrated with microfluidic electrochemical cell for the evaluation of enzyme kinetics,”

Microfluid. Nanofluidics, 2010. **8**(5): p. 565–573.

[82] “Book Review of Bioconjugate Techniques Bioconjugate Techniques , 2nd ed. By Greg T. Hermanson (Pierce Biotechnology, Thermo Fisher Scientific, Rockford, IL). Academic Press (an imprint of Elsevier): London, Amsterdam, Burlington, San Diego . 2008 . xxx + ,” *J. Am. Chem. Soc.*, 2008. **130**(30): p. 10031–10034.

[83] “‘Instructions – Coomassie (Bradford) Protein Assay Kit – Thermo Scientific, USA.’ [Online]. Available in: https://www.thermofisher.com/order/catalog/product/23200. Accessed: 15.October.2019.

[84] M. R. Hormozi-Nezhad, A. Moslehipour, and A. Bigdeli, “Simple and rapid detection of L-dopa based on in situ formation of polylevodopa nanoparticles,” *Sensors Actuators, B Chem.*, 2017. **243**: p. 715–720.

[85] C. A. Schneider, W. S. Rasband, and K. W. Eliceiri, “NIH Image to ImageJ: 25 years of image analysis,” *Nature Methods*. 2012. **9**(7): p. 671–675.

[86] C. Muzzi *et al.*, “Simultaneous determination of serum concentrations of levodopa, dopamine, 3-O-methyldopa and α-methyldopa by HPLC,” *Biomed. Pharmacother.*, 2008. **62**(4): p. 253–258.

[87] I. F. Pinto, M. R. Aires-Barros, and A. M. Azevedo, “Multimodal chromatography: debottlenecking the downstream processing of monoclonal antibodies,” *Pharm. Bioprocess.*, 2015. **3**(3), 263–279.

[88] H. B. Yildiz, S. Caliskan, M. Kamaci, A. Caliskan, and H. Yilmaz, “L-Dopa synthesis catalyzed by tyrosinase immobilized in poly(ethyleneoxide) conducting polymers,” *Int. J. Biol. Macromol.*, 2013. **56**: p. 34–40.

[89] J. L. Muñoz-Muñoz *et al.*, “Suicide inactivation of the diphenolase and monophenolase activities of Tyrosinase,” *IUBMB Life*. 2010. **62**(7): p. 539–547.

[90] E. Vilanova, A. Manjon, and J. L. Iborra, “Tyrosine hydroxylase activity of immobilized tyrosinase on enzacryl-AA and CPG-AA supports: Stabilization and properties,” *Biotechnol. Bioeng.*, 1984. **26**(11): p. 1306–1312.

[91] A. Yildirim and M. Bayindir, “Turn-on fluorescent dopamine sensing based on in situ formation of visible light emitting polydopamine nanoparticles,” *Anal. Chem.*, 2014. **86**(11): p. 5508–5512.

[92] P. Y. Ho, M. S. Chiou, and A. C. Chao, “Production of L-DOPA by Tyrosinase Immobilized on Modified Polystyrene,” *Appl. Biochem. Biotechnol.*, vol. 111, no. 3, pp. 139–152, 2003. **111**(3): p. 139–152.

Annexes

Annexes 1. First calibration curve made.

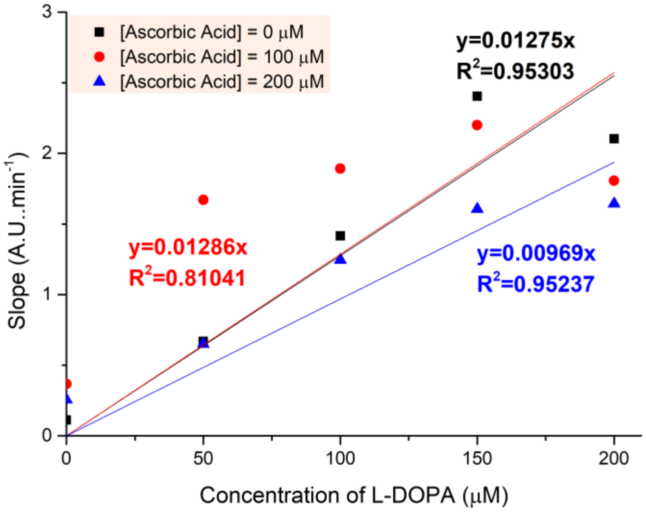

Figure 51. *Calibration Curve not considered. n=1*

Annexes 2. Example of treatment of results for second calibration curve made. Then analysis the results, as described in section 2.2.5 is considered the slope of the first three points corresponding to the first 2 minutes for each L-DOPA concentration and for each ascorbic acid concentration. This is an example for n=1. This was made 4 times, because I did this experiments 4 times. After, was made the average of slope for each concentration of L-DOPA and with this average of slopes previously obtained, the calibration curves were made as a function of L-DOPA concentration. In **Figure 52**, is possible to see the different slopes obtained for each concentration of L-DOPA and for different concentration of ascorbic acid.

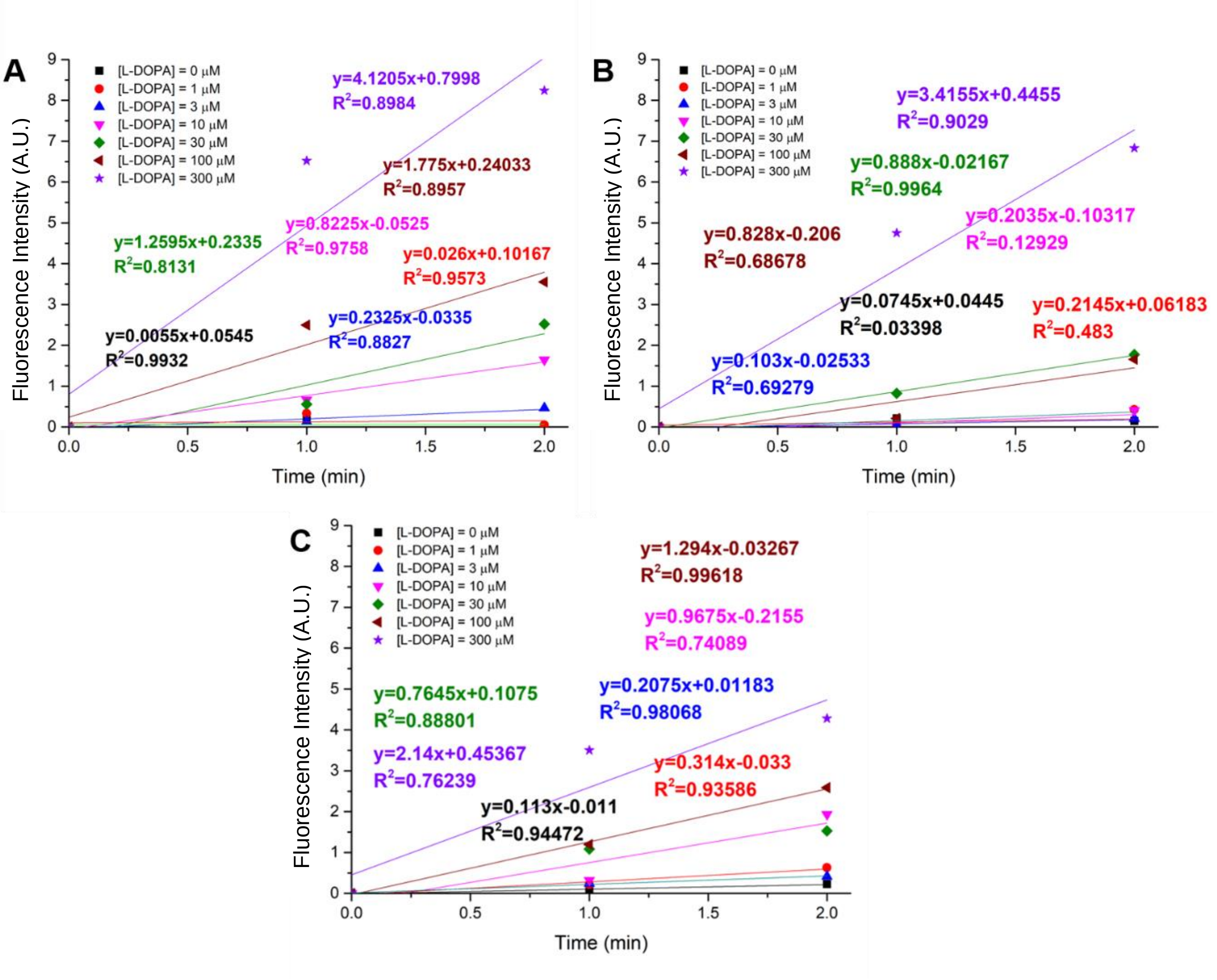

Figure 52. *Different slopes obtained for each concentration of L-DOPA and for each concentration of ascorbic acid in function of time:* ***(A)*** *0 μM of ascorbic acid;* ***(B)*** *100 μM of ascorbic acid and* ***(C)*** *200 μM of ascorbic acid. n=1*